INFORMATION TO USERS

This manuscript has been reproduced from the microfilm master. UMI films the text directly from the original or copy submitted. Thus, some thesis and dissertation copies are in typewriter face, while others may be from any type of computer printer.

The quality of this reproduction is dependent upon the quality of the copy submitted. Broken or indistinct print, colored or poor quality illustrations and photographs, print bleedthrough, substandard margins, and improper alignment can adversely affect reproduction.

In the unlikely event that the author did not send UMI a complete manuscript and there are missing pages, these will be noted. Also, if unauthorized copyright material had to be removed, a note will indicate the deletion.

Oversize materials (e.g., maps, drawings, charts) are reproduced by sectioning the original, beginning at the upper left-hand corner and continuing from left to right in equal sections with small overlaps.

ProQuest Information and Learning
300 North Zeeb Road, Ann Arbor, MI 48106-1346 USA
800-521-0600

8C

DEFORMATION KINETICS OF CREEP

by

Melek G. Akben

A Thesis Submitted to the School of
Graduate Studies of the
University of Ottawa
In Partial Fulfillment of the Requirements
for the degree of
Master of Applied Science
in Mechanical Engineering
Ottawa, Ontario, Canada
April, 1977

ABSTRACT

The deformation kinetics analysis of room temperature creep of high purity iron indicates two rate controlling mechanisms. The first of these is predominant during the initial part of the creep process and the second in the latter part when the internal stress increases and therefore the effective stress decreases. It is suggested that these mechanisms are associated with the overcoming of the Peierls-Nabarro stress field by the formation of a double kink and the lateral spreading of the kink. Strain rates diminishing to zero are believed to be a possible result of non-negligible backward activation over the double barrier system.

It is shown that, for the proposed system of two consecutive barriers, the limiting strain and the limiting effective stress at which the rate becomes zero are proportional to the activation parameters of the kinetics term associated with the backward activation over the double barrier system. This also indicates that the effective stress is not necessarily zero for zero strain rates.

A model of exponential strain dependence of the dislocation density has been proposed. The use of this model in the deformation kinetics description explicitly includes the effects of the initial dislocation density, dislocation multiplication, temperature, the initial effective stress and the work hardening coefficient on the calculated creep behavior. Results from this model indicate that the observed sharp levelling off may be due to dislocation multiplication.

LIST OF FIGURES

LIST OF TABLES

LIST OF SYMBOLS

Symbol	Definition
b	Burger's vector
h	Planck's constant
k	rate constant
$\bar{k}$	Boltzmann constant
t	time
v_o	a constant
A	pre-exponential factor in the rate equation
B	dislocation multiplication factor for linear normal strain dependence of the dislocation density
B'	dislocation multiplication factor for the linear shear strain dependence of the dislocation density
C	a constant
C_1, C_2, C_3, C_4	pre-exponential constants
ΔE	potential energy
ΔG	Gibb's free energy
H	work hardening coefficient in terms of shear stress and normal strain
H	work hardening coefficient in terms of shear stress and shear strain
M	dislocation multiplication factor for the exponential strain dependence of the dislocation density

Symbol	Definition
Q	partition function
T	absolute temperature
V	activation volume
W	work
α	a constant
β	a constant
γ	shear strain
$\dot{\gamma}$	shear strain rate
δ	contribution of one activation to the macroscopic rate
ϵ	normal strain
$\dot{\epsilon}$	normal strain rate
ϵ_o	a constant
κ	a constant
κ	transmission coefficient
μ	shear modulus
ν	frequency factor
ρ	concentration of flow units
σ	normal stress
τ	shear stress
$\Delta\sigma$	change in stress

Superscripts

lim	limiting
o	initial
$\ddagger$	activation

Subscripts

Symbol	Definition
a	applied
b	backward
e	experimental
eff	effective
f	forward
i	internal
i	counter
j	counter
r	reactant
t	total

ACKNOWLEDGEMENT

The author gratefully acknowledges the guidance, encouragement and constructive critisizm given by her advisor Dr.A.S.Krausz.

Many thanks to Mr.B.Faucher, who through discussions trigerred the work on the dislocation multiplication model, and to Dr.W.Ginman and Mr.C.Laforce for their valuable discussions.

Many thanks, also to Mr.G.Toth and members of the machine shop for their technical assistance, and to Mr.D.Seaman for his assistance.

TABLE OF CONTENTS

1. INTRODUCTION

Plastic deformation in polycrystalline metals is a complex process. The redistribution of the atoms-the plastic flow-is controlled by a system of energy barriers. To understand the mechanism, first a kinetics analysis followed by the analysis of the rate constants have to be carried out. Each of these two stages of the study of plastic deformation of a metal is a major research undertaking, as will be discussed in this chapter.

It is the purpose of this thesis to study the deformation kinetics of pure iron in creep and compare it with the findings of a stress relaxation study on the same batch of specimens. This kind of comparison is currently of interest bacause our understanding is deficient, or lacking in completeness, and is sought after in major laboratories.[2,33,37,38,44,45]

Creep is a thermally activated deformation process that takes place under constant applied load or stress at any temperature. At high temperatures, creep deformation is extensive. In most engineering applications high temperature creep is of great concern, but it has been shown by Glen[1] that creep occurs at very low temperatures, even near absolute zero.

Conventional creep curves for low and high temperatures are shown in Fig.1.1.1. The three stages of creep are gene-

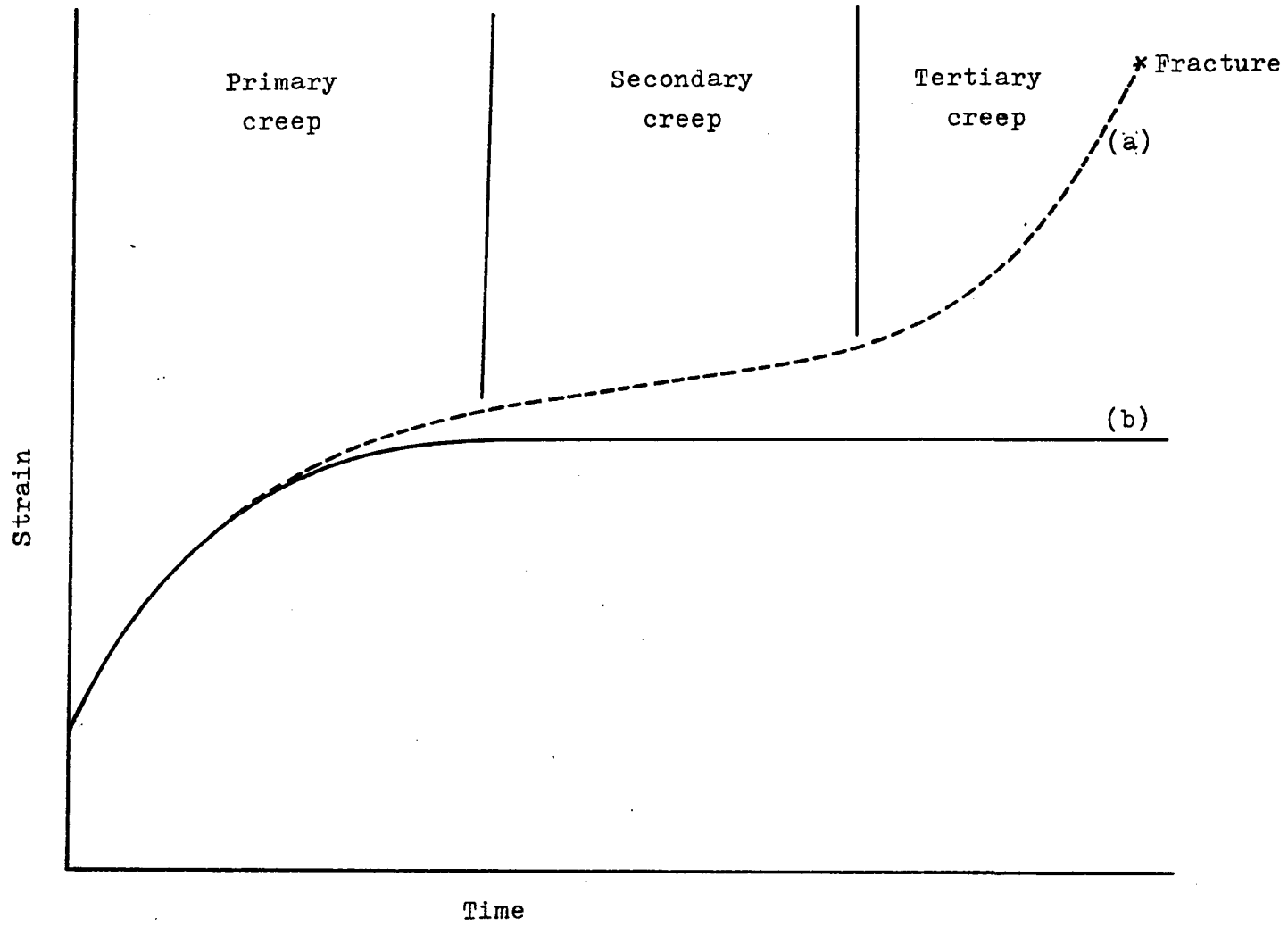

Figure 1.1.1. Conventional creep curves showing (a) primary, secondary and tertiary creep stages, (b) decelerating (primary) creep which occurs at low temperatures and stresses.

rally observed at higher temperatures and stresses. Diminishing strain rates are characteristic of low temperatures and stresses.

One of the earliest descriptions of creep was given by Andrade[2] as

$$\epsilon = \epsilon_0(1 + \beta t^{1/3})\, e^{\kappa t} \qquad 1.1.1$$

where ϵ is the strain, t is the time, and ϵ_0, κ, and β are experimental constants. In low temperature creep, κ is very small, thus Eq.1.1.1 reduces to

$$\epsilon = \epsilon_0 \beta t^{1/3}. \qquad 1.1.2$$

This is a purely empirical description. A logarithmic relation between strain and time was given by Phillips[4] as

$$\epsilon = \alpha \log t + C \qquad 1.1.3$$

where α and C are experimental constants.

Results reported by Wyatt for the creep of pure copper and aluminum showed that high temperature creep is better described by Eq.1.1.1 and low temperature creep by Eq.1.1.3.

Creep behavior can also be described by deformation kinetics-a branch of chemical kinetics.Deformation kinetics description of creep, or any thermally activated deformation

process, allows a complete description over the whole range of the process and is based on the rigorous Rate Theory of Chemical Kinetics.

1.2. THE RATE THEORY DESCRIPTION OF PLASTIC DEFORMATION

It was shown by Eyring[6] in 1936 that plastic flow can be considerd as a form of viscous flow. He has developed the theory of time dependent plastic deformation. The flow of any material is essentially a rearrangement of the atoms. During this process, interatomic distances change to the extent that bonds are broken and new bonds are established. The result of this is called plastic flow or plastic deformation. Plastic deformation is therefore like a chemical reaction and is identical to the isomerization of a giant molecule. The giant molecule is the plastically deformed material in which the atomic arrangement changes but the composition remains constant. Because plastic deformation and chemical reactions are identical processes, time dependent deformation can be described by rate theory. This argument is valid for all thermally activated deformation processes.

In the following a non-rigorous derivation of rate theory is given for the specific case of thermally activated deformation in crystalline materials. A rigorous derivation of rate theory was given, among others, by Laidler[7] and Eyring[7.1].

Consider the energy barrier represented in Fig.1.2.1. The height of this energy barrier is $\Delta G^{\ddagger}$. It should be noted that the height of this barrier is from the ground state of the reactant. When a stress τ_a is applied, the height of the barrier is reduced by the amount of work W_f introduced into the system by the applied force in the direction of the force, referred to as the forward direction, and is increased by W_b in the opposite direction, referred to as the backward direction.

The activation free energy $\Delta G_f^{\ddagger}$ associated with the forward direction is related to the partition functions of the reactant and the activated states, the latter being the configuration of the atoms from which the system can proceed to the product state. The activation free energy $\Delta G^{\ddagger}$ was defined by Eyring[7.1] as

$$\Delta G_i^{\ddagger} = \Delta E_i^{\ddagger} - \bar{k}T \ln\left(\frac{Q_{\ddagger}}{Q_r}\right)_i \qquad 1.2.1$$

where Q_r and $Q_{\ddagger}$ are the partition functions associated with the reactant and activated states respectively, $\bar{k}$ is the Boltzmann constant, $\Delta E_i^{\ddagger}$ the potential energy of the barrier, and T is the absolute temperature. The partition functions considered here are of one degree of vibrational freedom less than given in Statistical Thermodynamics. The one degree of freedom is considered as a "loose vibration"[7] -as a translational degree of freedom- whereby the bond is broken

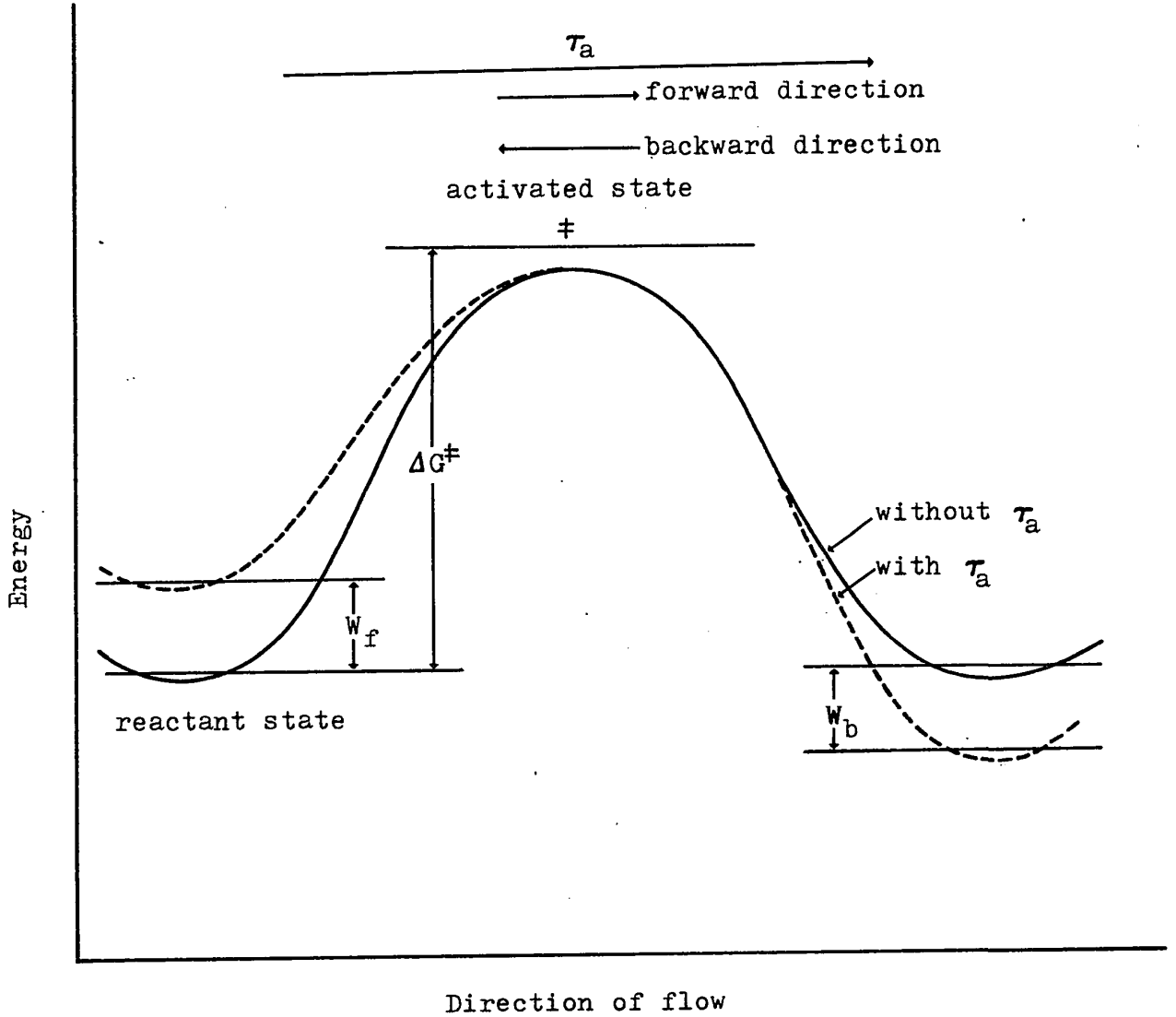

Figure 1.2.1. The distortion of the energy barrier due to the application of stress τ_a.

but not re-established-thus overcoming the energy barrier.[7]

For a unit deformation process to take place, a flow unit must overcome the barrier. The flow unit passes over the barrier $k_f^{\ddagger}$ times per second due to thermal vibrations. The relation between $k_f^{\ddagger}$ and the activation free energy is expressed as

$$k_f^{\ddagger} = \kappa \frac{\bar{k}T}{h} \exp\left(-\frac{\Delta G_f^{\ddagger}}{\bar{k}T}\right) \qquad 1.2.2$$

where κ is the transmission coefficient, h is the Plank's constant, and $\bar{k}T/h$ is a frequency factor. For low temperature deformation in metals, the transmission coefficient is unity.It is a term introduced to represent the probability of the activated complex going to the product state. It can be greater than unity when a quantum mechanical effect known as tunneling takes place.[7]

When a stress is applied to the system, the height of the barrier is reduced in the forward direction by the amount of work W_f externally introduced into the system and is increased by the work W_b in the backward direction.Using Eq.1.2.2, the rate constant in the forward direction is

$$k_f = k_f^{\ddagger} \exp\left(\frac{W_f}{\bar{k}T}\right) \qquad 1.2.3$$

In other words, the flow unit will move over the barrier k_f times per second under the stress τ_a.

The overall rate of the process also depends on the contribution of each activation, δ, and on the number of flow units, ρ_{f1}, in front of the barrier. In low temperature thermally activated deformation processes, the mobile dislocation density is considered as the concentration of flow units. Hence, the rate in the forward direction for a single barrier is

$$\text{Rate} = \delta \rho_{f1} k_{f1} \qquad 1.2.4$$

where $k_{f1} = k_f$ as defined in Eq.1.2.3.

Similarly, the rate constant in the backward direction is

$$k_{b1} = k_{b1}^{\pm} \exp\left(-\frac{W_b}{\bar{k}T}\right) \qquad 1.2.5$$

The negative sign in the exponent for the work term is due to the increase in the height of the energy barrier as a result of the applied stress.

Hence the net rate is

$$\text{Rate} = \delta \rho_{f1} k_{f1} - \delta \rho_{b1} k_{b1} \qquad 1.2.6$$

1.3. DEFORMATION KINETICS

During macroscopic deformation processes, the flow units have to pass over a large number of energy barriers. These barriers may all be identical or some may be different. The various kinds of barriers may be combined in a parallel, consecutive, or in the most general case, a parallel-consecutive system. Deformation kinetics, as a branch of chemical kinetics, is used to analyze and define the combination of the energy barriers associated with the deformation process under consideration.

In deformation kinetics, the simplest possible system is a single barrier with activation in the forward direction only. In this case, the elementary rate constant is equal to the Arrhenius rate constant. This simple description was used to describe a variety of deformation processes, e.g. Wyatt,[5] Altshuler and Christian,[9] and Dorn[8] for creep, Rhode and Pitt[11] for stress relaxation. The activation energy values reported, where evaluated[7,8] were misleading because these values include the work term. These values are therefore only apparent activation energies.

In thermally activated processes, as the contribution of the external work decreases, the system approaches equilibrium. Equilibrium is always a dynamic state in which the flow over a barrier in the forward and backward directions are equal. At low stresses the backward activation is not

negligible and must be considered as a reality at the microscopic level. For a large number of cases, the system cannot be described by a single barrier with activation in the forward direction alone; the backward activation must also be included. There is usually one other barrier or more that is rate controlling which becomes noticeable at low effective stresses.

In determining the kinetics, one should go from the simplest possible case of a single barrier with activation in the forward direction only, to the more complex forms given below.

1.3.1. Parallel Energy Barriers

The overall rate of deformation of a system comprising of m barriers in a parallel combination can be described in deformation kinetics as[12]

$$\text{Rate} = \sum_{l=1}^{m} \delta(\rho_{fl}k_{fl} - \rho_{bl}k_{bl}). \qquad 1.3.1$$

This type of system is very much like fluid flow through pipes that are joined in parallel as shown in Fig.1.3.1.

1.3.2.Consecutive Energy Barriers

The description given for a system of n consecutive barriers in deformation kinetics is[12]

$$\text{Rate} = \delta \frac{\rho_1 - \rho_{n+1}(k_{n+1}/\nu)}{\sum_{j=1}^{n}(1/k_j)_1} \qquad 1.3.2$$

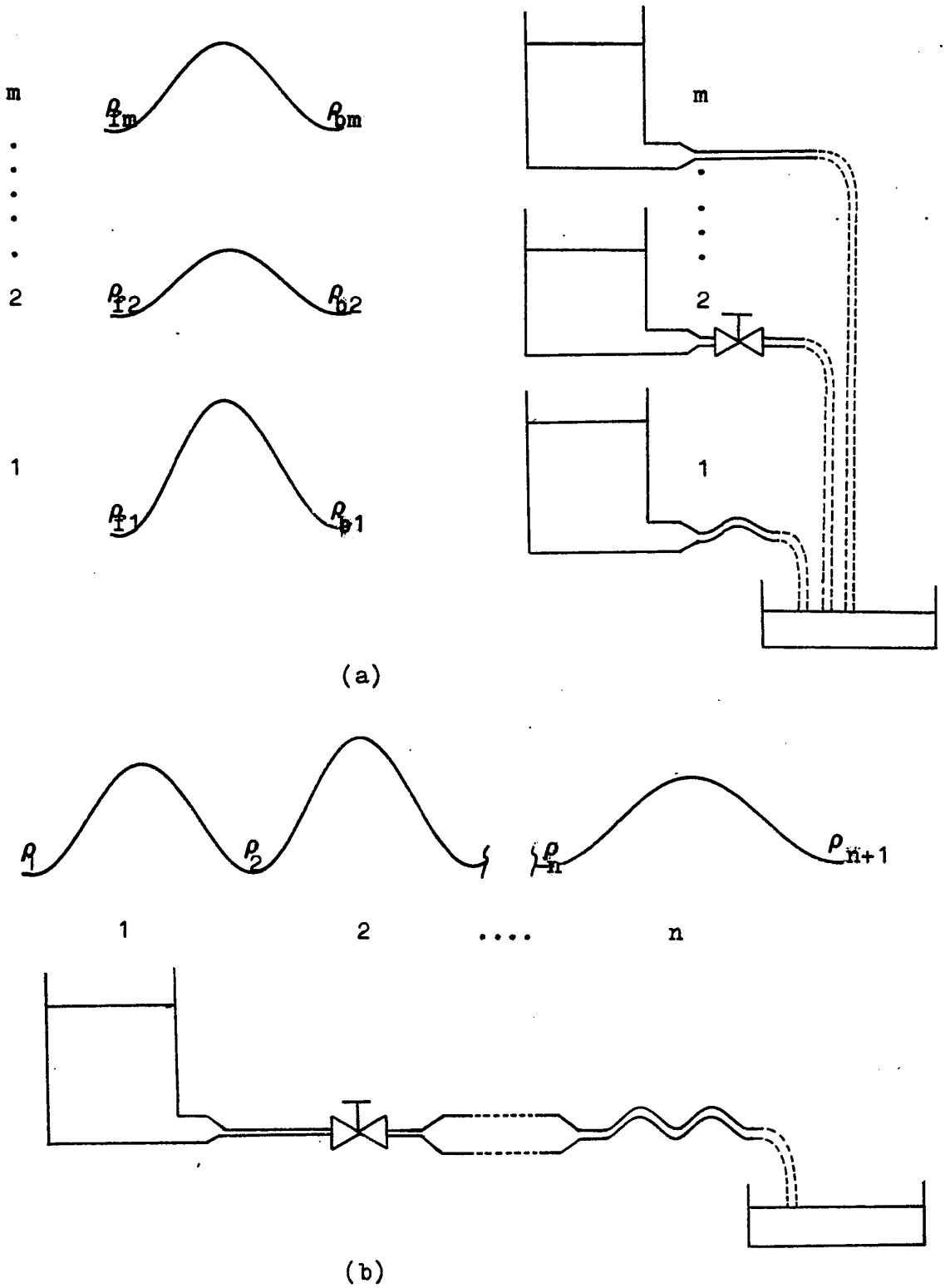

Fig. 1.3.1. Illustration of fluid flow equivalents of (a) parallel barriers, and (b) consecutive barriers systems.[12]

where ν is a frequency factor equal to $\bar{k}T/h$, and

$$(k_j)_1 = \prod_{i=1}^{j} \frac{k_{bi-1}}{k_{fi}} .$$

where $k_{b0} = 1$, and the subscript 1 on the LHS indicates reference to the ground state of the reactant in front of the first barrier. The fluid flow equivalent of this system is represented in Fig. 1.3.1.

1.3.3. Parallel-Consecutive Energy barriers

The description of the rate of a system comprising of m parallel barriers each consisting of n consecutive barriers is given in deformation kinetics as[12]

$$\text{Rate} = \sum_{l=1}^{m} \delta \frac{\rho_1 - \rho_{n+1}(k_{n+1}/\nu)}{\sum_{j=1}^{n} (1/k_j)_l} . \qquad 1.3.3$$

1.4. DETERMINATION OF ACTIVATION PARAMETERS

A kinetics approach gives a simple and systematic method by which thermally activated deformation processes can be analyzed. It is important to note that first the kinetics equation of simplest mathematical form that describes the behavior over the whole range of the experiment should be determined, then the individual rate constant, k_i, should be analyzed. In other words, first the possible combination of the rate constants should be determined for the process, e.g. parallel, consecutive, etc., then each of these rate constants should be analyzed to determine the activation parameters V_i, the activation volume which is defined in section 1.4.2, and the activation energy $\Delta G_i^{\ddagger}$.

The activation parameters determined from such analyses should have physical significance. They should be compatible with mechanisms that may be associated with the process under the given experimental conditions.

There are two methods used for thedetermination of the activation parameters:the temperature change method, and the stress change method.

1.4.1. Temperature Change Method

Temperature change methods at the same stress are used to determine the activation free energy, expressed as

$$\Delta G_i = -\bar{k} \left(\frac{d\ln k_i}{d(1/T)}\right)_{\tau,\text{structure}} \qquad 1.4.1$$

where ΔG_i is the apparent activation free energy.It includes the work introduced by the application of force on the system as

$$\Delta G_i = \Delta G_i^{\ddagger} \pm V_i \tau_{eff} \qquad 1.4.2$$

where $\Delta G_i^{\ddagger}$ is the "true" activation free energy for the i^{th} type of barrier, and τ_{eff} is the effective stress.

1.4.2. Stress Change Methods

Activation volume is a non-geometrical volume related to the work required to change the system from the reactant to the activated state. In chemical kinetics,[7] it is defined as

$$V_i = \pm \bar{k}T \left(\frac{d\ln k_i}{d\tau}\right)_{T,\text{structure}} \qquad 1.4.3$$

The order of magnitude of the ratio V/b^3, where b is the Burger's vector, gives an indication of the rate controlling mechanism.(In Appendix I a listing of these mechanisms is given.)The activation free energy gives a clearer indication of the rate controlling mechanism, however, temperature change tests are more difficult to perform than stress change tests.

Only a part of the applied stress-the effective stress-contributes to the work performed on the system and is expressed as

$$\tau_{eff} = \tau_a - \tau_i \qquad 1.4.4$$

where τ_i is the internal stress. The internal stress is the consequence of the lattice imperfections, and the residual strain.[25]

In constant load and constant temperature creep tests, time and elongation are measured,the strain and strain rates are calculated.The effective stress decreases with the strain according to the following approximate expression

$$\tau_{eff} = \tau^o_{eff} - H\gamma \qquad 1.4.5$$

where τ^o_{eff} is the effective stress at the beginning of the experiment, γ is the shear strain, and H is the work hardening coefficient. The latter is often taken as the slope of

the stress-strain curve at the stress level applied in the creep test and is assumed to be constant throughout the test.

The rate constant can hence be expressed in terms of the creep strain in a general form as

$$k_i = \frac{\bar{k}T}{h} \exp\left(-\frac{\Delta G_i^{\mp}}{\bar{k}T}\right) \exp\left(\pm V_i \frac{\tau_{eff}^{o} - H\gamma}{\bar{k}T}\right) \qquad 1.4.6$$

and therefore

$$k_i = A_i \exp\left(\mp \frac{V_i H}{\bar{k}T} \gamma\right) \qquad 1.4.7$$

For the simplest kinetics, there is a single barrier with forward activation only and the rate is

$$\text{Rate} = \delta \rho_1 A_1 \exp\left(-\frac{V_1 H}{\bar{k}T} \gamma\right) \qquad 1.4.8$$

The rate equation (Eq.1.4.8) can be analyzed by two methods:

a) the time dependence of creep strain, or

b) the strain dependence of the strain rate.

The first method, as will be shown, involves an approximation and therefore the second one is preferable.

a) <u>The time dependence of creep strain.</u> From Eq.1.4.8,

$$\text{Rate} = \frac{d\gamma}{dt} = \delta \rho_1 A_1 \exp\left(-\frac{V_1 H}{\bar{k}T} \gamma\right) \qquad 1.4.9$$

Taking the reciprocal and multiplying both sides by $d\gamma$, Eq.1.4.9 can be integrated,i.e.

$$\int_0^t dt = \int_0^\gamma \frac{1}{\delta \rho_1 A_1} \exp\left(\frac{V_1 H}{\bar{k}T}\gamma\right) d\gamma \,. \qquad 1.4.10$$

Therefore,

$$t = \frac{1}{\delta \rho_1 A_1} \frac{\bar{k}T}{V_1 H}\left[\exp\left(\frac{V_1 H}{\bar{k}T}\gamma\right) - 1\right]$$

For sufficiently large strain

$$\exp\left(\frac{V_1 H}{\bar{k}T}\gamma\right) >> 1$$

therefore,Eq.1.4.10 is approximately

$$t \cong \frac{1}{\delta \rho_1 A_1} \frac{\bar{k}T}{V_1 H} \exp\left(\frac{V_1 H}{\bar{k}T}\gamma\right) \qquad 1.4.11$$

From this we find that

$$\ln t = \ln\left(\frac{1}{\delta \rho_1 A_1} \frac{\bar{k}T}{V_1 H}\right) + \frac{V_1 H}{\bar{k}T}\gamma \qquad 1.4.12$$

Thus the slope of a semilogarithmic plot of time vs. creep strain, as shown in Fig.1.4.1 is proportional to the activation volume associated with the forward activation over a single barrier as

$$\frac{d\ln t}{d\gamma} = \frac{V_1 H}{\bar{k}T}$$

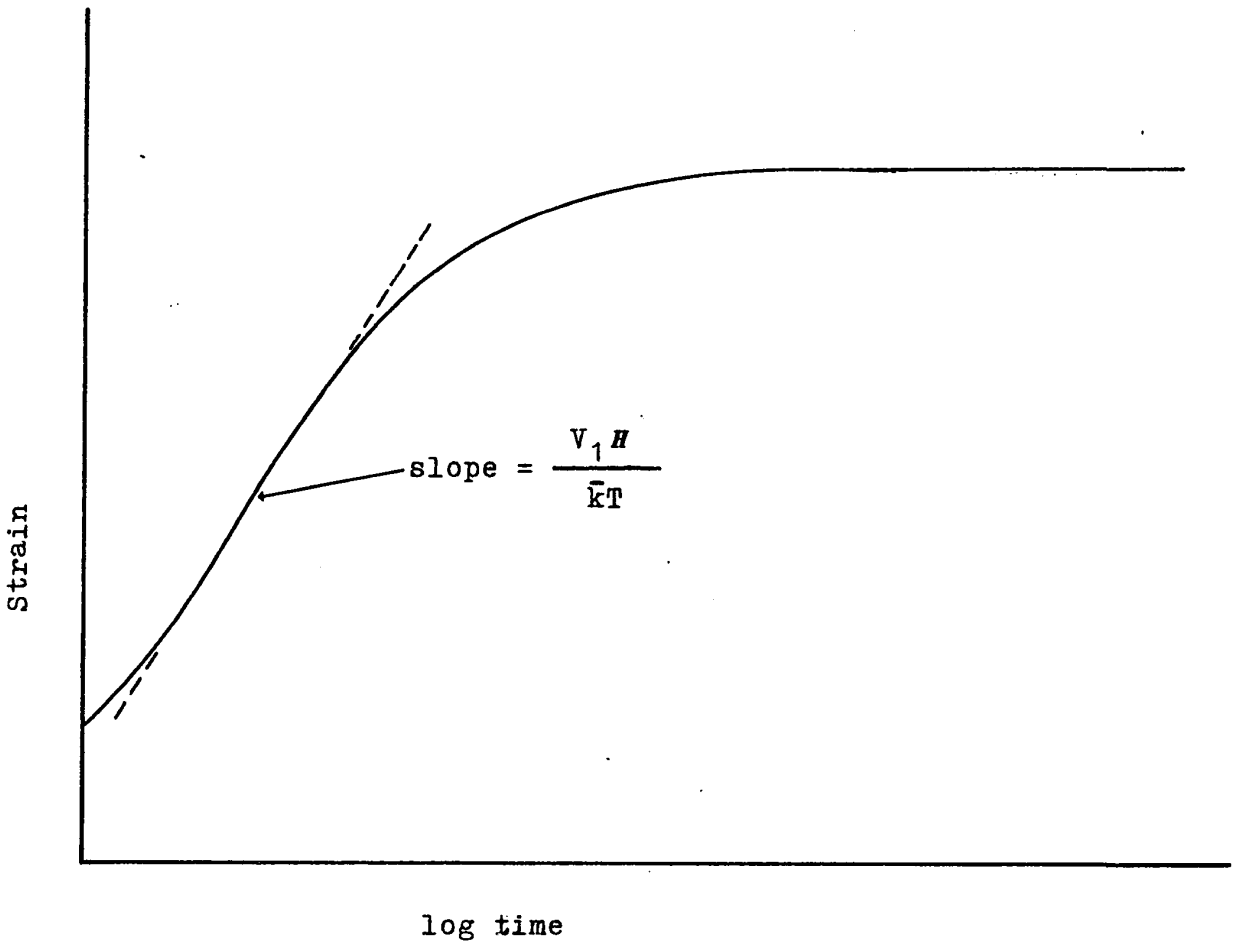

Fig. 1.4.1. The determination of V_1 from a creep curve.

Over the early part of the experiment where the second term in Eq.1.4.10 is not negligible, this method should not be used.

b) The strain dependence of the strain rate. From Eq.1.4.9,

$$\ln \text{Rate} = \ln \delta \rho_1 A_1 - \frac{V_1 H}{kT} \gamma$$

Again a plot of the logarithm of the strain rate vs. the creep strain is proportional to the activation volume. Figure 1.4.2 shows such a plot.

1.5. THE DETERMINATION OF THE INTERNAL STRESS

All of the methods described in the preceeding sections require the determination of the effective stress. It is not possible or easy to determine the effective stress directly, therefore, it must be determined through a relation between the applied stress τ_a, and a measurable value. From Eq.1.4.5, the effective stress is related to the creep strain as

$$\tau_{eff} = \tau^o_{eff} - H \gamma$$

and from Eq.1.4.4, τ^o_{eff} is expressed as

$$\tau^o_{eff} = \tau_a - \tau^o_i$$

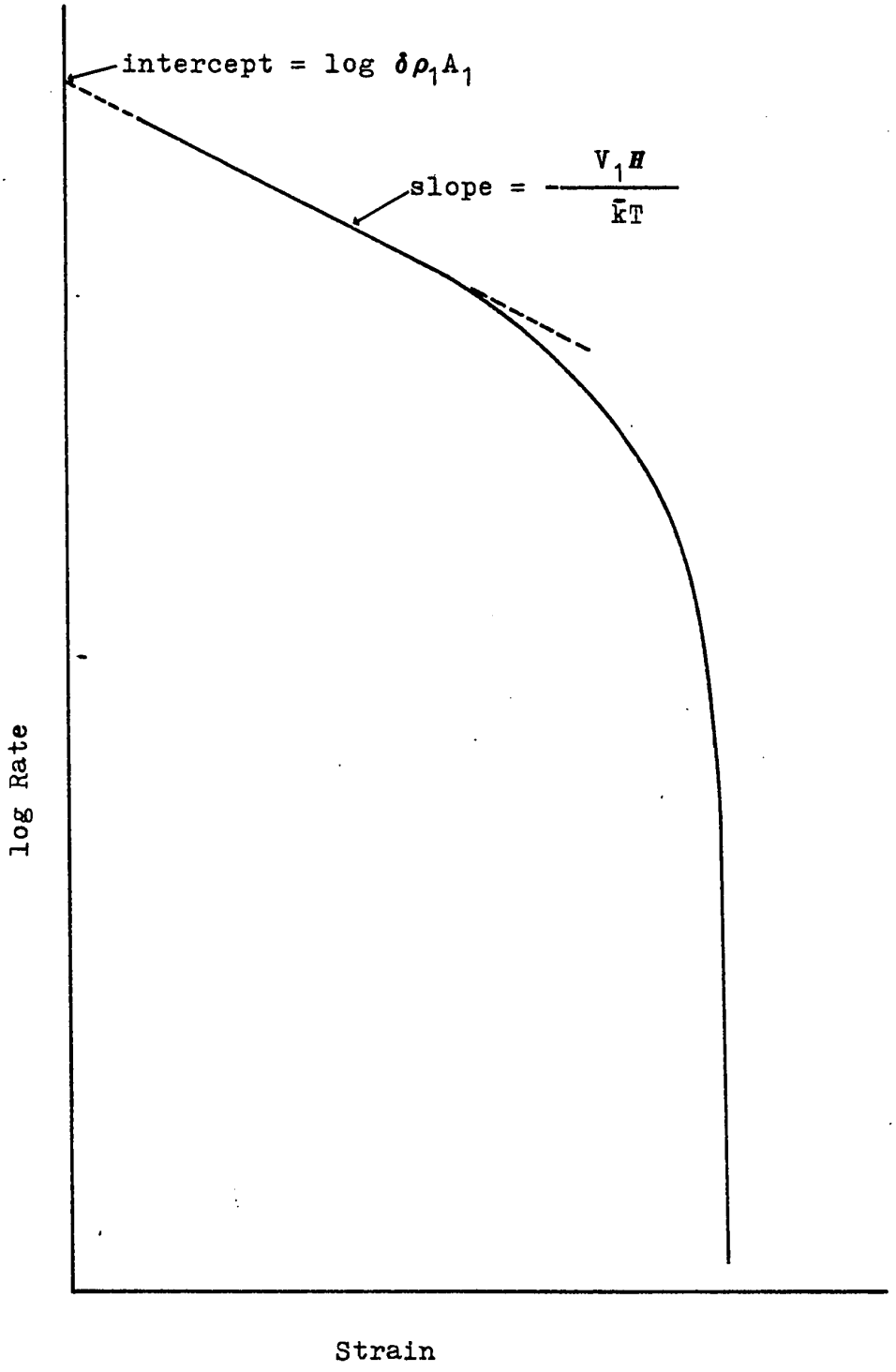

Fig. 1.4.2. The determination of V_1 from log Rate vs. strain curve.

where τ_i^o is the initial internal stress.

In the following, a brief description of some of the methods used to determine the internal stress is given.

1.5.1. Creep Test Method

In low temperature creep when only primary creep is observed, the strain rate decreases to zero. When the strain rate is zero, the internal stress and the applied stress are approximately equal. This method is illustrated in Fig. 1.5.1,a.

This method allows the approximate determination of the internal stress when a creep test is performed and the rate is zero. The time involved in performing a creep test can be long, therefore, unless one is already performing a creep test, the method may not be advantageous. It should be noted that the strain rate can be zero without the internal stress being equal to the applied stress, as will be shown in section 3.3.

1.5.2. Strain Transient Dip Test

This method[16,17] is based on the assumption that for applied stress levels below τ_i, creep recovery takes place, and above τ_i, creep occurs. This method consists of observing the creep behavior under the applied load conditions. The load is incremented or decremented depending on whether creep recovery or creep occurs untill the strain rate is zero for a sufficiently long time. This method gives a range of internal stress as illustrated in Fig.1.5.1,b.

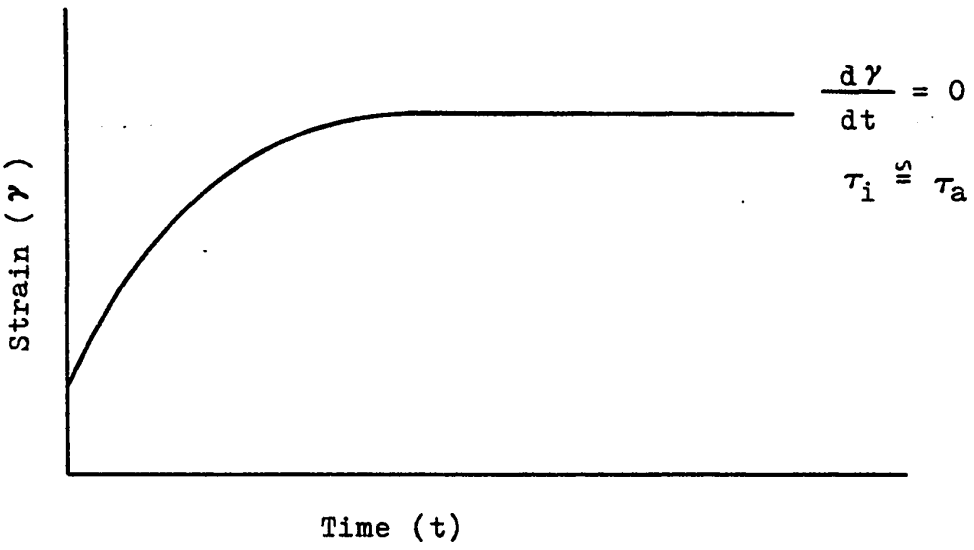

(a)

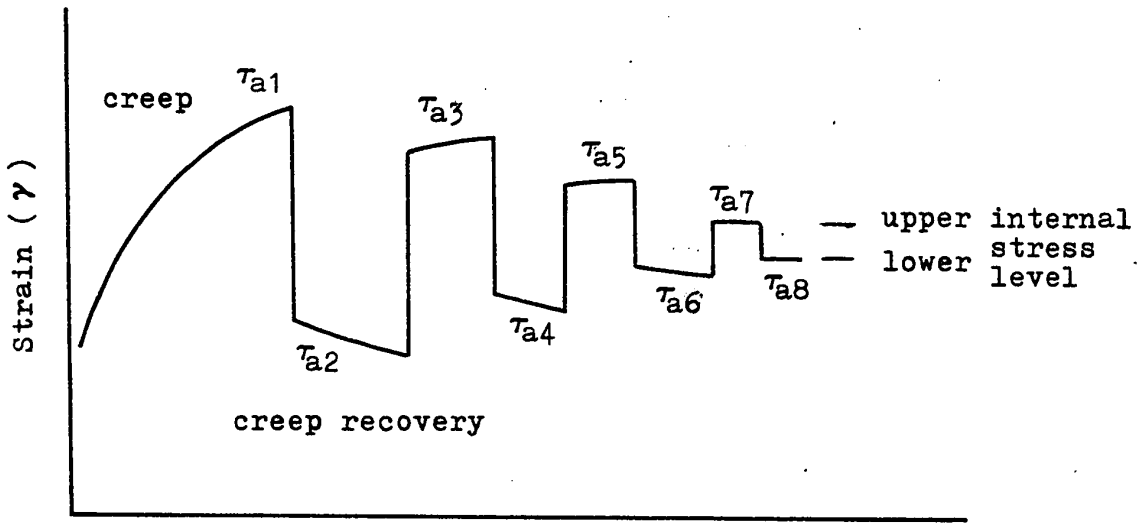

(b)

Fig.1.5.1. Illustration of the internal stress measurement methods.

1.5.3. Stress Relaxation Method

When the rate of stress relaxation is zero, the applied stress is approximately equal to the internal stress.[18] As in the creep test method, the time involved in the application of this method could be long. There is also a similar uncertainty in the evaluated internal stress because the stress relaxation rate can be zero without the applied stress being equal to the internal stress level. (Fig. 1.5.1, c)

1.5.4. Stress Transient Dip Test

This method is based on the assumption that when the stress level is below τ_i, negative stress relaxation will occur. First the material is allowed to undergo stress relaxation at constant strain, then the applied stress level is alternately decreased or increased depending on whether positive or negative stress relaxation occurs.[19] This method gives a range of internal stress for which the rate $(d\tau/dt)_\epsilon$ is zero, as illustrated in Fig. 1.5.1, d.

1.5.5. Dislocation Density Dependence

The dependence of τ_i on the dislocation density ρ is expressed empirically as[20]

$$\tau_i = \alpha \mu b \rho^{\frac{1}{2}}$$

where α is a constant, μ is the shear modulus, and b is the Burger's vector. Knowledge of the dislocation density could, therefore, give an indication of the internal stress. (Fig. 1.5.1, e)

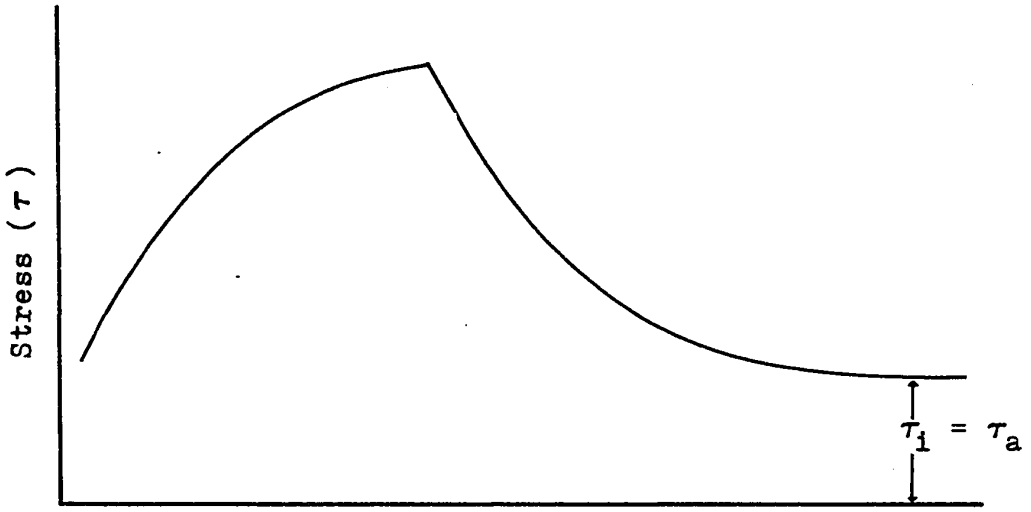

(c)

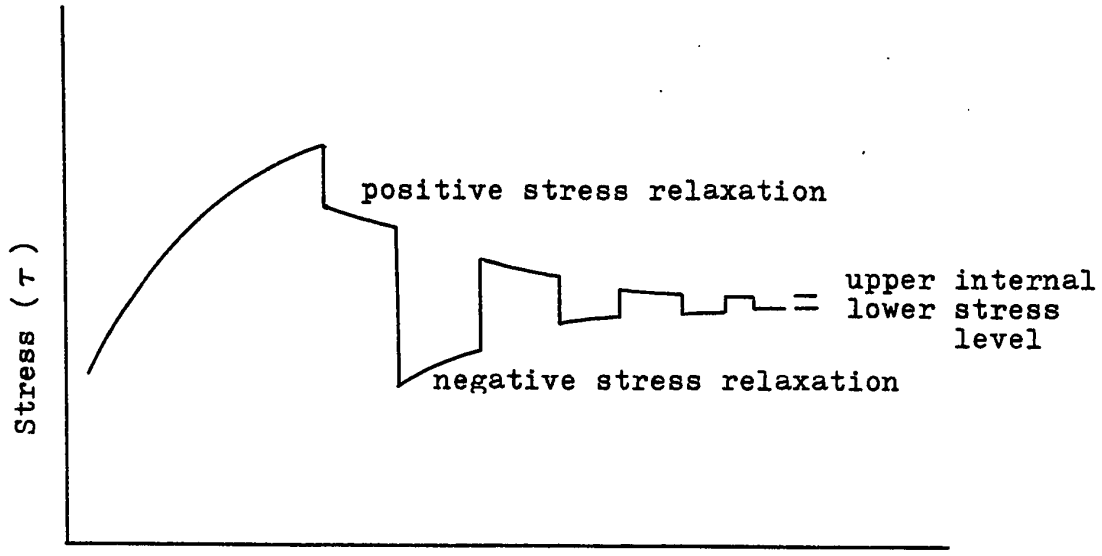

(d)

Fig.1.5.1. Illustration of the internal stress measurement methods.(cont'd.)

1.5.6 Grain Size Dependence

Conrad and Sargent[21] utilized Petch's relation between the grain size d and the internal stress, expressed as

$$\tau_i = Cd^{\frac{1}{2}}$$

where C is a constant. (Fig. 1.5.1,f)

The value of internal stress determined with these methods is only an appriximation. It is of interest to note that methods 1.5.2 to 1.5.6 have been compared by Conrad[15] on Titanium, and methods 1.5.2 and 1.5.4 by Ahlquist[16] on polycrystalline high purity aluminum. They have found that these methods give approximately the same internal stress when the assumptions upon which the methods are based are applicable to the test conditions.

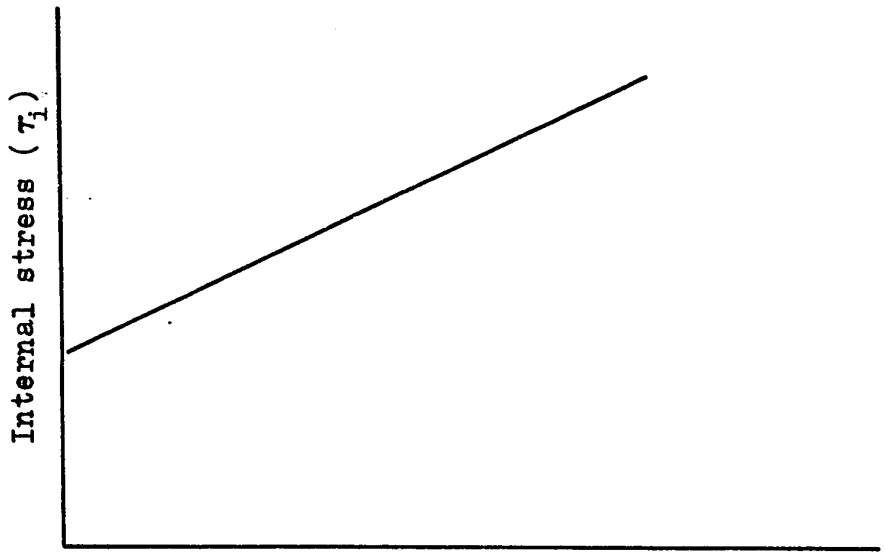

(e)

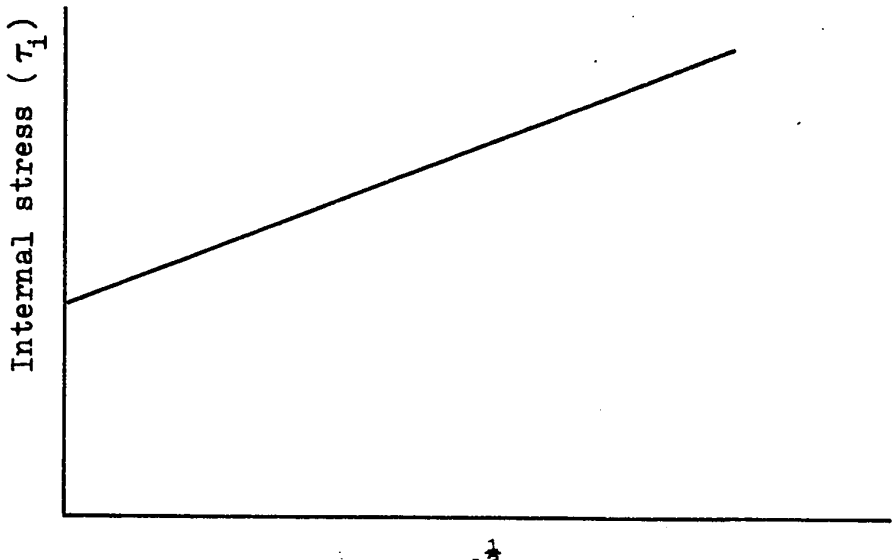

(f)

Fig.1.5.1. Illustration of the internal stress measurement methods. (cont'd.)

2.EXPERIMENTAL PROCEDURE AND RESULTS

2.1.MATERIAL SPECIFICATIONS

The high purity polycrystalline iron was recieved from Johnson Matthey & Mallory Ltd. in form of 5mm diameter rods. The impurity content was reported by the company to be 10ppm (Mainly Si and Mn.)

The grain size was determined to be ranging from 95×10^{-3} to 70×10^{-3}mm with an average of 120 to 203 grains per square milimeter.[23]

The specimens were machined from the 5mm diameter rods to 3mm diameter and 42mm gage length.(Fig.2.1.1)

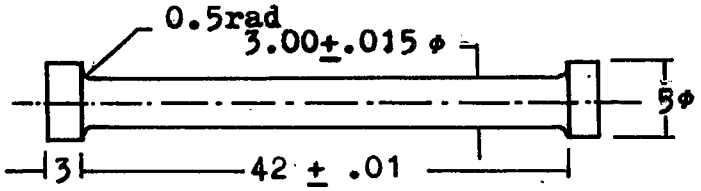

Note: All dimensions are in mm.

Fig.2.1.1. High purity polycrystalline iron specimens used for the creep tests.

2.2. TESTING PROCEDURE

Two types of testing procedures were followed.

2.2.1. Standard Constant Load Creep Tests

The initial internal stress σ_i^o, was measured by the strain transient dip test method described in section 1.5.2. Then a constant load was applied and the specimen allowed to creep. Only three of the tests were performed with this method due to the advantages of the second method. (Fig.2.2.1)

2.2.2. Incremental Load Type Tests

Measurement of σ_i^o for the first test on each specimen was carried out by the strain transient dip test method. A constant load was applied and the specimen was allowed to creep for an average of 3000 seconds (50 minutes). The creep rates were found to reduce to zero in this time for the selected stress level. The specimen was then fully unloaded and the load was incremented. The incremented load was then applied. This procedure of unloading and reloading was repeated two or three times for each specimen. An example of the typical testing sequence for this method is shown in Fig.2.2.2.

In these tests, the internal stress was approximately equal to the applied stress at the end of each test period. Consequently, the internal stress level was established for the test at the next stress level by the creep test method described in section 1.5.1. Results of all σ_i^o measurements are given in Table I.

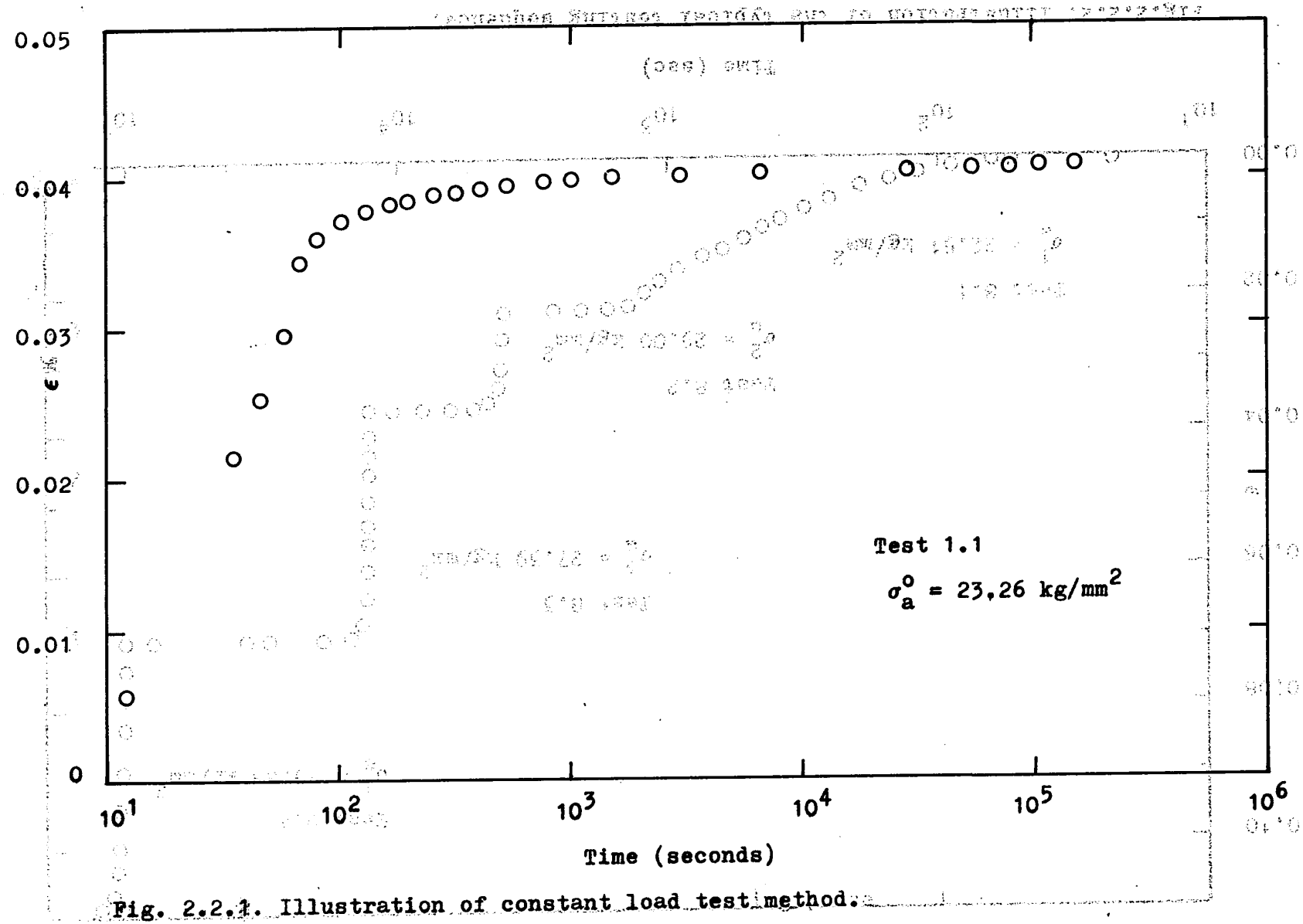

Fig. 2.2.1. Illustration of constant load test method.

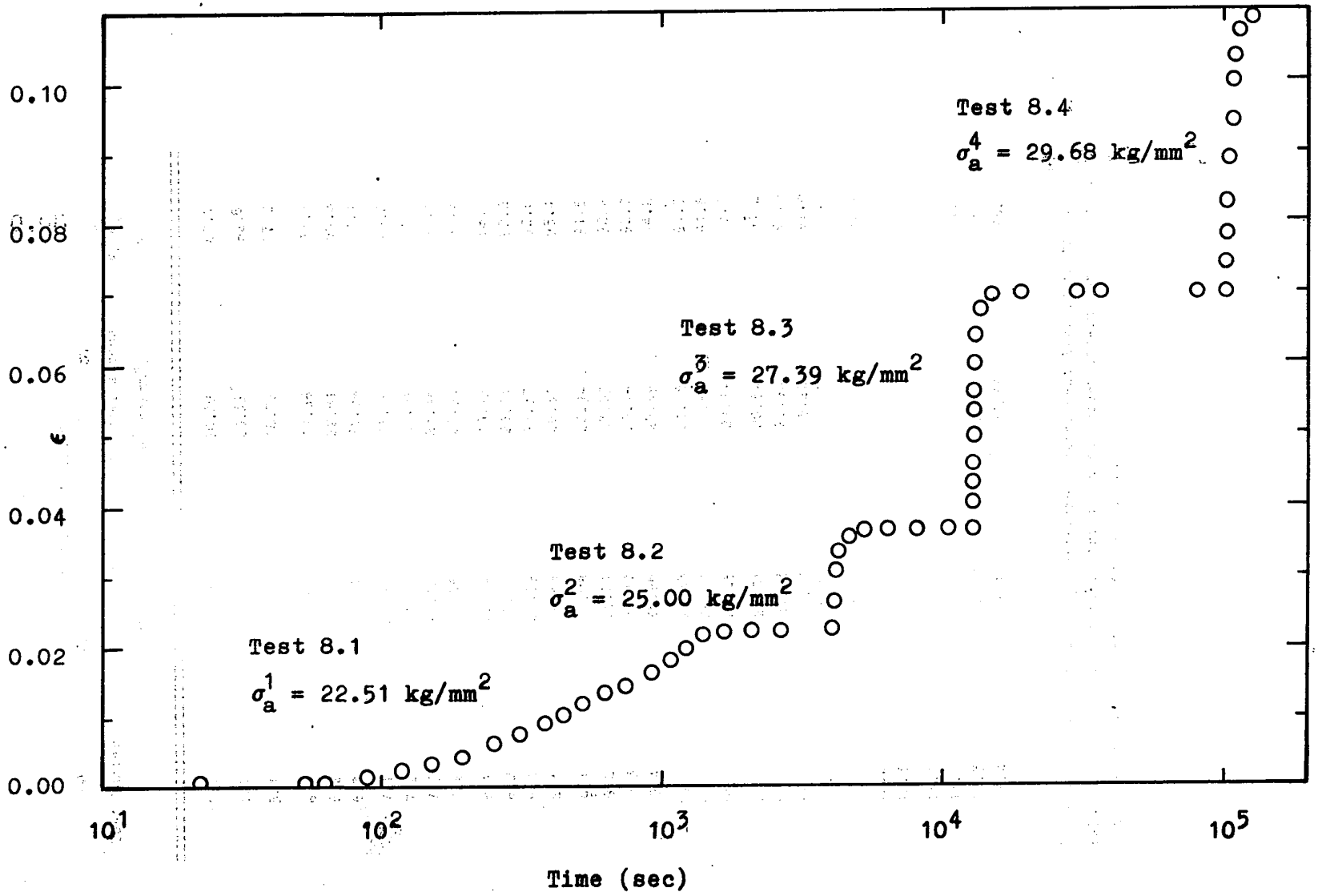

Fig.2.2.2. Illustration of the typical testing sequence.

TABLE I

INTERNAL STRESSES

Test Number	Applied stress (σ_a^o kg/mm^2)	Internal stress (σ_i^o kg/mm^2)	σ_i^o/σ_a^o (%)
1.1	23.26	20.39*	87.7
3.1	24.62	20.39*	82.8
5.1	24.24	18.72	77.2
6.1	22.45	19.86	88.5
6.2	25.39	22.81	89.8
6.3	27.84	25.94	93.1
7.1	22.57	21.16	93.8
7.2	24.36	23.04	94.6
7.3	27.10	24.46	90.3
7.4	29.05	27.94	96.2
8.1	22.54	19.99	88.7
8.2	25.00	23.04	92.2
8.3	27.39	25.37	92.6
8.4	29.68	28.31	95.4
9.1	22.88	20.94	91.5
9.2	25.01	23.05	92.2
9.3	27.17	25.19	92.7
9.4	28.96	27.29	94.2
10.1	23.83	21.75	91.3
10.2	26.81	24.56	91.6
10.3	29.65	27.59	93.1
11.1	22.51	20.54	91.2
11.2	24.93	22.90	91.9
11.3	27.23	25.22	92.6
11.4	29.40	28.00	95.2
12.1	23.63	19.46	82.4
12.2	26.55	24.45	92.1
12.3	29.46	27.48	93.3
13.1	22.93	20.66	90.1
13.2	25.51	23.50	92.1
13.3	26.90	25.60	95.2
13.4	28.91	27.77	96.1

* These values of σ_i^o were not determined experimentally. It is the value of the relation between the internal stress and the creep strain for zero strain. (This relation is given in section 3.6,c.)

In this test method, creep tests at different σ_a^o can be performed on the same specimen. It also eliminates the necessity of measuring σ_i^o for each test by a separate test since it is known approximately from the preceeding creep test.

2.3. EQUIPMENT

2.3.1.Creep Machine

The creep machine was designed in a previous thesis.[24] It is a constant load, tensile creep testing machine. A minor change in the loading system was effected and temperature control was introduced.

2.3.2.Temperature Control and Measurement

The testing machine was enclosed with styrofoam. Heating tape was mounted onto this enclosure. The temperature was controlled by a Fisher 15-179 Laboratory Immersion type thermoregulator with a sensitivity of $\pm$.06 K. The temperature in the chamber was kept slightly above room temperature. In few experiments the temperature varied about $\pm$.5 K and for the large majority of them, the temperature variation was less than $\pm$.25 K.

The temperature was measured with copper-constantan thermocouple wires with an ice water mixture reference junction. The temperature was recorded with a Hewlett Packard 7100B type strip chart recorder.

2.3.3. Extensometry

The elongation of the specimens was measured with a Hewlett Packard 7DCDT 250 linear variable differential transformer. Two rod guides were made for the transformer to prevent the lateral movement of the transformer rod and to reduce the hysteresis losses during the loading and unloading of the specimens.

The transformer was mounted on the grip system as shown in Fig. 2.3.1. The grip system was designed to prevent the relative lateral movement of the upper and lower grips during loading and unloading. This was done through the use of three solid guide bars. The grip system was joined to the weight pan rod by means of a universal joint for the same reason.

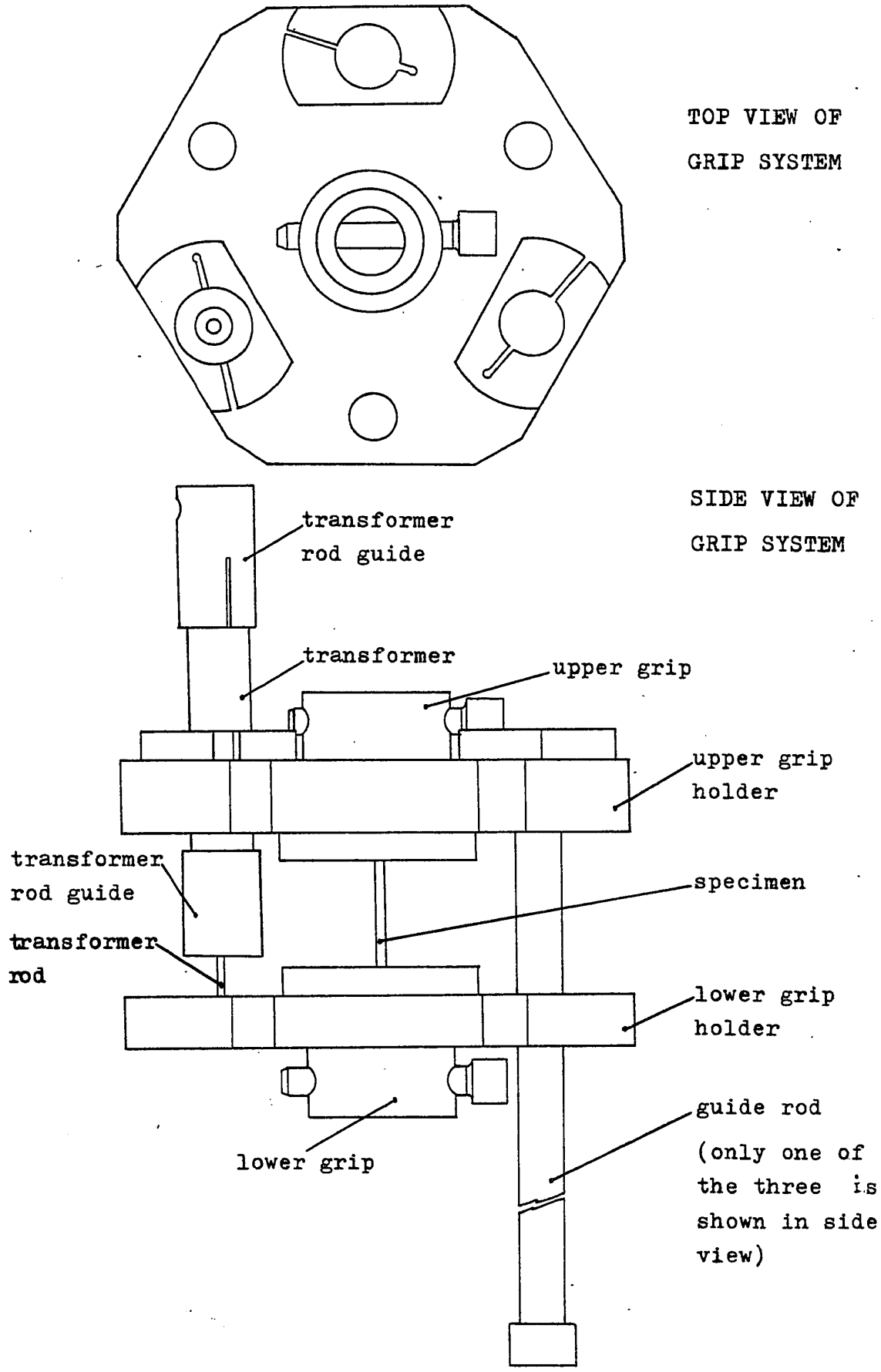

Fig. 2.3.1. Schematic illustration of grip system with transformer.

3.DISCUSSION

3.1.CREEP TESTS

A total of thirty two tests were carried out. The results of these tests are represented in Figures 3.1.1 to 3.1.5 in terms of the creep strain vs. the logarithm of the time, and in Figures 3.1.6 to 3.1.10 in terms of the logarithm of the strain rate vs. the creep strain. To facilitate the analysis, these tests were divided into four groups with respect to the initial effective stress, σ^{o}_{eff}. These groups are given in Table II. The first digit of the code identifies the specimen and the second the applied stress level.

TABLE II

GROUPING OF CREEP TESTS

Group Number	σ^{o}_{eff} (kg/mm^2)	Test Number
I	$4.63 \pm .77$	3.1, 5.1, 12.1
II	$2.51 \pm .20$	1.1, 6.1, 6.2, 7.3, 8.1, 10.2, 10.3, 13.1
III	$2.00 \pm .05$	6.3, 8.2, 8.3, 9.1, 9.2, 9.3, 10.1, 11.1, 11.2, 11.3, 12.2, 12.3, 13.2
IV	$1.30 \pm .12$	7.1, 7.2, 7.4, 8.4, 9.4, 11.4, 13.3, 13.4

Note1. All variations are one standard deviation.

Note2. Group III was subdivided into two groups for clearer graphical presentation.

Note3. For iron $\tau = 0.5\sigma$.

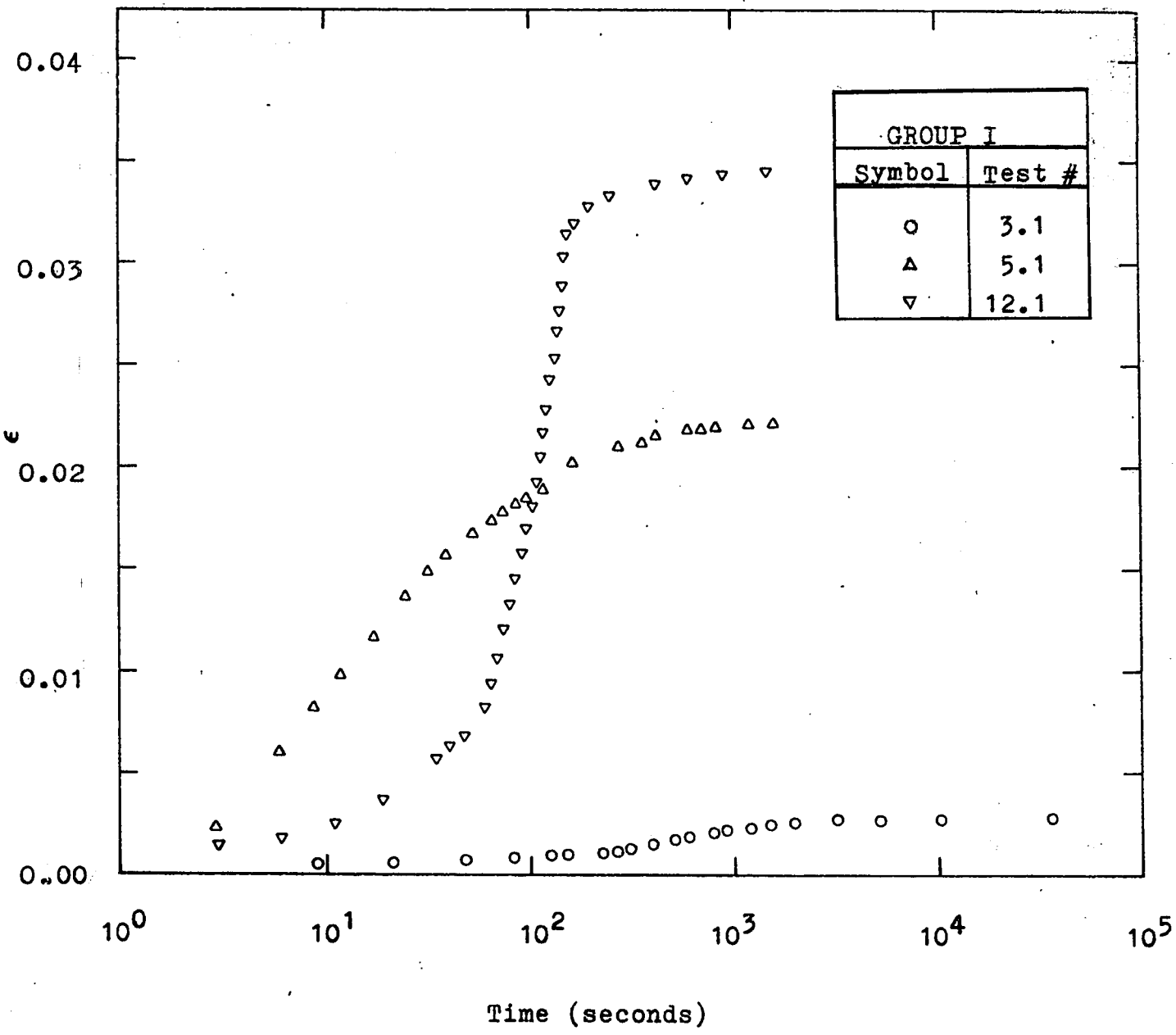

Fig. 3.1.1. Time dependence of creep strain for Group I.

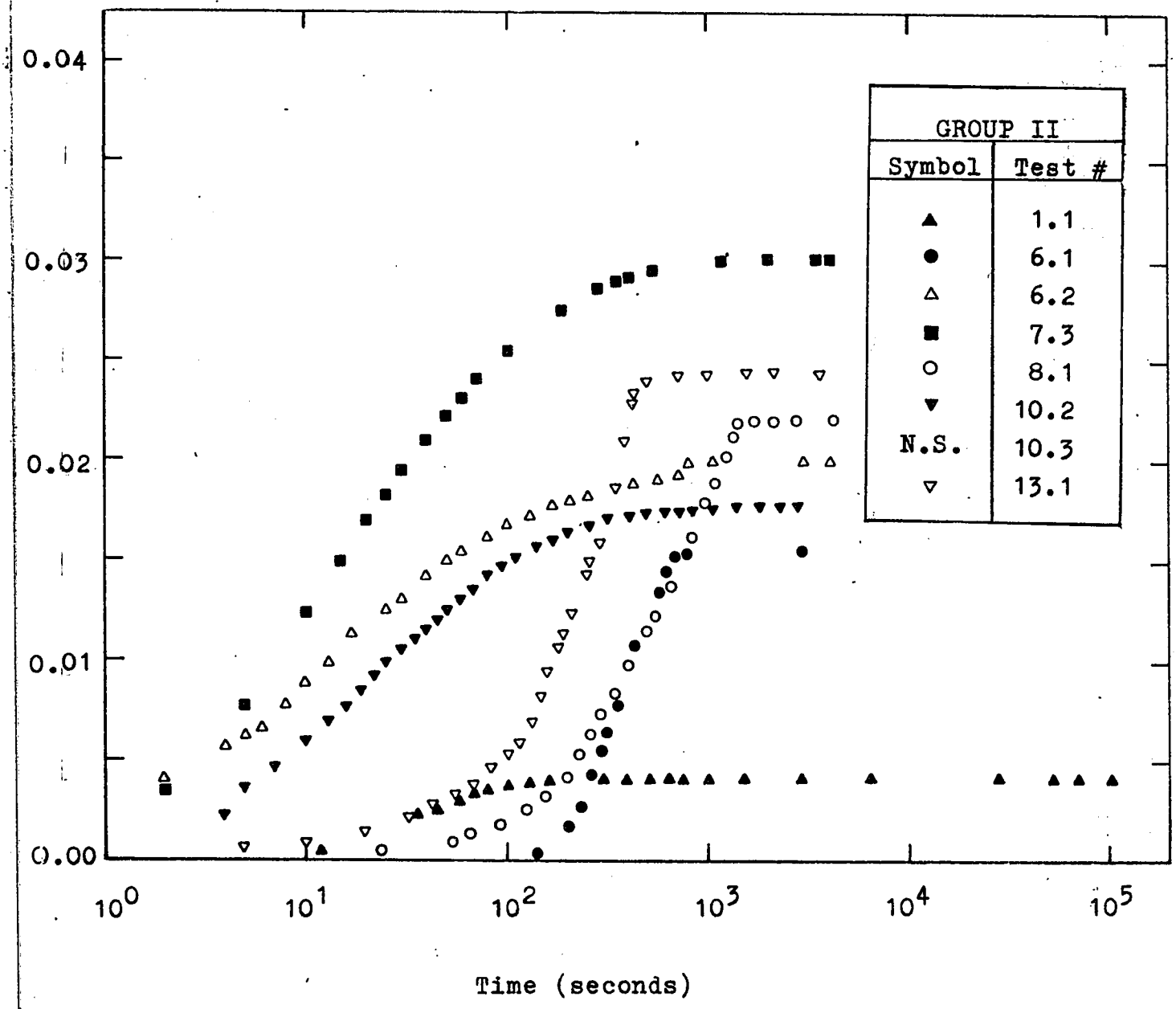

Fig. 3.1.2: The time dependence of creep strain for Group II. (N.S. : Not shown.)

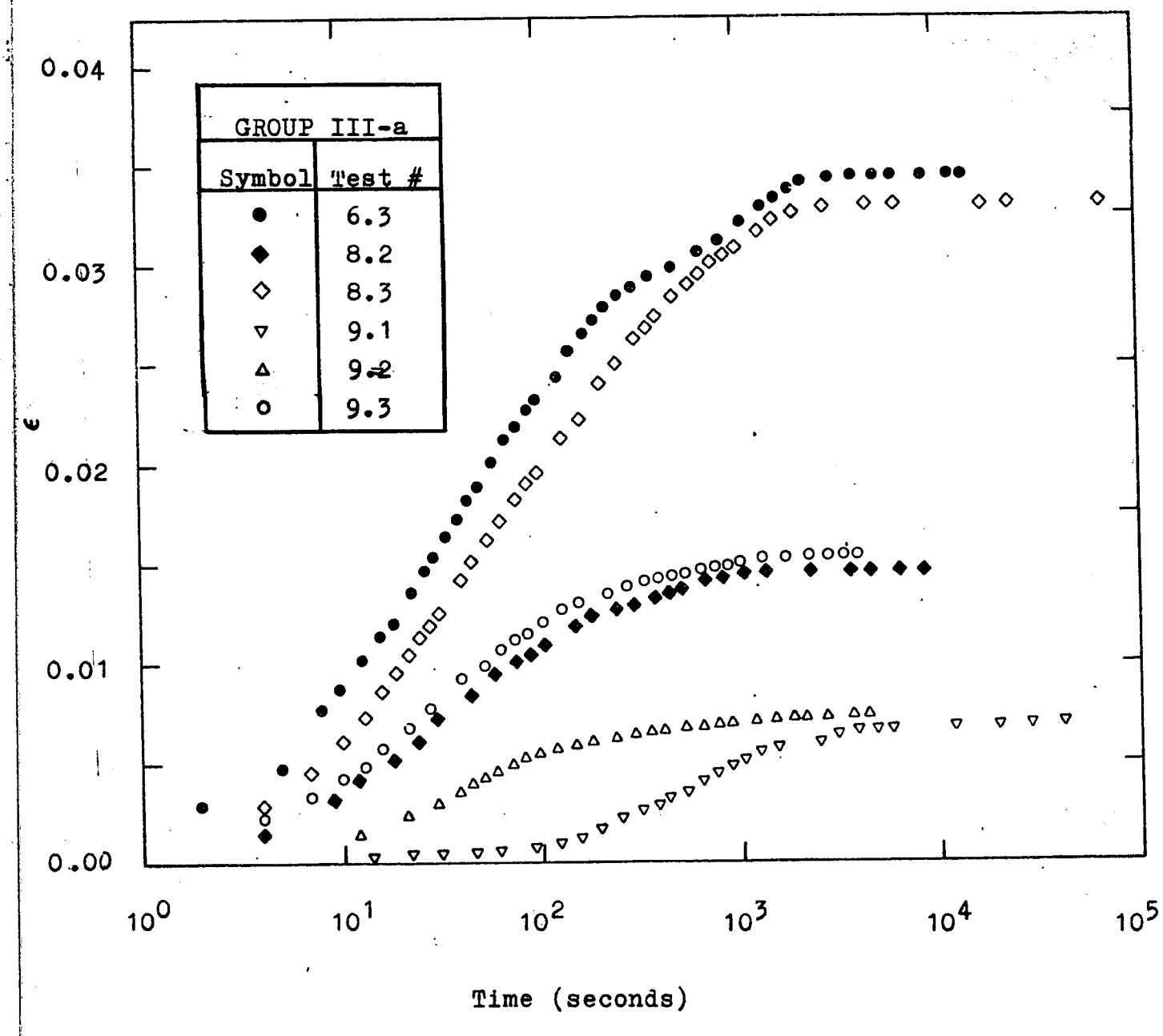

Fig. 3.1. 4. The time dependence of creep strain for Group III-a.

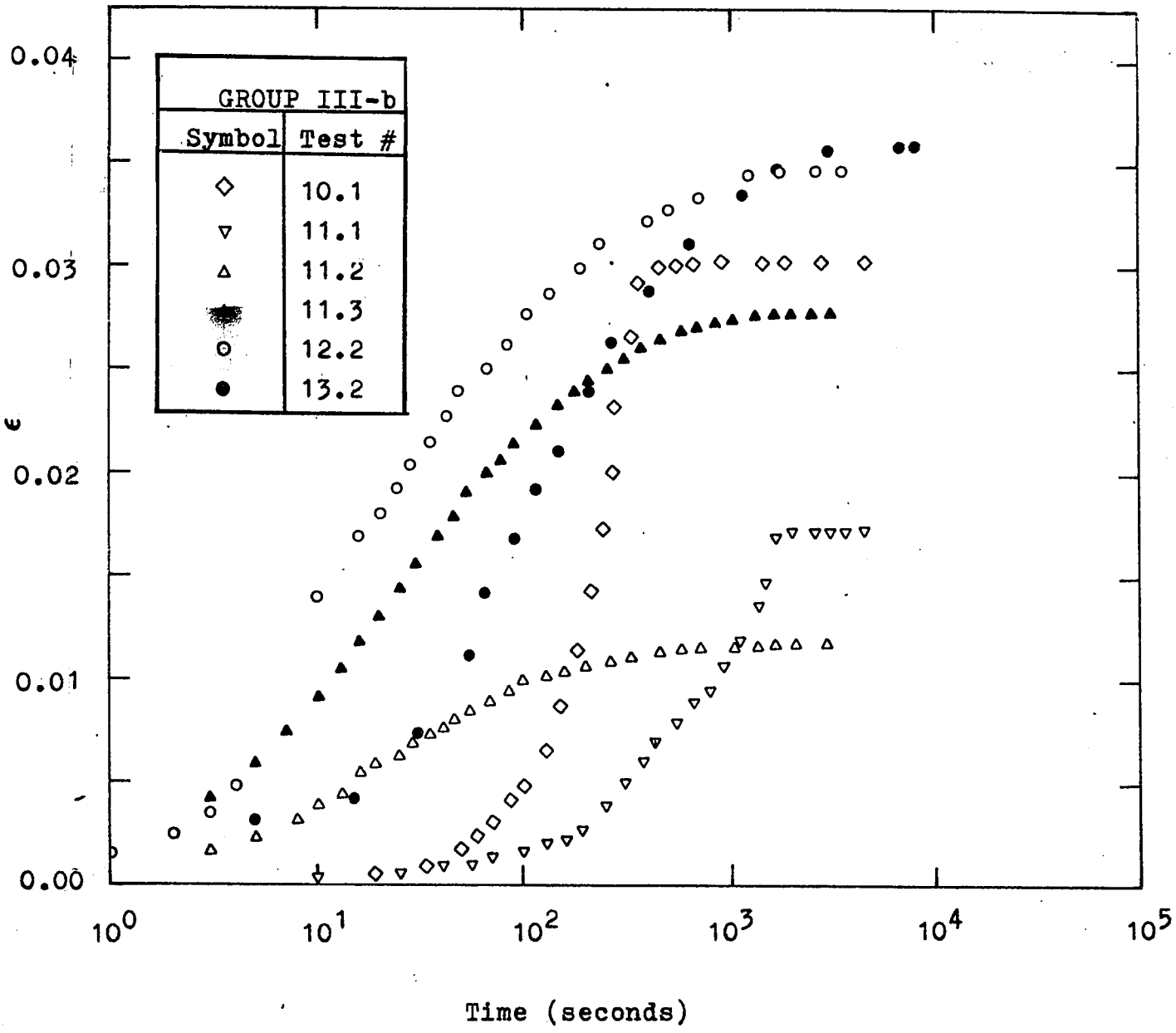

Fig. 3.1.4. The time dependence of creep strain for Group III-b.

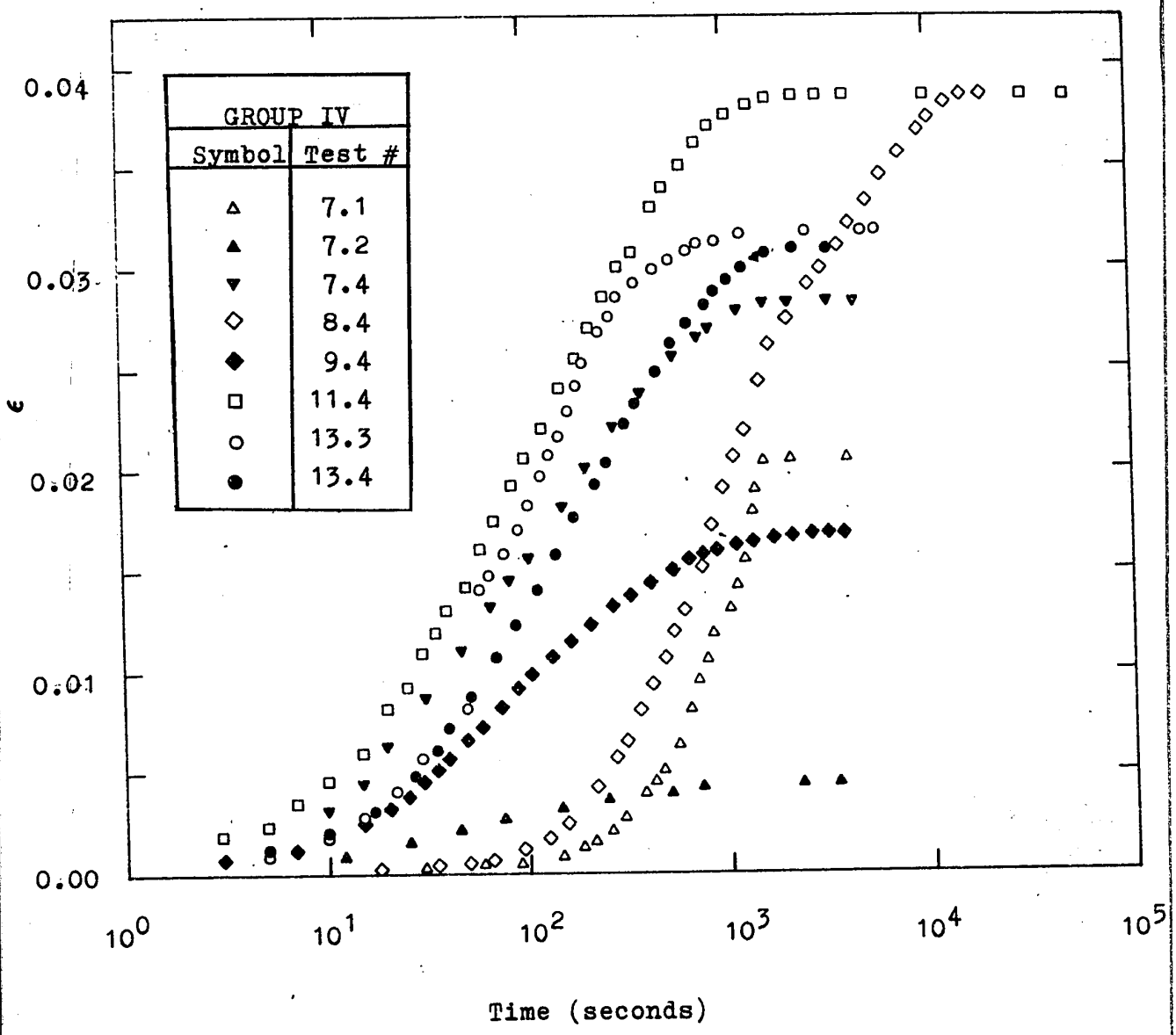

Fig. 3.1.5. Time dependence of creep strain for Group IV.

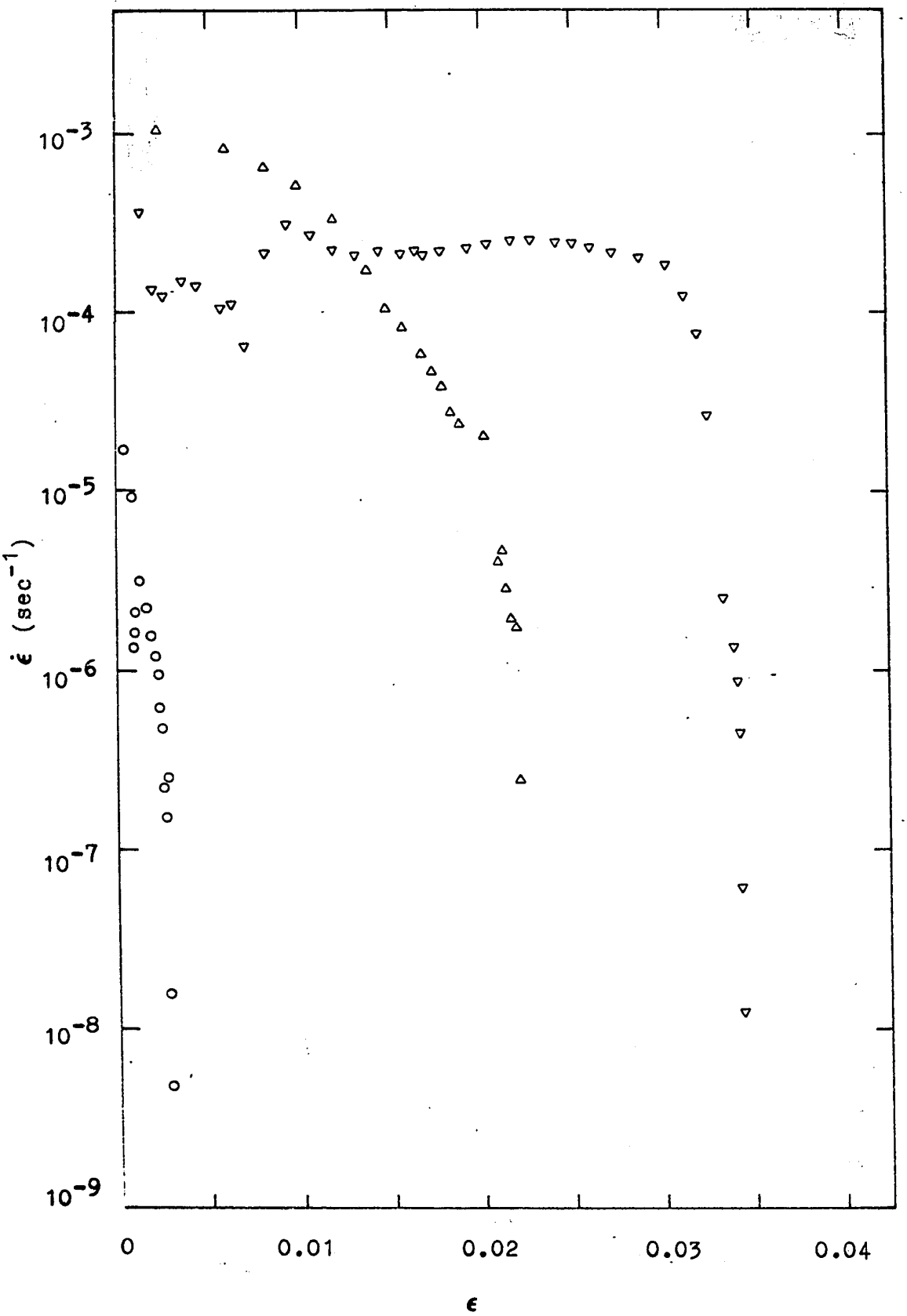

Fig. 3.1.6. Strain dependence of strain rate for Group I.

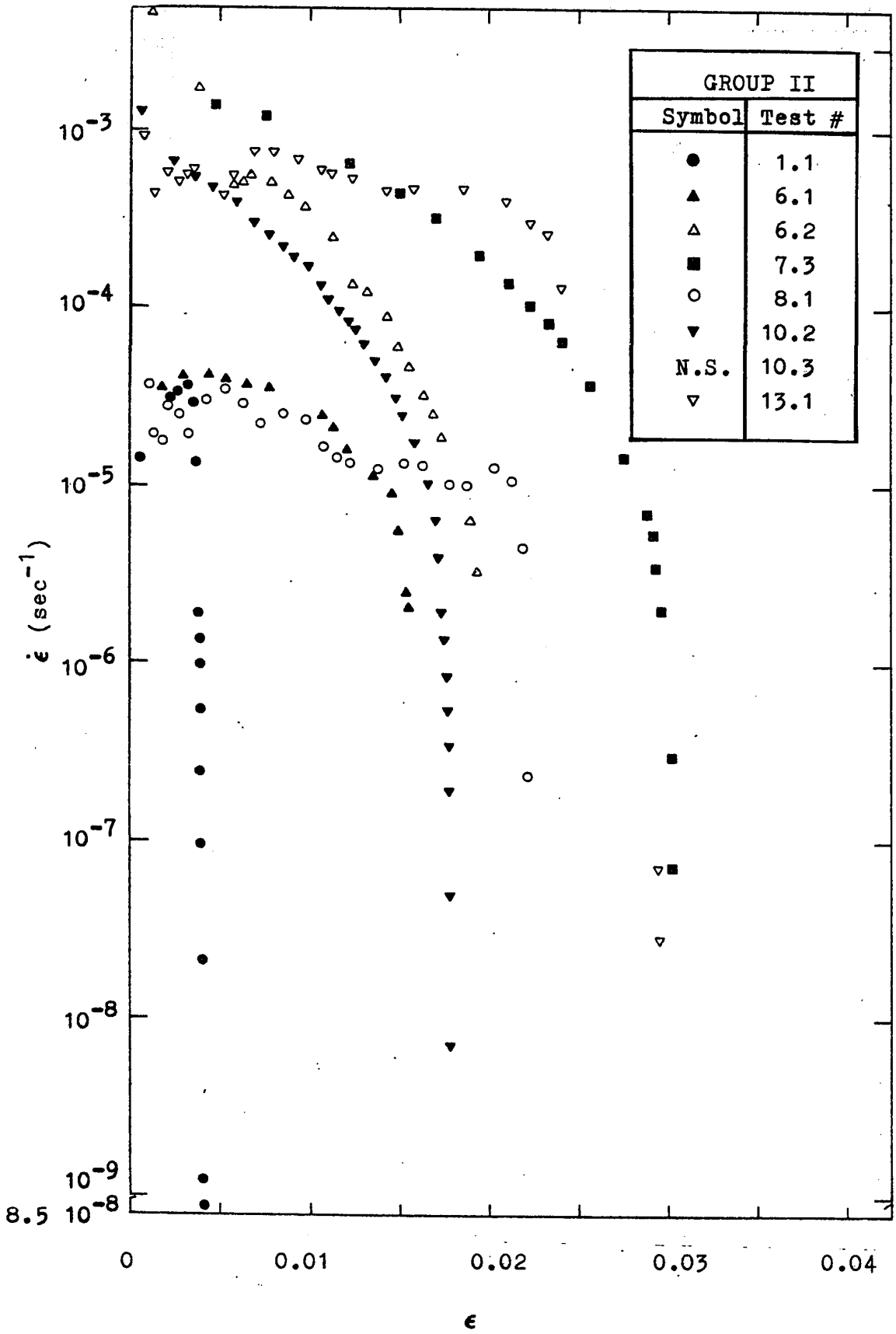

Fig. 3.1.7. The strain dependence of strain rate for Group II.

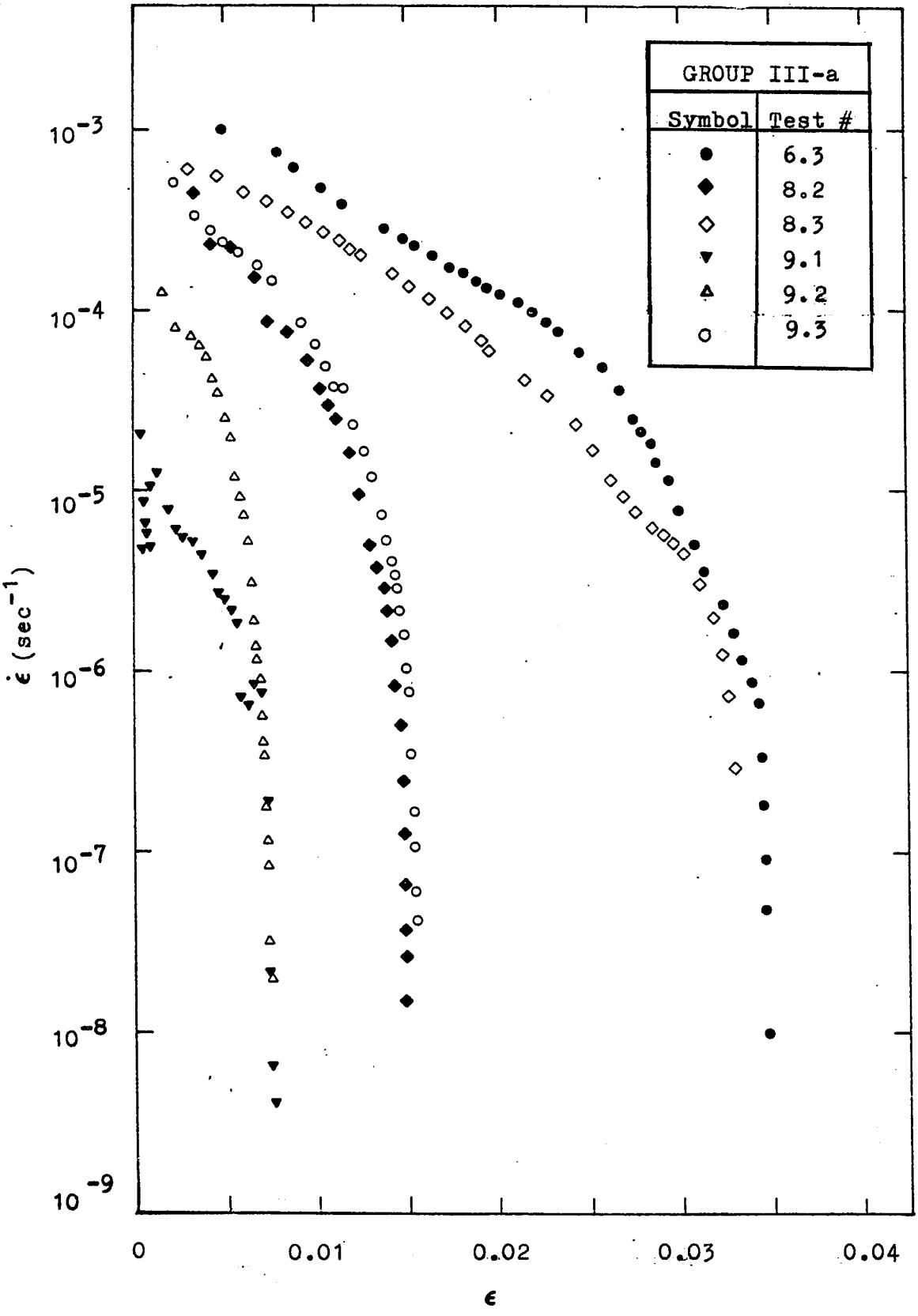

Fig. 3.1.8. Strain dependence of strain rate for Group III-a.

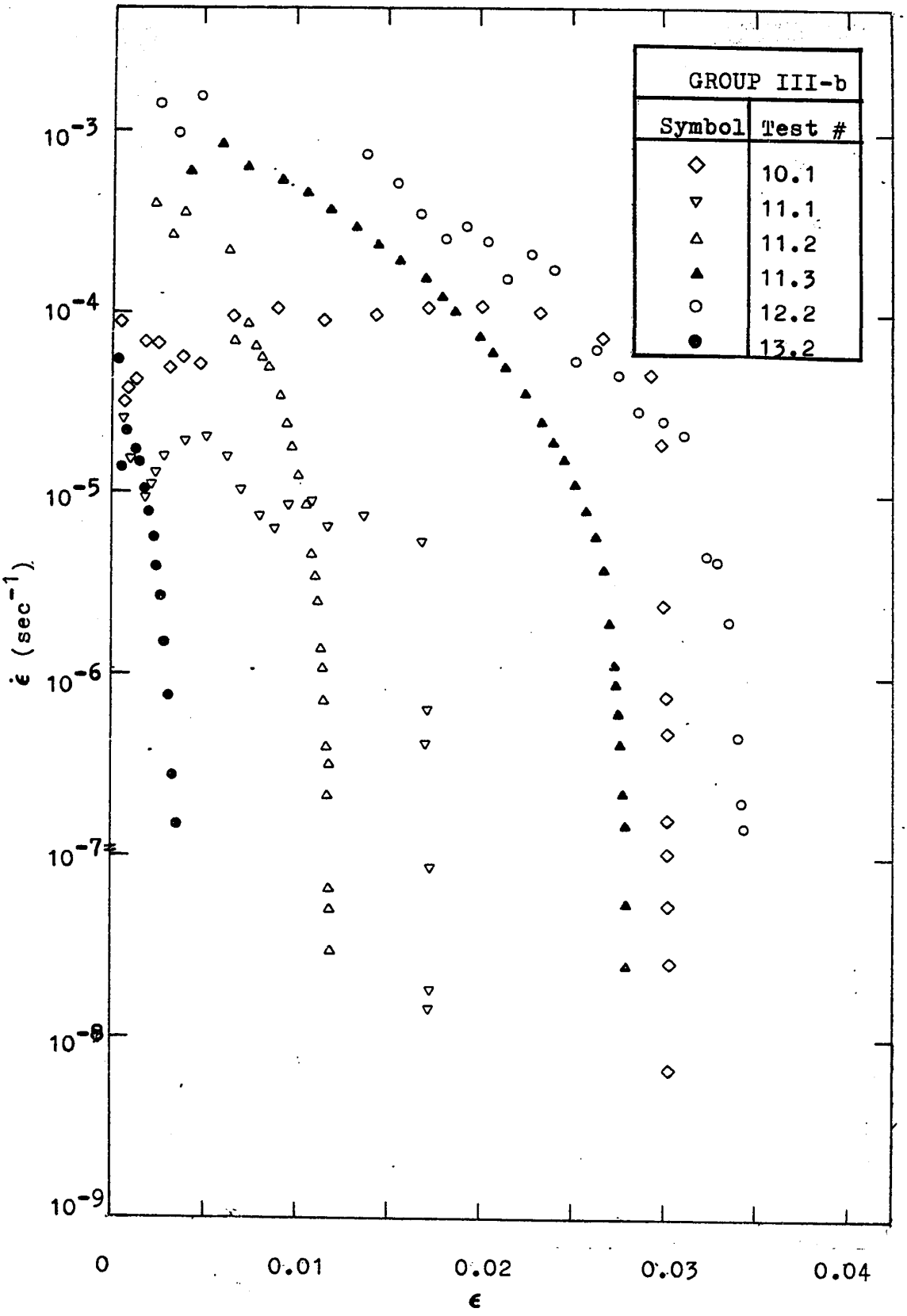

Fig. 3.1.9. Strain dependence of strain rate for Group III-b.

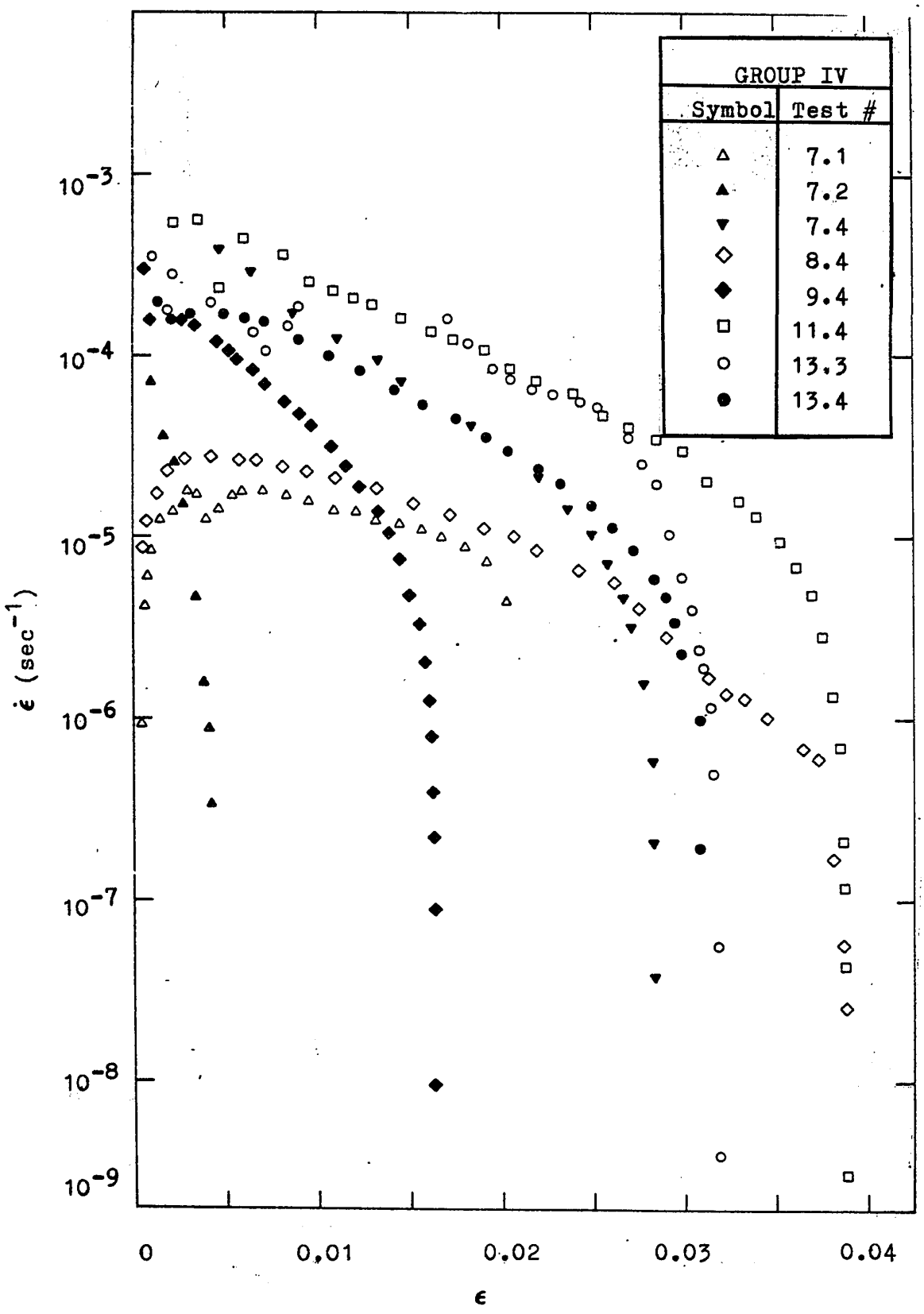

Fig. 3.1.10. Strain dependence of strain rate for Group IV.

In the tests at the first applied stress levels, the creep curves level off sharply. These stress levels correspond to the lower yield region.(See Figures 3.1.1 to 3.1.5) . As seen from the stress-strain diagram[23] in Fig.3.1.11, there is a pronounced yield effect.The typical sharp levelling off is believed to be due to a relatively large change in the mobile dislocation density in this stress region.The dislocation density of the untested specimens is expected to be low, therefore, upon application of the stress, the effect of dislocation multiplication can be quite pronounced. Results reported in literature[14] indicate a change in the dislocation density accompanying the yielding. This effect is noticable in iron.[25-32] This possibility and the consequences will be further discussed. The sharp levelling off behavior has also been observed in the stress relaxation of nickel.[11]

The scatter in results represented in Figures 3.1.1 to 3.1.10 may be due to the following reasons: Plastic deformation processes are structure dependent. For low stresses and strains, the effects of the production methods and any previous deformation are more noticable. Another reason might be the difference in the applied stress levels; the work hardening behavior is different at different applied stress levels as can be seen from the stress-strain curve shown in Fig.3.1.11.

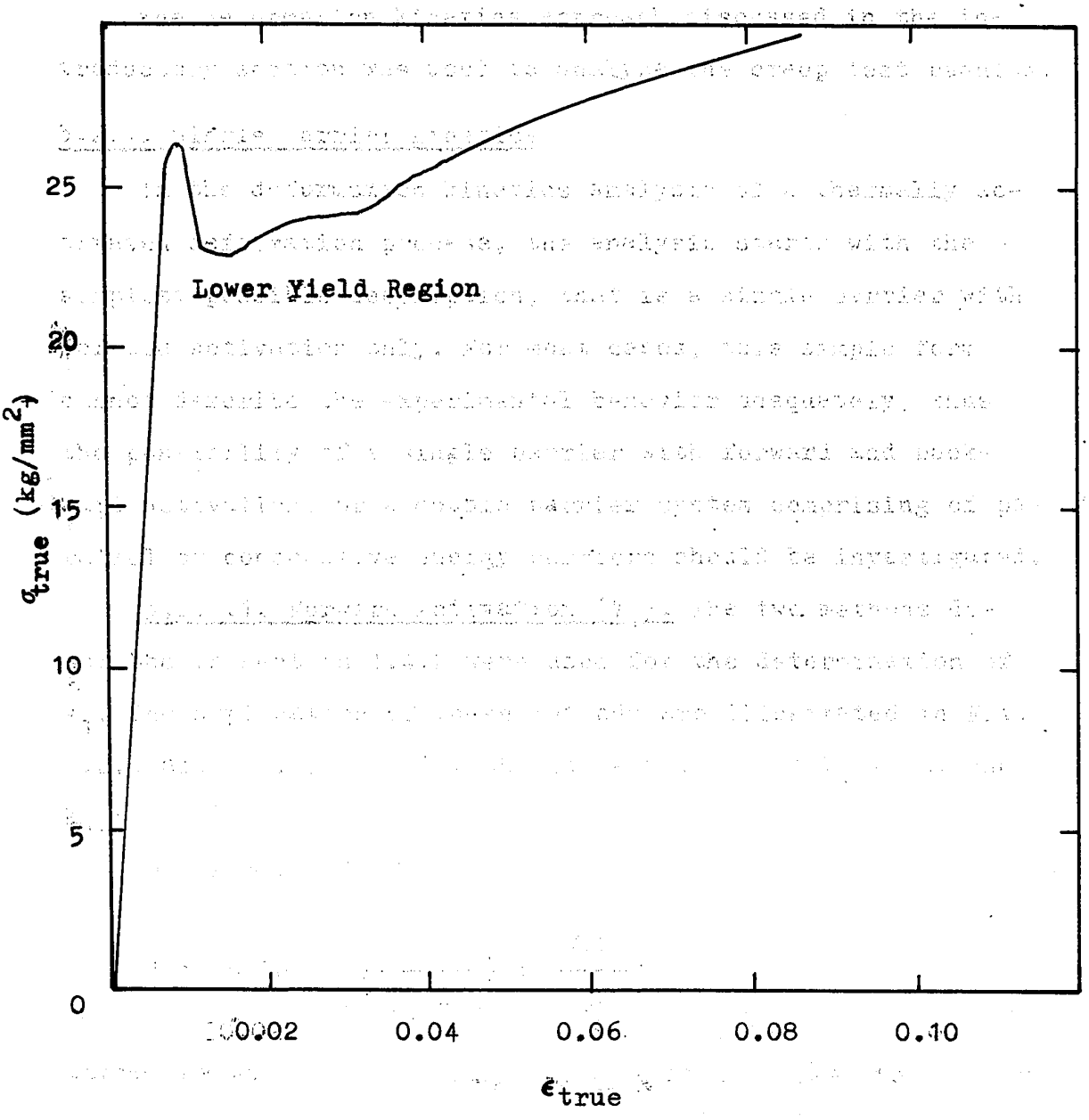

Fig. 3.1.11. Typical true stress-strain curve[23]

3.2. THE DETERMINATION OF THE DEFORMATION KINETICS

The deformation kinetics approach discussed in the introductory section was used to analyze the creep test results.

3.2.1. Single Barrier Kinetics

In the deformation kinetics analysis of a thermally activated deformation process, the analysis starts with the simplest possible description, that is a single barrier with forward activation only. For most cases, this simple form cannot describe the experimental behavior adequately, thus the possibility of a single barrier with forward and backward activation, or a double barrier system comprising of parallel or consecutive energy barriers should be investigated.

3.2.1.1. Forward Activation (V_1). The two methods described in section 1.4.2 were used for the determination of V_1. The application of these methods are illustrated in Fig. 3.2.1 and Fig. 3.2.2. (It should be noted that $V_1 = V_{f1}$ and $k_1 = k_{f1}$.)

Using Eq. 1.4.12

$$\ln t_1 = \ln\left(\frac{1}{\delta \rho_1 A_1}\frac{\bar{k}T}{V_1 H}\right) + \frac{V_1 H}{\bar{k}T}\epsilon$$

where the work hardening coefficient is $H = 0.5\mu$ to account for the use of σ instead of τ. For iron,[28] $\gamma = 1.4\epsilon . V_1$ can thus be determined from the creep test results represented in the logt vs. ϵ coordinate system, as illustrated in Fig. 3.2.1.

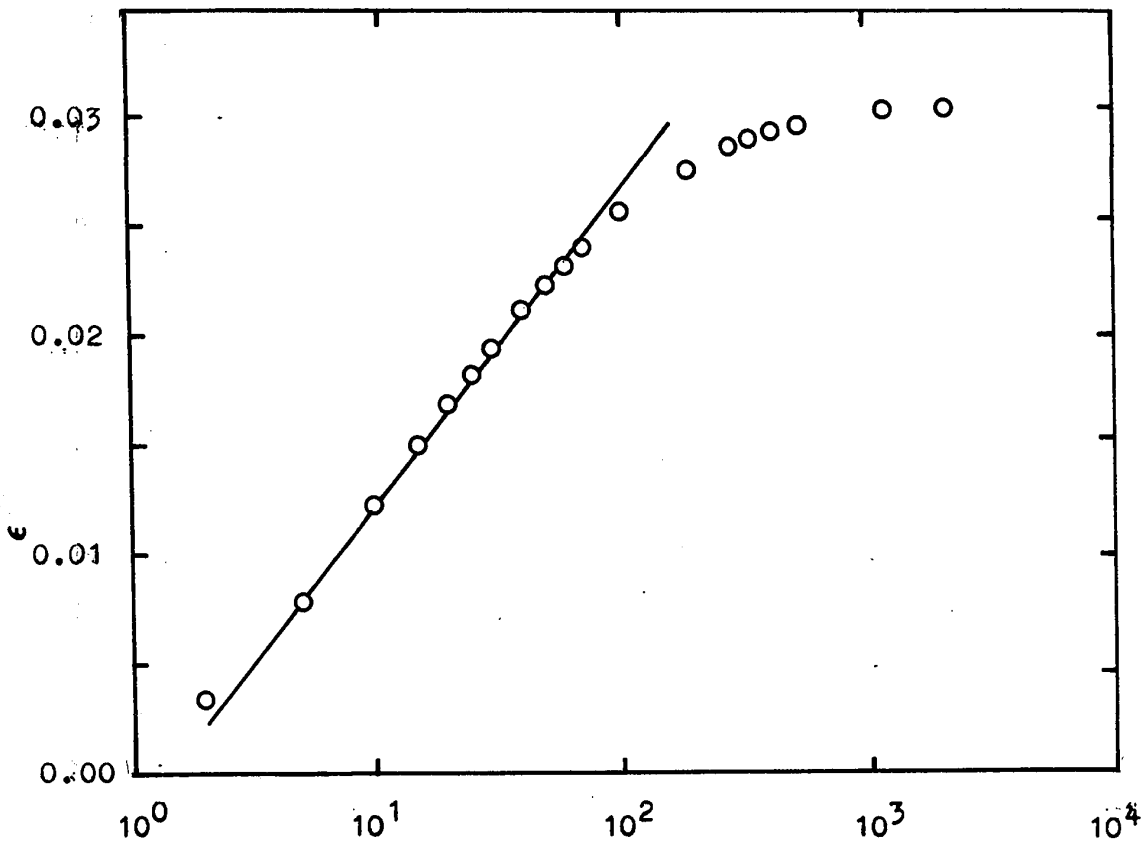

Fig. 3.2.1. Illustration of the determination of V_1 from the creep curve of test 7.3. From the slope, $V_1 = 81b^3$, and from the intercept, $\delta\rho_1 A_1 = 4.73 \times 10^{-3} sec^{-1}$.

Similarly, from Eq. 1.4.9, V_1 can be determined from

$$\ln \dot{\epsilon}_1 = \ln(\delta \rho_1 A_1) - \frac{V_1 H}{\bar{k}T} \epsilon$$

The application of this method is illustrated in Fig. 3.2.2.

The calculated activation volumes are listed in Table III. There appears to be an increase in V_1 as the effective stress τ^o_{eff} decreases. (For iron,[28] $\tau = 0.5\sigma$) This behavior has been observed by many investigators.[13,20,33]

The observed scatter in V_1 values is not unacceptable and all values of V_1 confirm the possibility[9,10,13,22,33] that the primary rate controlling mechanism is the Peierls-Nabarro mechanism.

It should be noted that if a different set of points were considered to represent a linear section in the evaluation, the values of t_1 and $\dot{\epsilon}_1$, and therefore V_1 would be obtained. The difference in V_1 would not be large enough to indicate a different mechanism, however, the effects of the differences in t_1 and $\dot{\epsilon}_1$ would be carried into the evaluation of all subsequent kinetics terms where they are used. Comparing Fig. 3.2.2 with Fig. 3.2.2,a, one can see that for the evaluation in some tests, the linear region is easily determined, but for others it is a matter of judgement as to which section is linear.

3.2.1.2. Backward Activation (V_{b1}). The single term expression does not describe the creep behavior over the range of the experiment. The next level of complexity that should

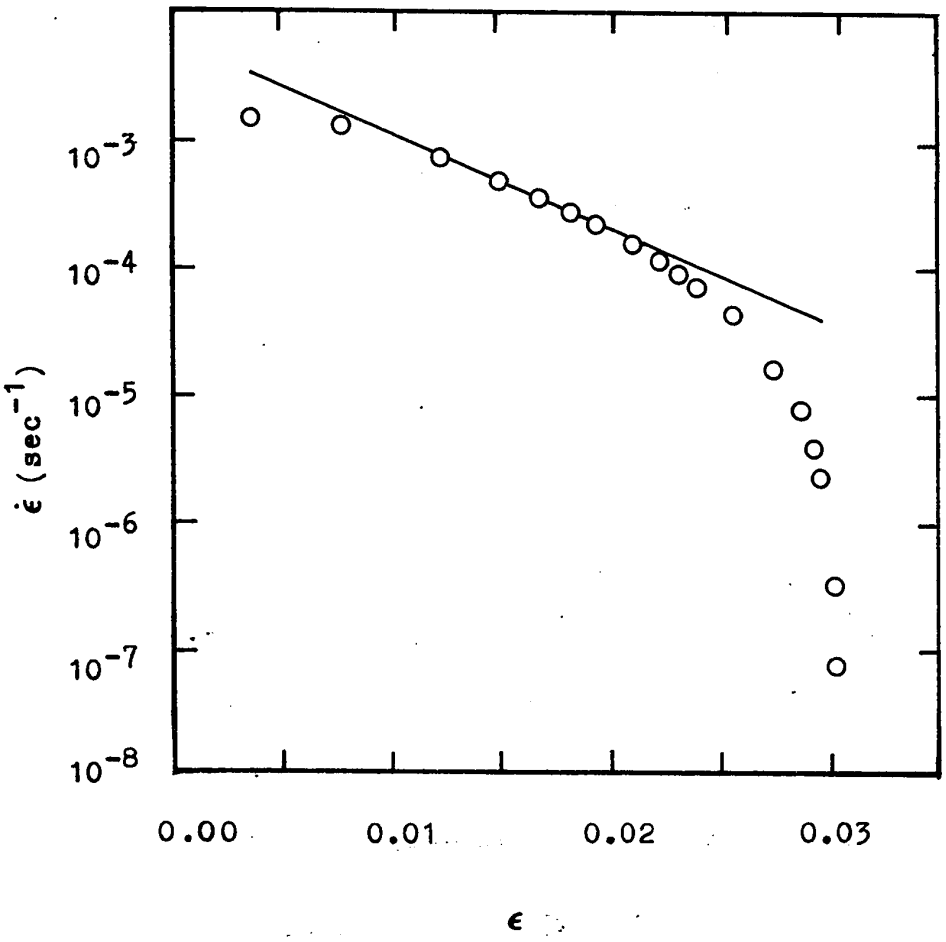

Fig. 3.2.2. The strain dependence of the strain rate for test 7.3 and the determination of V_1. From slope, $V_1 = 82b^3$ and from intercept, $\delta\rho_1 A_1 = 5.63 \times 10^{-3} sec^{-1}$.

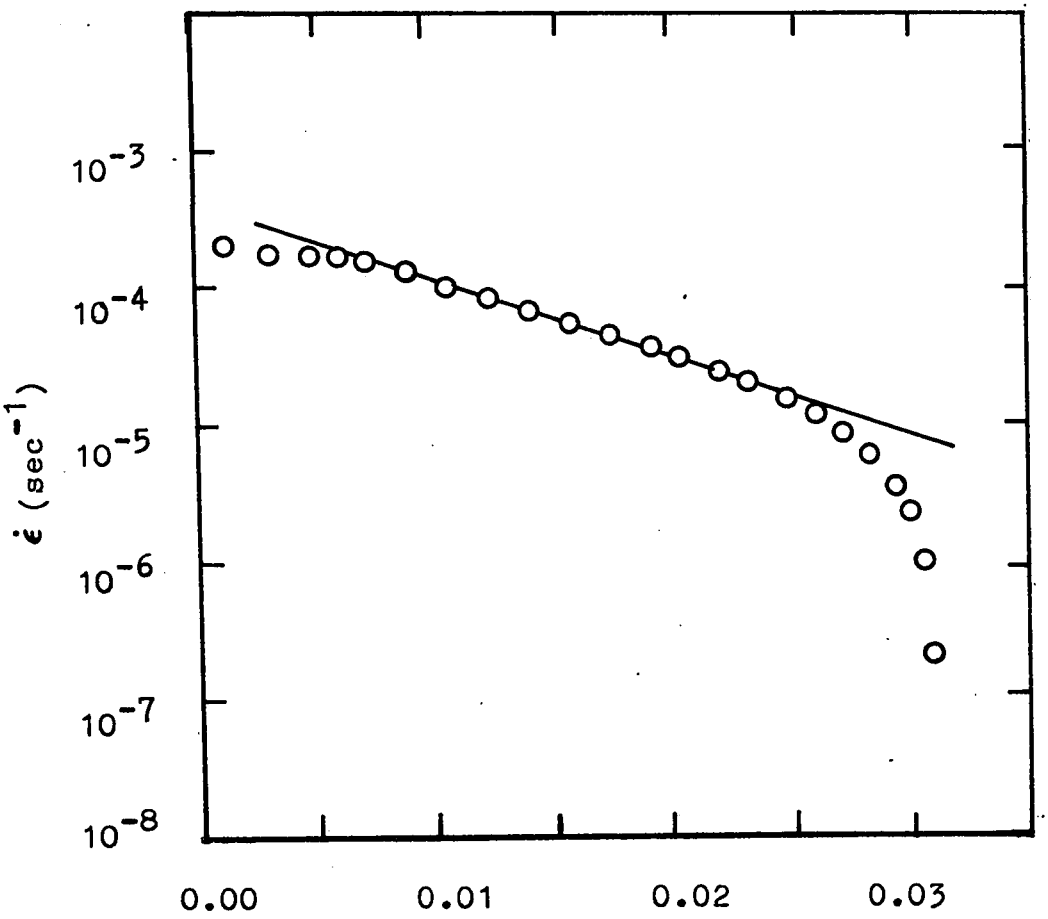

Fig. 3.2.2,a. The strain dependence of the strain rate for test 13.4. The figure illustrates a test result with a longer initial linear portion which facilitates the analysis for V_1.

be investigated is a single barrier with forward and backward activation. The deformation kinetics description of such a system is

$$\text{Rate} = \delta \rho_1 A_1 \exp\left(-\frac{V_1 H}{\bar{k}T}\epsilon\right) - \delta \rho_{b1} A_{b1} \exp\left(\frac{V_{b1} H}{\bar{k}T}\epsilon\right) \qquad 3.2.1$$

where the subscript "b1" refers to the backward direction associated with the first barrier. Eq. 3.2.1 can be expressed as

$$\dot{\epsilon} = \dot{\epsilon}_1 - \dot{\epsilon}_{b1} \qquad 3.2.2$$

where $\dot{\epsilon}_1$ and $\dot{\epsilon}_{b1}$ represent the first and second terms on the RHS of Eq. 3.2.1 respectively. Therefore

$$\dot{\epsilon}_{b1} = \dot{\epsilon}_1 - \dot{\epsilon} \qquad 3.2.3$$

The activation volume V_{b1} can thus be obtained, as illustrated in Fig. 3.2.3. Out of the thirty two tests, twenty five indicated the existence of a backward term V_{b1}. Four tests gave no indication of this backward term. No indication of this term is believed to be due to experimental scatter and the method of analysis used, i.e. the use of semi-logarithmic graphs.

The results indicated that there was activation over the single barrier in the forward and possibly in the backward direction as well. The single barrier kinetics discussed

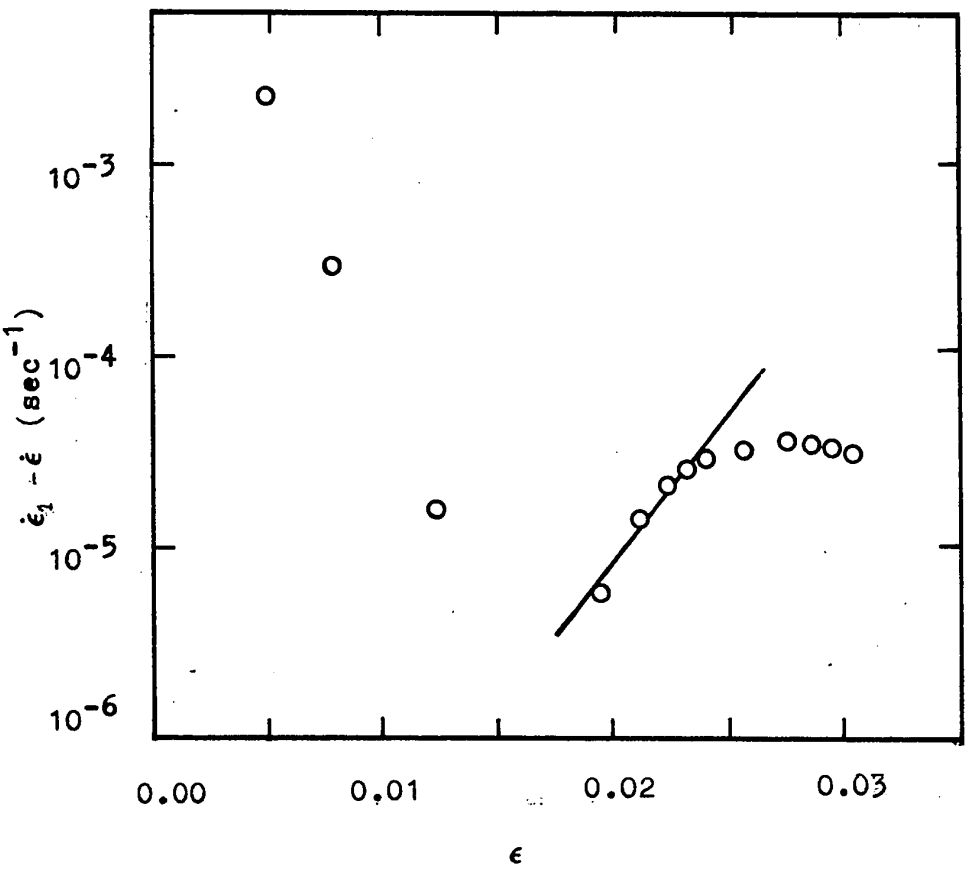

Fig. 3.2.3. The determination of V_{b1} for test 7.3.

From slope, $V_{b1} = 192b^3$ and from intercept, $\delta\rho_{b1}A_{b1} = 2.81\times10^{-9}\text{sec}^{-1}$.

above, however, does not describe the behavior over the whole range of the experiment. It was therefore necessary to consider the next level of complexity indicated by theory, that is the possibility that the effect of a second barrier was also observed.

3.2.2. Double Barrier Kinetics

In general, the second barrier may be associated with the first in parallel or in series. Both possibilities were investigated.

3.2.2.1. Parallel Barriers. All tests were analyzed with the assumption that the two barriers may be in parallel. Only five indicated the possibility of a second parallel barrier. It was concluded that the rate of the process cannot be controlled by a system of two parallel barriers.

3.2.2. Consecutive Barriers (V_2). Previous investigations [13,23] on the same batch of specimens indicated the possibility of a second consecutive barrier. In the present study, twenty eight tests gave a clear indication of the existence of a second consecutive barrier. Two test gave no indication of this term.

Theory requires that V_2, as well as the activation volume of any subsequent barrier be greater than V_1. Only one of these twenty eight results indicated a V_2 smaller than V_1, and even this is expected to be due to the inaccuracy inherent in the graphical method.

For the evaluation of V_2, consider the rate equation (Eq.1.3.2) with two barriers (n=2).Hence

$$\text{Rate} = \dot{\epsilon} = \delta \frac{\rho_1 - \rho_3(k_3/\nu)}{\frac{1}{k_1} + \frac{1}{k_2}} \qquad 3.2.4$$

In the early part of the experiment

$$\rho_3(k_3/\nu) \ll \rho_1 ,$$

therefore Eq.3.2.5 can be simplified to

$$\dot{\epsilon} = \frac{d\epsilon}{dt} = \delta\rho_1 \left(\frac{1}{k_1} + \frac{1}{k_2}\right)^{-1} \qquad 3.2.5$$

Thus

$$dt = \frac{1}{\delta \rho_1} \left(\frac{1}{k_1} + \frac{1}{k_2}\right) d\epsilon . \qquad 3.2.6$$

Substituting for k_1 and k_2 from Eq.1.4.7

$$\int_0^t dt = \frac{1}{\delta \rho_1} \int_0^{\epsilon} \left[\frac{1}{A_1} \exp\left(\frac{V_1 H}{\bar{k}T} \epsilon\right) + \frac{1}{A_2} \exp\left(\frac{V_2 H}{\bar{k}T} \epsilon\right) \right] d\epsilon \qquad 3.2.7$$

Therefore

$$t = \frac{1}{\delta \rho_1 A_1} \frac{\bar{k}T}{V_1 H} \left[\exp\left(\frac{V_1 H}{\bar{k}T} \epsilon\right) - 1 \right] + \frac{1}{\delta \rho_1 A_1} \frac{\bar{k}T}{V_2 H} \left[\exp\left(\frac{V_2 H}{\bar{k}T} \epsilon\right) - 1 \right] . \qquad 3.2.8$$

Rearranging Eq.3.2.8 leads to

$$\frac{1}{\delta \rho_1 A_2} \frac{\bar{k}T}{V_2 H} \left[\exp\left(\frac{V_2 H}{\bar{k}T} \epsilon\right) - 1\right] =$$

$$t - \frac{1}{\delta \rho_1 A_1} \frac{\bar{k}T}{V_1 H} \left[\exp\left(\frac{V_1 H}{\bar{k}T} \epsilon\right) - 1\right]. \quad 3.2.9$$

Because over the range where the effect of the second barrier is noticable

$$\exp\left(\frac{V_2 H}{\bar{k}T} \epsilon\right) >> 1,$$

therefore,

$$\frac{1}{\delta \rho_1 A_2} \frac{\bar{k}T}{V_2 H} \exp\left(\frac{V_2 H}{\bar{k}T} \epsilon\right) =$$

$$t - \frac{1}{\delta \rho_1 A_1} \frac{\bar{k}T}{V_1 H} \left[\exp\left(\frac{V_1 H}{\bar{k}T} \epsilon\right) - 1\right]. \quad 3.2.10$$

Thus

$$\ln \frac{1}{\delta \rho_1 A_2} \frac{\bar{k}T}{V_2 H} + \frac{V_2 H}{\bar{k}T} \epsilon =$$

$$\ln\left\{t - \frac{1}{\delta \rho_1 A_1} \frac{\bar{k}T}{V_1 H} \left[\exp\left(\frac{V_1 H}{\bar{k}T} \epsilon\right) - 1\right]\right\}. \quad 3.2.11$$

Eq. 3.2.11 can also be expressed as

$$\ln \frac{1}{\delta \rho_1 A_1} \frac{\bar{k}T}{V_2 H} + \frac{V_2 H}{\bar{k}T} \epsilon = \ln(t - t_1) \qquad 3.2.12$$

where t is the experimental time and t_1 is as determined in section 3.2.1.1. The graphical representation of Eq. 3.2.12 is shown in Fig. 3.2.4.

Another possible method by which the existence of a second consecutive barrier can be tested is in the following: Eq. 3.2.6 can be rearranged to give [12]

$$\ln\left(\frac{\dot{\epsilon}_1}{\dot{\epsilon}} - 1\right) = \ln C + \frac{V_{b1}+V_{f2}}{\bar{k}T} H\epsilon \qquad 3.2.13$$

where C is a constant expressed as

$$C = \frac{A_1}{\frac{\bar{k}T}{h} \exp\left(\frac{\Delta G^{\ddagger}_{f1} - \Delta G^{\ddagger}_{b1} + \Delta G^{\ddagger}_{f2}}{\bar{k}T}\right)},$$

and

$$\dot{\epsilon}_1 = \delta \rho_1 A_1 \exp\left(-\frac{V_1 H}{\bar{k}T} \epsilon\right) ,$$

and V_{f2} is an activation volume different than V_2. The reference state of the former is the ground state in front of the second barrier, whereas for the latter it is the ground state in front of the first barrier. A graphical representation of Eq. 3.2.13 is given in Fig. 3.2.5.

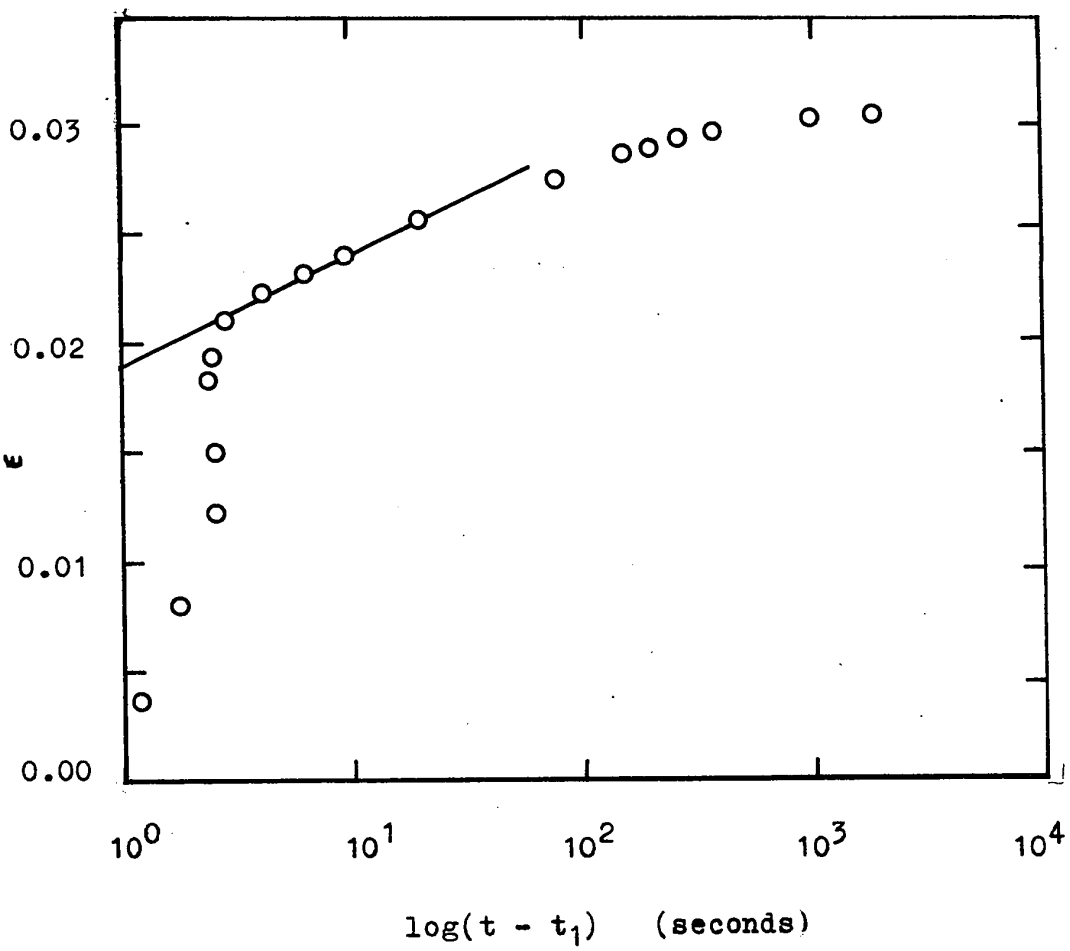

Fig. 3.2.4. The determination of V_2 for test 7.3. From slope, $V_2 = 330b^3$ and from intercept, $\delta \rho_1 A_2 = 3.07 \times 10^3 sec^{-1}$.

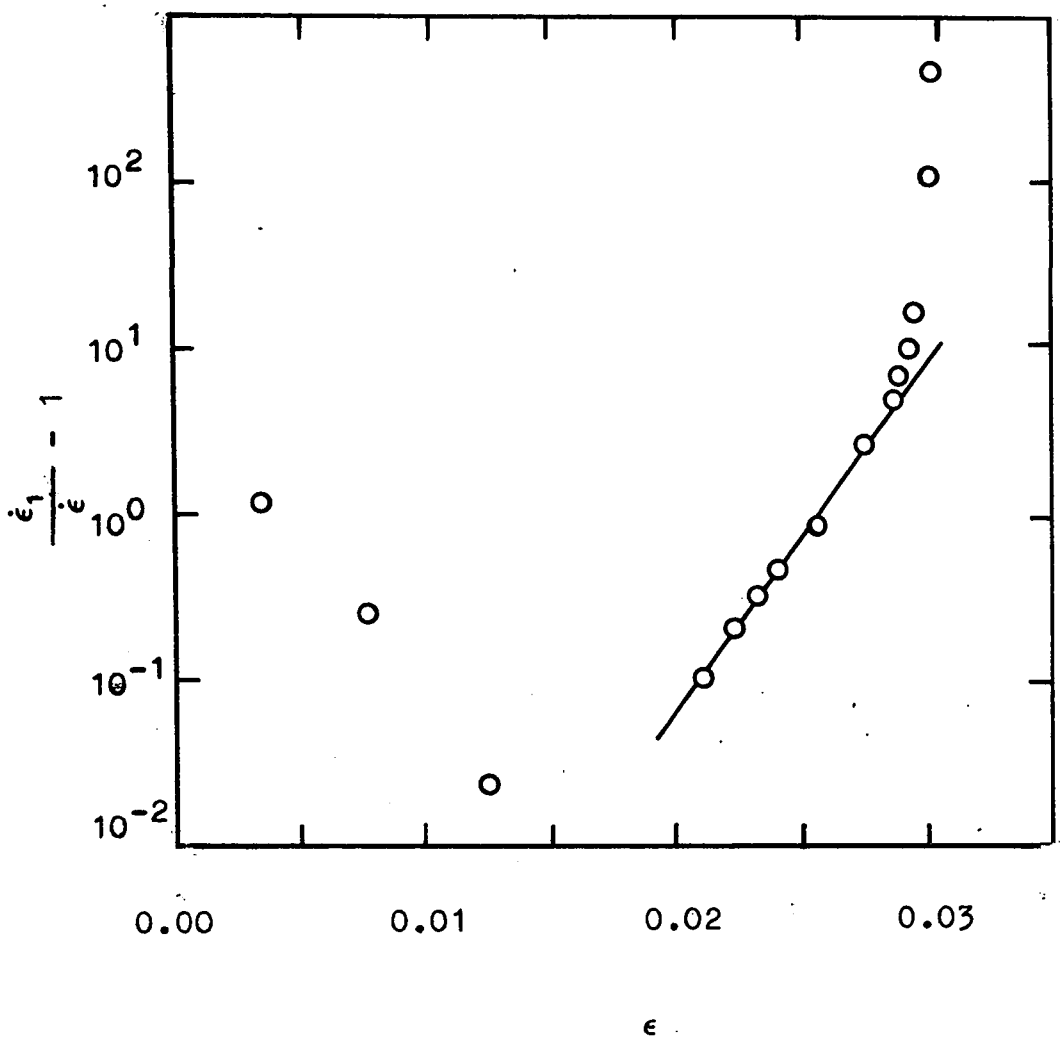

Fig. 3.2.5. The determination of $V_{b1}+V_{f2}$ for test 7.3. From slope, $V_{b1} = 400b^3$.

3.2.2.3. Backward Activation Over The Two Barriers(V_3).

In the pevious evaluation of V_2, the backward activation over the two barriers was ignored. For low effective stresses, it is no longer negligible. During low temperature creep, as the material deforms, the internal stress increases, leading to strain rates decreasing to zero.

The rate of deformation over a system of two consecutive barriers can be expressed as

$$\text{Rate} = \delta \frac{\rho_1 - \rho_3(k_3/\nu)}{\frac{1}{k_1} + \frac{1}{k_2}}. \qquad 3.2.14$$

Because for high effective stresses

$$\frac{\rho_3}{\rho_1} k_3/\nu << 1,$$

this term is ignored in the evaluation of V_2. This simplification is no longer applicable for low effective stresses and Eq. 3.2.14 must be used for the evaluation. In order to determine V_3 from this expression, it should be noted that $\rho_1 = \rho_3$. Thus Eq. 3.2.14 becomes

$$\text{Rate} = \dot{\epsilon} = \delta\rho_1 \frac{1 - k_3/\nu}{\frac{1}{k_1} + \frac{1}{k_2}} \qquad 3.2.15$$

or, rearranging Eq. 3.2.15

$$k_3/\nu = 1 - \dot{\epsilon}\left(\frac{1}{\delta\rho_1 k_1} + \frac{1}{\delta\rho_1 k_2}\right) \qquad 3.2.15,a$$

where it is reminded that

$$k_3/\nu = A_3 \exp\left(\frac{V_3 H}{\bar{k}T}\epsilon\right).$$

A semi-logarithmic representation of Eq. 3.2.15,a is given in Fig. 3.2.6. V_3 can be determined from the slope. Of the thirty two tests, six gave no indication of the existence of a backward term V_3. Six of the remaining twenty six were from a two or three point evaluation and were therefore not included in the averages shown in Table III. Thus twenty of the results gave a clear indication of backward activation. These results therefore gave no conclusive indication of the presence of such a backward term. The reasons may be the following:

i)Most tests were terminated shortly after the rates went to zero. The effects of the k_3 term are noticable in these parts of the experiments where the rates are diminishing to zero. There was not always enough data for the determination or detection of this term.

ii)The strain rates for the latter parts of the experiments were very low, ranging from 10^{-6} to 10^{-11} sec^{-1}. The rates ranged over six orders of magnitude in some tests. It is not easy or always possible to record data over such a wide range. Any calculation with low strain rates mentioned has considerable inaccuracies.

iii)Determination of all activation volumes is done from semi-logarithmic graphs. This introduces inaccuracies. For

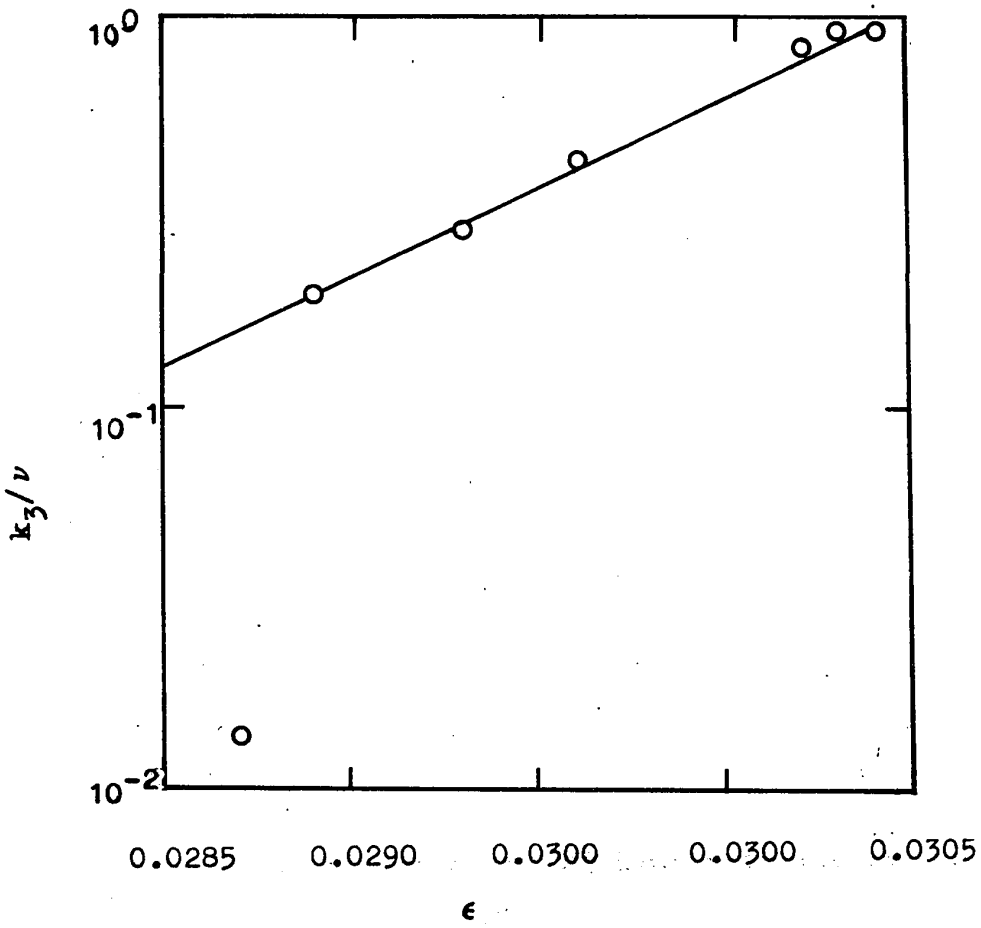

Fig. 3.2.6. Determination of V_3 for test 7.3. From slope, $V_3 = 840b^3$ and from intercept, $A_3 = 1.75 \times 10^{-15}$.

the determination of each subsequent term, these inaccuracies add on. Thus, along with low strain rates, the k_3 term, and therefore V_3 term is difficult to obtain.

iv)Throughout the investigation, only ρ_1 was considered as the concentration of flow units, and it was considered to be constant. Recently it has been shown by Krausz[34] that a more complete description is given by

$$\rho_t = \rho_1 + \rho_2 \qquad 3.2.16$$

where ρ_t is the total concentration of flow units, and ρ_2 is the concentration of flow units in front of the second barrier. The model considers a consecutive system of two barriers and this leads to a rate equation with four kinetics terms in the denominator of Eq.3.2.14, and the rate constants are described somewhat differently. This requires the determination of all four kinetics terms in the denominator before determining the backward term k_3. The analysis is much more complicated for this case and was not looked into in the present investigation.

v)It is also possible that there are more consecutive barriers may be rate controlling. This possibility was also not looked into.

For cases in which there was a clear indication of backward activation, the rates were calculated from the experi-

mentally determined values. The calculated curves were in good agrrement with the experimental data.

In terms of creep strain, the strain rate is expressed as

$$\dot{\epsilon} = \frac{1 - A_3 \exp(\frac{V_3 H}{\bar{k}T}\epsilon)}{\frac{1}{\delta\rho_1 A_1} \exp(\frac{V_1 H}{\bar{k}T}\epsilon) + \frac{1}{\delta\rho_1 A_2} \exp(\frac{V_2 H}{\bar{k}T}\epsilon)}$$

where $\delta\rho_1 A_1$, $\delta\rho_1 A_2$ and A_3 are determined experimentally and are constants, H is the work hardening coefficient, and the activation volumes are calculated as described. In Fig.3.2.7, the calculated and experimentally determined rates are shown.

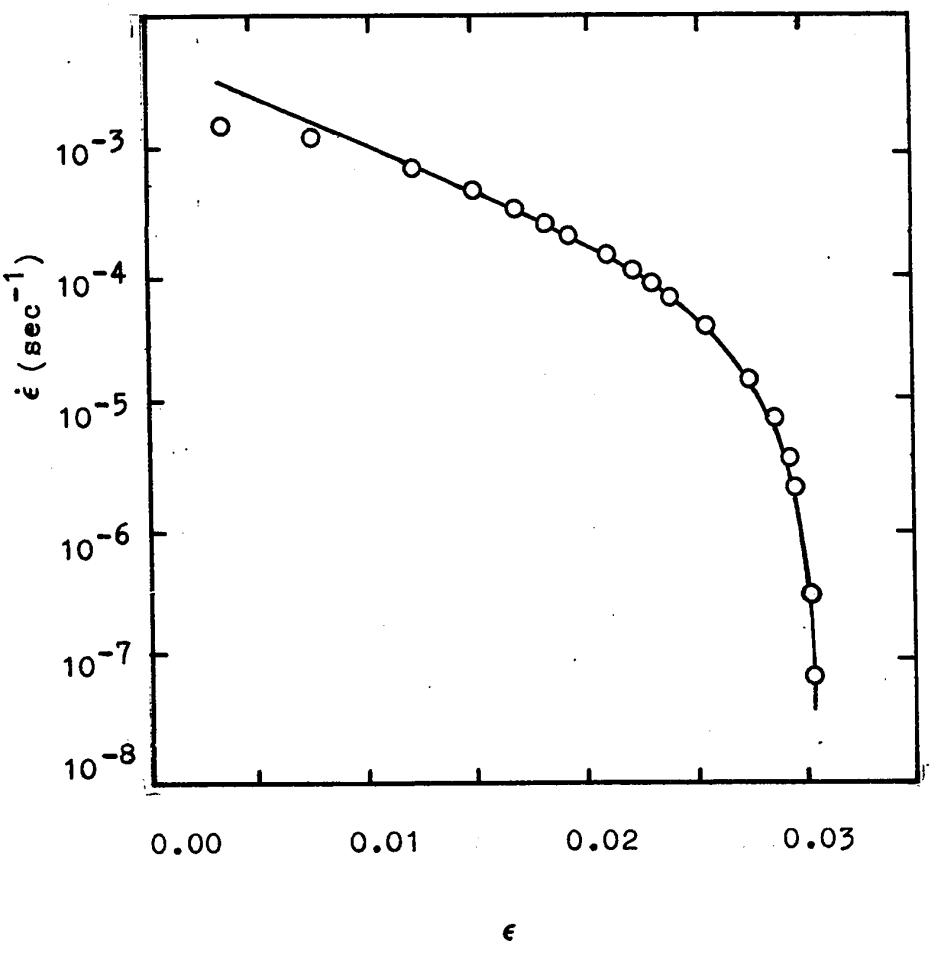

Fig. 3.2.7. Full representation of $\dot{\epsilon}$ vs. ϵ for test 7.3.according to $\dot{\epsilon} = (1 - A_3 \exp\frac{V_3 H}{\bar{k}T}\epsilon) \div (\frac{1}{\delta\rho_1 A_1} \exp\frac{V_1 H}{\bar{k}T}\epsilon + \frac{1}{\delta\rho_1 A_2} \exp\frac{V_2 H}{\bar{k}T}\epsilon)$, where A_i and V_i are as determined from Fig. 3.2.1 to Fig. 3.2.6.

TABLE III

ACTIVATION VOLUMES

Group Number	τ^o_{eff} (kg/mm^2)	σ^o_a (kg/mm^2)	V_1/b^3‡ (a)	V_1/b^3‡ (b)	V_{b1}/b^3	$(V_{b1}+V_{f2})/b^3$	V_2/b^3	V_3/b^3
I	2.32±.38	24.2±0.50	34±13	50±17	220±217	403±328	864±1250	1425±2034
II	1.26±.10	25.0±2.65	61±24	66±25	185±163	551±383	956±1292	1005± 355
III	1.00±.03	25.8±2.04	91±23	104±46	244±125	925±1047	890±1123	3240±6838
IV	0.65±.06	27.5±2.66	97±45	97±45	367±232	506±289	574±296	516±271

Note: All variations are one standard deviation.

(a) V_1 in this column is derived from Eq. 1.4.12.

(b) V_1 in this column is derived from Eq. 1.4.9.

‡ V_1 is identical to V_{f1}.

$\tau = \frac{1}{2}\sigma$

3.3.LIMITING CREEP STRAIN,EFFECTIVE STRESS AND INTERNAL STRESS

In low temperature and low stress creep the strain rate decreases to zero as the material deforms. The rate of a creep process that is controlled by a system of two consecutive barriers is expressed as

$$\dot{\epsilon} = \delta \rho_1 \frac{1 - k_3/\nu}{\frac{1}{k_1} + \frac{1}{k_2}} \qquad 3.3.1$$

For the limiting case in which the rate is zero, the expression in the numerator of Eq.3.3.1 must be zero,therefore

$$1 - k_3/\nu = 0. \qquad 3.3.2$$

Expressing k_3 more explicitly from Eq.1.4.7,the Equation 3.3.2 becomes

$$1 - \exp(-\frac{\Delta G_3^{\ddagger}}{\bar{k}T}) \exp(-V_3 \frac{\tau_{eff}^{o} - H\epsilon^{lim}}{\bar{k}T}) = 0, \qquad 3.3.3$$

where ϵ^{lim} is the limiting creep strain at which the rate becomes zero. It should be noted here once again that $\Delta G_3^{\ddagger}$ is referenced to the ground state of the reactant in front of the first barrier.

Rearranging Eq.3.3.3 we obtain

$$-\Delta G_3^{\ddagger} - V_3 \tau_{eff}^{o} + V_3 H \epsilon^{lim} = 0 \qquad 3.3.4$$

Thus, as the creep strain approaches the limiting value ϵ^{lim}, the rate approaches zero. The limiting strain can be obtained from Eq.3.3.4 as

$$\epsilon^{lim} = \frac{V_3 \tau^o_{eff} + \Delta G_3^{\mp}}{V_3 H} . \qquad 3.3.5$$

The evaluation of ϵ^{lim} from experimental results is also possible. The expression of Eq.3.3.1 in terms of experimentally determined constants (Eq.3.2.17) leads to

$$1 - A_3 \exp(\frac{V_3 H}{\bar{k}T} \epsilon^{lim}) = 0 \qquad 3.3.6$$

thus

$$\epsilon^{lim} = -\frac{\ln A_3}{V_3 H/\bar{k}T} \qquad 3.3.7$$

The evaluation of ϵ^{lim} is a means by which the experimental results for k_3 can be cross checked. Of all tests for which V_3 could be determined, most calculated ϵ^{lim} were within 0.5% of the experimentally observed limiting creep strain. Three were within 1.5% and only one varied by 4.6%.

In order to illustrate that the limiting effective stress τ^{lim}_{eff} does not have to be zero for the limiting case of zero rate, consider Eq.3.3.2 in terms of stress rather than strain, i.e.

$$1 - \exp(-\frac{\Delta G_3^{\mp}}{\bar{k}T}) \exp(-\frac{V_3 \tau^{lim}_{eff}}{\bar{k}T}) = 0 \qquad 3.3.8$$

Thus, the limiting effective stress at which the rate is zero is

$$\tau_{eff}^{lim} = -\frac{\Delta G_3^{\ddagger}}{V_3} \qquad 3.3.9$$

The limiting effective stress is related to the limiting internal stress τ_i^{lim} as (Eq.1.4.5)

$$\tau_{eff}^{lim} = \tau_a - \tau_i^{lim} .$$

From this

$$\tau_{eff}^{lim} = \tau_a - \tau_i^{lim} = \tau_a + \frac{\Delta G_3^{\ddagger}}{kT} . \qquad 3.3.10$$

For low $\Delta G_3^{\ddagger}$ and high V_3, τ_{eff}^{lim} is small and therefore, τ_i^{lim} is approximately equal to the applied stress. In these cases, the creep and stress relaxation methods of internal stress measurement described in section 1.5.1 and 1.5.3 respectively, do not always involve much approximation. For the most general case, the internal stress can be evaluated from Eq.3.3.10 using the activation free energy $\Delta G_3^{\ddagger}$ and the activation volume V_3. This line of thought corrects and completes the recently introduced methods of internal stress measurement.

3.4. DISLOCATION DENSITY EFFECTS

It has already been pointed out that for the low temperature deformation of metals, the concentration of flow units is considered as the mobile dislocation density. In the foregoing discussions, the dislocation density has entered the description as ρ_1 (or ρ_{f1}), i.e. the concentration of flow units in front of the first barrier. The mobile dislocation density is known to change during plastic deformation. During creep, where there can be considerable deformation, the dislocation multiplication effect can be pronounced. The relative effect will be greater when the initial dislocation density ρ_1^o is low, as will be shown. The possible effects of dislocation density on the creep behavior are briefly discussed below.

3.4.1. Effect of Initial Dislocation Density (ρ_1^o)

In the early 1960's, Gilman[36] and Gilman and Johnston[14] showed the effects of ρ_1^o on early creep behavior. In low temperature creep, for low initial dislocation density, there is an initial delay time, also referred to as the incubation period. It is the period of non-measurable or negligible creep strain. Longer delay times are expected for lower ρ_1^o.

It has been shown[3,35,36] that delay time is the general behavior of creep and is a parallel phenomenon of yield drop. The empirical description used by these authors is based on Orowan's equation and is expressed as

$$\dot{\gamma} = \alpha b(\rho^{o} + B'\gamma)v_{o}\left(\frac{\tau^{o}_{eff}}{\tau_{o}}\right) \qquad 3.4.1$$

where ρ^{o} is the initial dislocation density, α is a geometrical factor, b is the Burger's vector, B' is the dislocation multiplication factor, and v_{o} and τ_{o} are empirical parameters. Prediction of longer delay times for lower ρ^{o} follows from this description. Results show[3,35,36] the parallel between delay times and yield .

Studies by Krausz[3] on ice show that delay times are no longer observed after repeated loading and that delay times are observed for low initial dislocation densities. The correlation between constant load compression tests on polycrystalline ice where yield is observed, and creep behavior where dislocation multiplication leading to delay times has been shown by Krausz.[3]

Studies by Johnston[35] also showed that with increasing stress the delay time also decreases. His explanation of the correlation between delay times and yielding is the following: Delay times are observed when there is no work hardening. Decelerating creep is a consequence of work hardening and thus corresponds to the appearance of the lower yield point.

The general behavior of delay times associated with yielding, absence or shorter delay times for increasing stress and repeated loading have been observed in the present investigation.

3.4.2. Dislocation Multiplication Effects

The strain dependence of dislocation multiplication is generally expressed by the approximate empirical relation

$$\rho_1 = \rho_1^o + B\epsilon \qquad 3.4.2$$

Substituting this into the simplest form of the rate equation (Eq.1.4.8.) leads to

$$\dot{\epsilon} = \delta A_1(\rho_1^o + B\epsilon)\ \exp(-\frac{V_1 H}{\bar{k}T}\epsilon) \qquad 3.4.3$$

This equation cannot be integrated. It is possible to get an equation that can be integrated if the dislocation multiplication is expressed as

$$\rho_1 = \rho_1^o\ \exp(M\epsilon) \qquad 3.4.4$$

where M is a dislocation multiplication factor. Hence the rate in the simplest kinetics description becomes

$$\dot{\epsilon} = \rho_1^o\ \exp(M\epsilon) A_1\ \exp(-\frac{V_1 H}{\bar{k}T}\epsilon) \qquad 3.4.5$$

$$= \rho_1^o\ A_1\ \exp\left[(-\frac{V_1 H}{\bar{k}T} + M)\epsilon\right] \qquad 3.4.5$$

The integration of Eq.3.4.5 leads to

$$t = \frac{1}{\delta\rho_1^o A_1}\left(-\frac{V_1 H}{\bar{k}T} + M\right)^{-1}\left\{\exp\left[\left(\frac{V_1 H}{\bar{k}T} - M\right)\epsilon\right] - 1\right\} \qquad 3.4.6$$

It is worth noting that Eq.3.4.5 and the integrated form, Eq.3.4.6 consider the dislocation multiplication effect explicitly. These equations can be used in the evaluation of the rate constants for cases in which the multiplication effects are considerable.

Considering now the rate equation for two consecutive barriers (Eq.3.2.15) and substituting Eq.3.4.4 for ρ_1 leads to

$$\dot{\epsilon} = \delta\rho_1^o \exp(M\epsilon)\frac{1 - k_3/\nu}{\frac{1}{k_1} + \frac{1}{k_2}} \qquad 3.4.7$$

or, more explicitly

$$\dot{\epsilon} = \delta\rho_1^o \exp(M\epsilon) \times \frac{1 - A_3 \exp(\frac{V_3 H}{\bar{k}T}\epsilon)}{\frac{1}{A_1}\exp(\frac{V_1 H}{\bar{k}T}\epsilon) + \frac{1}{A_2}\exp(\frac{V_2 H}{\bar{k}T}\epsilon)} \qquad 3.4.8$$

An often more convenient form of Eq.3.4.8 is

$$\dot{\epsilon} = \frac{1 - A_3 \exp(\frac{V_3 H}{\bar{k}T}\epsilon)}{\frac{1}{\delta\rho_1 A_1}\exp\left[(\frac{V_1 H}{\bar{k}T} - M)\epsilon\right] + \frac{1}{\delta\rho_1 A_2}\exp\left[(\frac{V_2 H}{\bar{k}T} - M)\epsilon\right]} \qquad 3.4.9$$

Equations 3.4.8 and 3.4.9 allow the effects of dislocation density and dislocation multiplication to be included in the description.

3.4.3. Total Dislocation Density ρ_t Instead of ρ_1.

The effects of using ρ_t instead of ρ_1 were discussed in section 3.2,b.

3.5. CALCULATED CREEP CURVES

The rate of a system comprising of two consecutive barriers with backward activation given in Eq.3.4.8 can be written as

$$\dot{\epsilon} = \frac{d\epsilon}{dt} = C_4 \left[1 - C_3 \exp\left(\frac{V_3 H}{\bar{k}T}\epsilon\right)\right] \left[C_1 \exp\left(\frac{V_1 H - M\bar{k}T}{\bar{k}T}\epsilon\right) + C_2 \exp\left(\frac{V_2 H - M\bar{k}T}{\bar{k}T}\epsilon\right)\right]^{-1} \qquad 3.5.1$$

where

$$C_1 = \exp\left(\frac{\Delta G_1^{\ddagger} - V_1 \tau_{eff}^{o}}{\bar{k}T}\right)$$

$$C_2 = \exp\left(\frac{\Delta G_2^{\ddagger} - V_2 \tau_{eff}^{o}}{\bar{k}T}\right)$$

$$C_3 = \exp\left(\frac{\Delta G_3^{\ddagger} - V_3 \tau_{eff}^{o}}{\bar{k}T}\right)$$

$$C_4 = \delta \rho_1^o \frac{\bar{k}T}{h}$$

Rearranging Eq.3.5.1, we get

$$dt = \frac{1}{C_4}\left[1 - C_3 \exp(\frac{V_3H}{\bar{k}T}\epsilon)\right]^{-1}$$

$$\left[C_1 \exp(\frac{V_1H - M\bar{k}T}{\bar{k}T}\epsilon)) + C_2 \exp(\frac{V_2H - M\bar{k}T}{\bar{k}T}\epsilon)\right] d\epsilon$$

3.5.2

This is an equation of form

$$dy = \frac{a\, e^{bx} + c\, e^{fx}}{1 - g\, e^{hx}} dx \qquad 3.5.3$$

where the denominator can be approxamated by an infinite series as

$$\frac{1}{1 - g\, e^{hx}} = \sum_{j=1}^{\infty} g^j\, e^{jhx} \qquad 3.5.4$$

Thus Eq. 3.5.2 can be expressed as

$$dt = \frac{1}{C_4} \sum_{j=1}^{\infty} C_3^j \exp(\frac{jV_3H}{\bar{k}T}\epsilon)$$

$$\left[C_1 \exp(\frac{V_1H - M\bar{k}T}{\bar{k}T}\epsilon) + C_2 \exp(\frac{V_2H - M\bar{k}T}{\bar{k}T}\epsilon)\right] d\epsilon$$

therefore

$$t = \frac{1}{C_4} \sum_{j=1}^{\infty} C_1 C_3^j \left[\frac{V_1 H + jV_3 H - M\bar{k}T}{\bar{k}T} \right]^{-1}$$

$$\left[\exp\left(\frac{V_1 H + jV_3 H - M\bar{k}T}{\bar{k}T} \epsilon \right) - 1 \right]$$

$$+ \frac{1}{C_4} \sum_{j=1}^{\infty} C_2 C_3^j \left[\frac{V_2 H + jV_3 H - M\bar{k}T}{\bar{k}T} \right]^{-1}$$

$$\left[\exp\left(\frac{V_2 H + jV_3 H - M\bar{k}T}{\bar{k}T} \epsilon \right) - 1 \right] . \quad 3.5.5$$

The experimental variables in Eq.3.5.5 are ρ_1^o, temperature T, the initial effective stress τ_{eff}^o, dislocation multiplication M, and the work hardening coefficient H. The effects of the applied stress enter through H as the work hardening behavior differs with the applied stress as noticed in the stress-strain diagram (Fig.3.1.12). The effects of each of these variables are briefly discussed in the following.

a) Initial dislocation density ρ_1^o. The constant, C_4 is proportional to ρ_1^o. Longer delay times are predicted for lower initial dislocation densities. In Fig.3.5.1 calculated creep curves showing the effects of different initial dislocation densities are given. As seen in the figure, as the initial dislocation density increases the delay time decrea-

ses, and for $\rho_1^o = 1x10^{16}/m^2$ it is not observed at all. The limiting creep strain appears to be independent of the initial dislocation density.

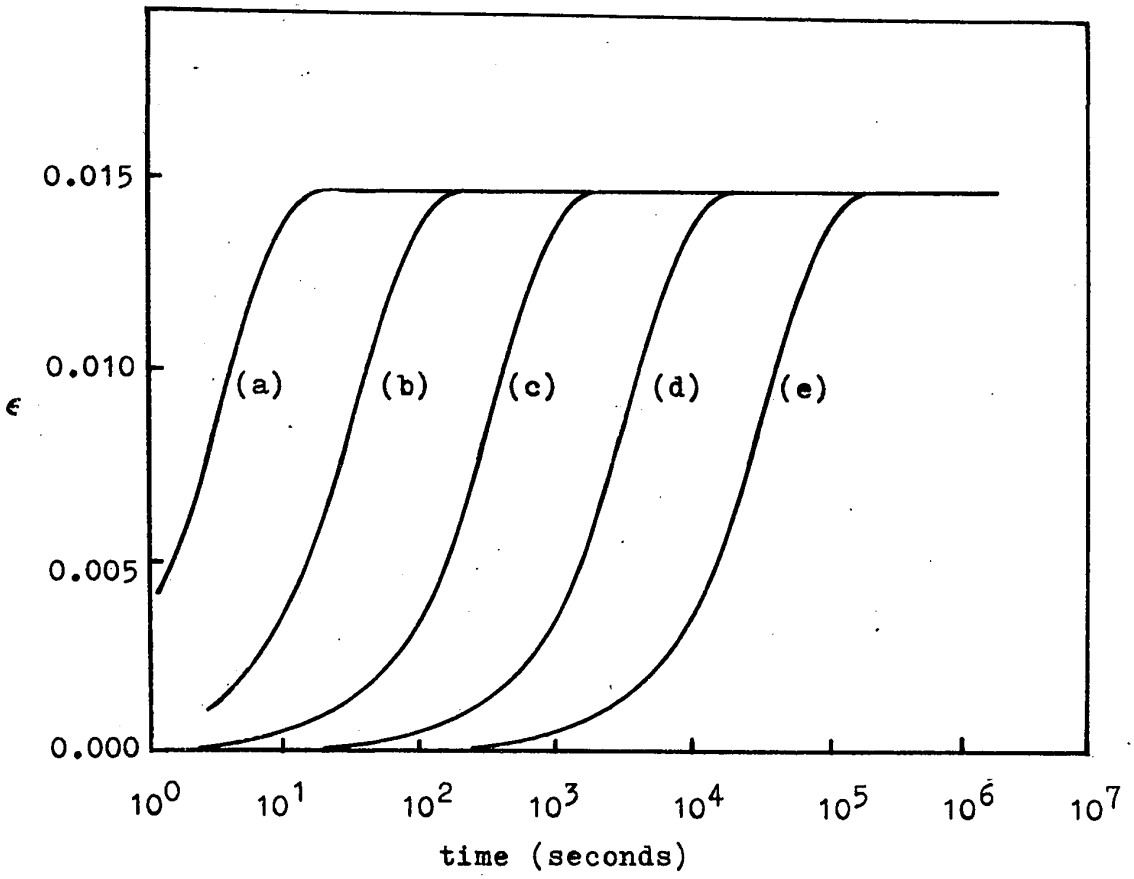

Fig. 3.5.1. Illustration of the effect of initial dislocation density on the creep curves calculated from Eq.3.5.5.The initial dislocation densities are for (a) $1x10^{16}/m^2$, (b) $1x10^{15}/m^2$ (c) $1x10^{14}/m^2$, (d) $1x10^{13}/m^2$, (e) $1x10^{12}/m^2$.

(Note. For Figures 3.5.1 to 3.5.5,the following values were used in the calculation of the creep curves from Eq.3.5.5; only the indicated variable's value has been changed, the va-

lues or which have been indicated: $\Delta G_1^{\pm} = 0.74$ev, $V_1 = 40b^3$, $\Delta G_2^{\pm} = 0.76$ ev, $V_2 = 196b^3$, $\Delta G_3^{\pm} = 0.013$ev, $V_3 = 275b^3$, $\delta = 6\times10^{-20}m^2$, $\rho_1^o = 1\times10^{14}/m^2$, M = 0, H = 7×10^8N/m^2 (71.36kg/mm^2), τ_{eff}^o = 1kg/mm^2 and T = 300K.)

b) Temperature T. All C_i and the exponential terms in Eq.3.5.5 include temperature. The effects of temperature on creep behavior are shown in Fig.3.5.2. As expected, it takes longer for the material to deform to the same strain at lower temperatures. The limiting creep strain is not effected by the temperature.

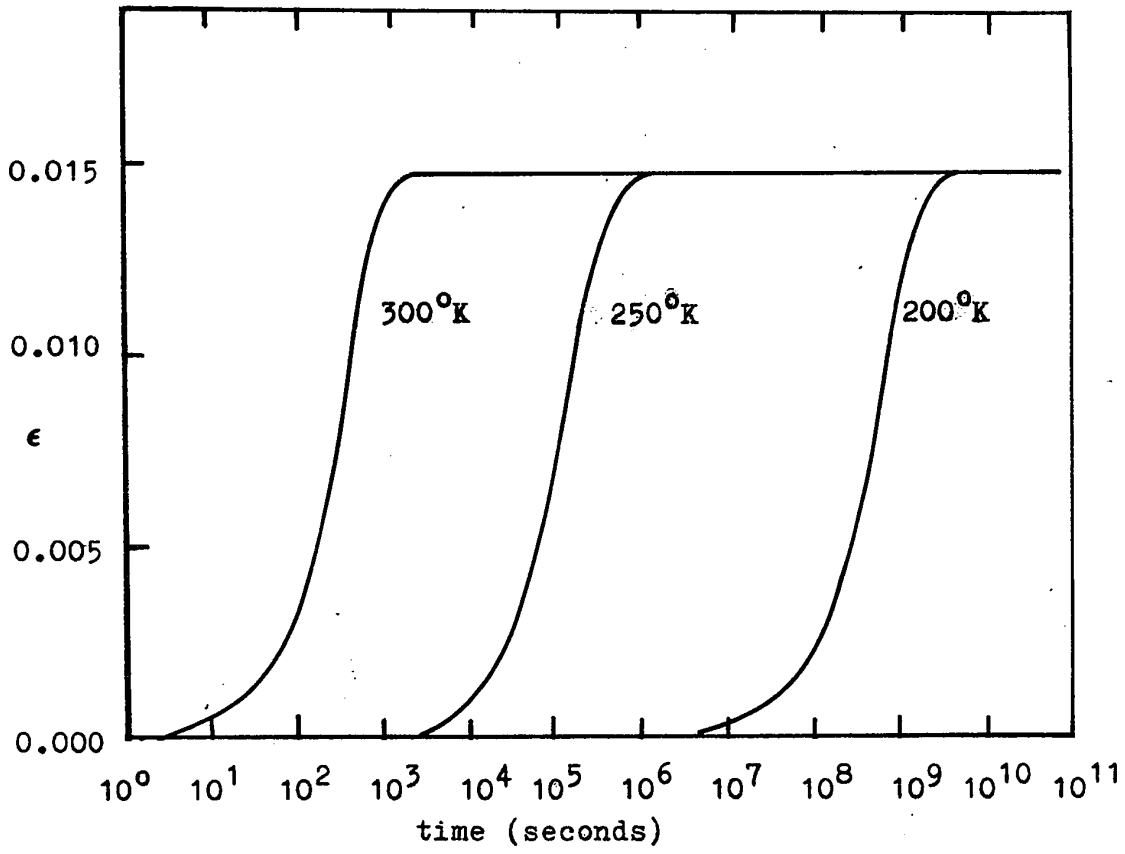

Fig. 3.5.2. Illustration of the effect of temperature on the calculated creep behavior.

c) The initial effective stress τ^{o}_{eff}. The constants C_1, C_2 and C_3 are proportional to the initial effective stress. The calculated creep curves for different τ^{o}_{eff} are shown in Fig. 3.5.3. The limiting creep strain increases with increasing initial effective stress, also the time required to reach the same strain decreases with higher initial effective stresses. It is of interest to note that the time at which

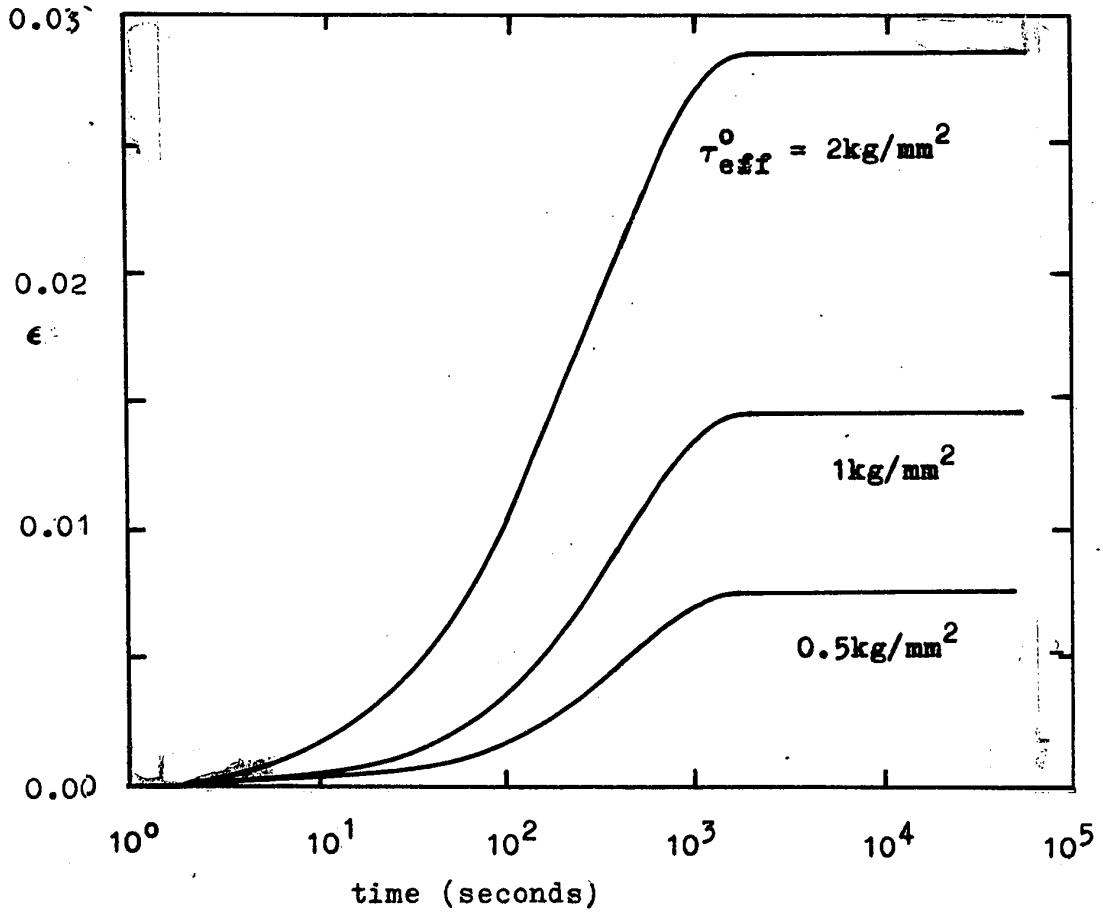

Fig. 3.5.3. Illustration of the effect of τ^{o}_{eff} on the calculated creep behavior.

the creep curve levels-off appears to be independent of τ^{o}_{eff}.

d) Dislocation multiplication. The effect of dislocation multiplication is entered into the description with an exponential term, M. Calculated creep curves for different values of M are shown in Fig. 3.5.4. The creep curves level off sharply for higher values of M. This increases the possibility that the observed sharp levelling-off of creep curves is a result of dislocation multiplication. The value of ϵ^{lim} is not affected by dislocation multiplication, how-

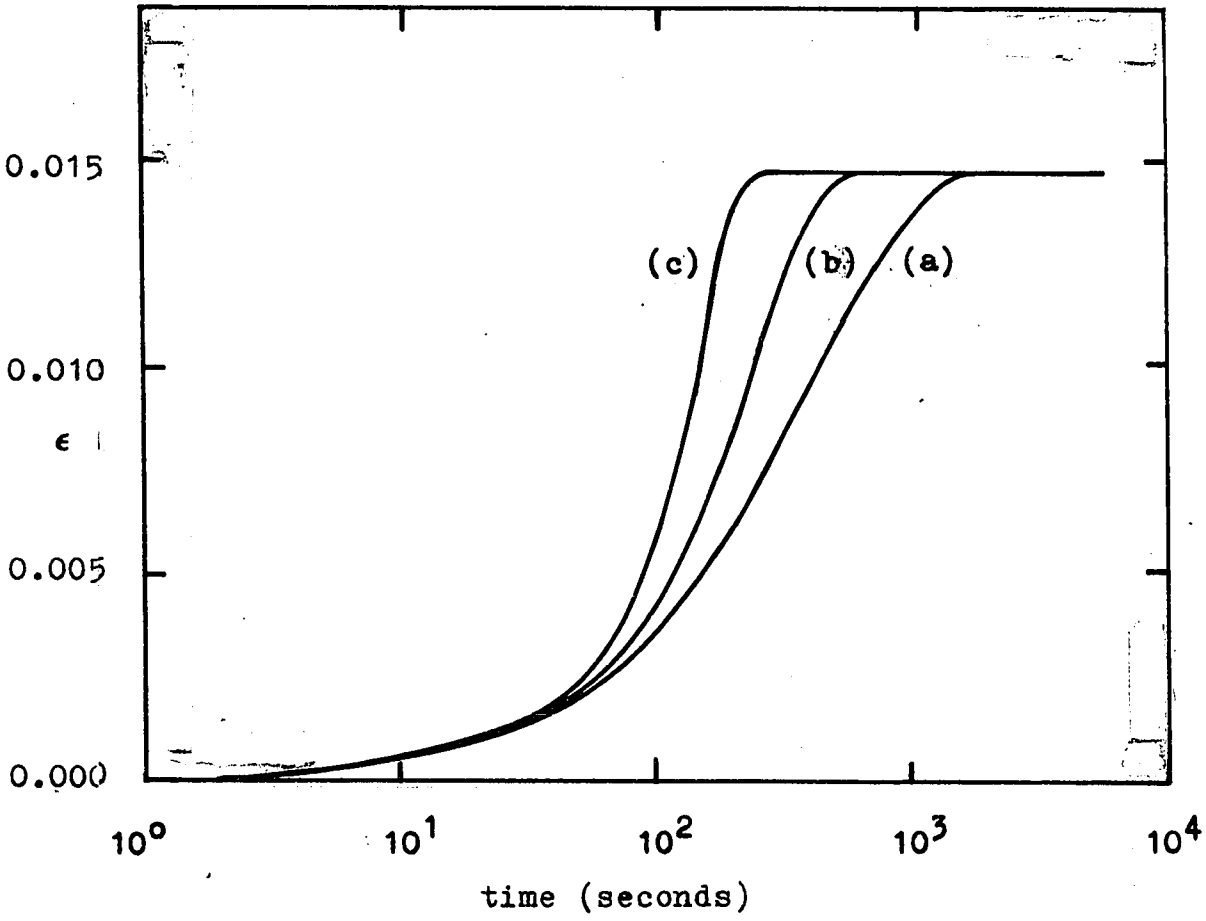

Fig. 3.5.4. Illustration of the effect of dislocation multiplication on the calculated creep behavior. The value for M is (a) 0, (b) 100 ,and (c) 200.

ever, the time required to reach it is reduced.

e) The applied stress. The work hardening coefficient varies with the applied stress.In Fig.3.5.5, calculated creep curves for various values of the work hardening coefficient H are shown. The limiting creep strain decreases as the work hardening coefficient increases. This is to be expected because the effective stress reduces faster at greater work hardening coefficients.

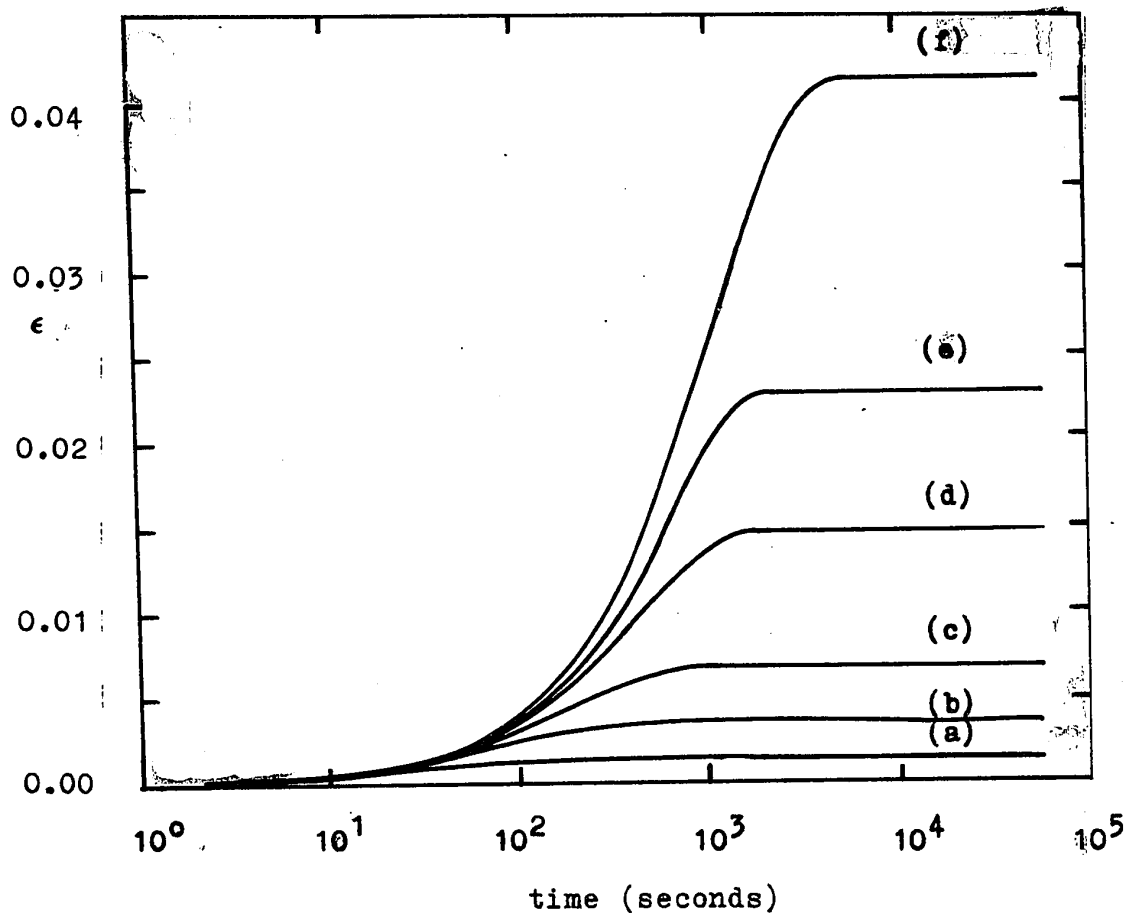

Fig. 3.5.5. Illustration of the effects of the work hardening coeeficient H. The value of H is (a) 815.49 kg/mm^2, (b) 305.81 kg/mm^2, (c) 152.91 kg/mm^2, (d) 71.36 kg/mm^2, (e)45.87 kg/mm^2, (f) 25.48 kg/mm^2.

The effects of the initial dislocation density, the effective stress, dislocation multiplication, and the work hardening have been investigated be Gilman.[36] He used an empirical description (Eq. 3.4.1). The essentially theoretically rigorous description (Eq. 3.5.5) and the empirical one lead to similar results. There is an advantage in the use of Eq. 3.5.5 introduced in this study because it directly allows the prediction of the behavior at different temperatures, whereas Eq. 3.4.1 includes this effect only through the temperature dependence of the constants as determined experimentally. Decrease in delay time is expected to accompany higher initial dislocation densities and lower H. The latter also indicates an increase in ϵ^{lim}. Such behavior is observed between tests 6.1, 6.2 and 6.3; 7.2 and 7.3; 8.2 and 8.3; 9.1,9.2 and 9.3; 11.2 and 11.3; and 13.1,13.2 and 13.3. It is of interest to note that H is the same for tests 13.3 and 13.4 and the creep curves exhibit very similar behavior. (Fig. 3.1.1 to Fig. 3.1.5)

3.6. DETERMINATION OF THE WORK HARDENING COEFFICIENT

The deformation kinetics analysis of creep requires that the work hardening coefficient be known. The relation between the effective stress and the strain was given in Eq. 1.4.6 as

$$\tau_{eff} = \tau^{o}_{eff} - H\epsilon$$

The work hardenign coefficient can be determined by one of the following methods.

a) The slope of the stress-strain curve is a good approximation of H. The inaccuracies involved would be those

arising from the change in the stress-strain behavior from specimen to specimen. Due to Lüders bands formation in iron, the stress-strain curve exhibits non-uniform strains at the lower yield stress region. This introduces inaccuracies in the determination of H in the yield region.

b) The effective stress is related to the applied stress, the internal stress and the creep strain as

$$\tau_{eff} = \tau_a - \tau_i$$

and also

$$\tau_{eff} = \tau^o_{eff} - H\epsilon$$

Therefore

$$\tau^o_{eff} = \tau_a - \tau^o_i$$

Thus

$$\tau_a - \tau_i = \tau^o_{eff} - H\epsilon$$

$$= \tau_a - \tau^o_i - H\epsilon$$

Therefore H can be expressed as

$$H = (\tau_i - \tau^o_i)/\epsilon \qquad 3.6.1$$

The work hardening coefficient can therefore be determined from the change in the internal stress. In the determination of the activation volumes from slopes, (section 3.2), the work hardening coefficient values used were determined

by this method.

There was up to 1.25% uncertainty in the determination of the initial internal stress τ_i^o at the first applied stress levels which lead to an average of 12.5% uncertainty in $(\tau_i - \tau_i^o)$ and therefore, in H, as well. It is usually difficult to determine an accurate value for H in the lower yield region regardless of the method used.

c) The internal stress is related to the strain as[46]

$$\tau_i = \tau_i^o + C\sqrt{\epsilon}$$

therefore

$$\tau_i - \tau_i^o = C\sqrt{\epsilon}$$

Substituting this in Eq. 3.6.1 we get

$$H = \frac{C}{\sqrt{\epsilon}}$$

The relation between the measured internal stress $(\tau_i \cong \frac{1}{2}\sigma_i)$ and $\sqrt{\epsilon}$ as shown in Fig.3.6.1. From a least squares fit, τ_i is related to $\sqrt{\epsilon}$ as

$$\tau_i = 10.195 + 14.735\sqrt{\epsilon}$$

therefore

$$H = \frac{14.735}{\sqrt{\epsilon}}$$

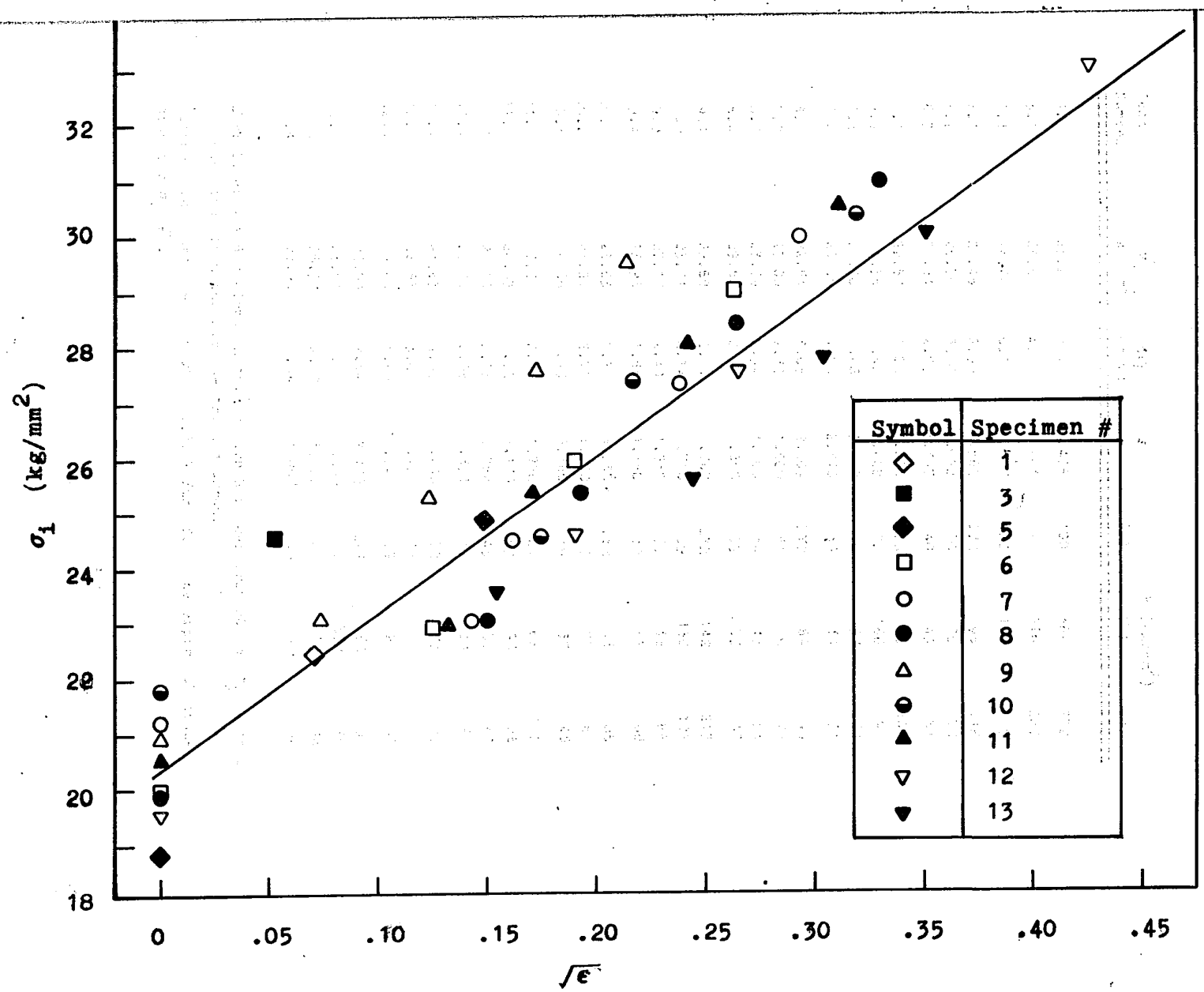

Fig. 3.6.1. The experimental dependence of σ_i on $\sqrt{\epsilon}$. The solid line is for the relation $\sigma_i = 2\tau_i = 29.47\sqrt{\epsilon} + 20.39$

TABLE IV

THE WORK HARDENING COEFFICIENT

Test Number	σ_a^o kg/mm^2	$\Delta\sigma_i$ kg/mm^2	ϵ %	H (kg/mm^2) (a)	(b)	(c)
1.1	23.26	2.97*	.405	100	367	232
3.1	24.62	4.29*	.263	120	816	287
5.1	24.24	6.06	2.208	120	137	99
6.1	22.45	2.95	1.562	LYR	94	118
6.2	25.39	3.10	2.028	70	76	78
6.3	28.84	2.89	3.397	40	43	81
7.1	22.57	1.88	2.060	LYR	46	102
7.2	24.36	1.42	.428	72	166	93
7.3	27.10	3.48	3.040	50	57	63
7.4	29.05	1.94	2.840	39	34	51
8.1	22.54	3.05	2.209	LYR	69	99
8.2	25.00	2.33	1.500	51	78	76
8.3	23.39	2.94	3.300	34	45	56
8.4	29.68	2.54	3.865	39	33	45
9.1	22.88	2.11	.747	LYR	142	213
9.2	25.01	2.14	.716	59	150	121
9.3	27.17	2.40	1.537	53	78	85
9.4	28.96	1.86	1.680	39	55	68
10.1	23.83	2.81	3.030	LYR	46	85
10.2	26.81	2.73	1.780	55	77	67
10.3	29.65	3.99	5.360	39	37	46
11.1	22.51	2.36	1.730	121	68	112
11.2	24.93	2.32	1.179	59	98	86
11.3	27.29	2.78	2.784	45	50	61
11.4	29.40	2.56	3.891	39	33	47
12.1	23.63	4.99	3.440	72	73	79
12.2	26.55	3.03	3.428	45	44	56
12.3	29.46	5.49	11.240	39	24	41
13.1	22.93	2.84	2.435	LYR	60	94
13.2	25.51	2.10	2.599	77	292	60
13.3	26.90	2.17	3.186	48	34	48
13.4	28.90	2.04	3.087	39	33	42

LYR: Lower yield region. In this region H ranges from 20 to 115 kg/mm^2, as determined from the stress-strain diagram.

*These values are based on σ_i^o = 20.39 kg/mm^2 from the empirical equation for $\sigma_i(/\bar{\epsilon})$.

The work hardening coefficient determined by these methods is presented in Table IV. The greatest discrepancy is in the region σ_a = 22.5 kg/mm^2 to 25 kg/mm^2. This discrepancy is believed to be due to the irregular stress-strain behavior in this stress region as shown in Fig. 3.1.11, as already mentioned.

3.7. COMPARISON OF RESULTS

Most investigations in literature cover the region in which only a one term rate equation is applicable. Comparison is therefore made of only the V_1 (which has already been pointed out to be identical to V_{f1}) and the $V_{1b}+V_2$ values. The summary of this comparison is given in Table V.

There is a good agreement between the present results and those reported in literature for both activation volumes. The results reported by Hanley and Krausz[12] are from the same data as Maheshwaris[23], therefore the results of the latter have not been included in the table. All results indicate the primary rate controlling mechanism to be Peierls-Nabarro mechanism.

TABLE V

COMPARISON OF RESULTS

τ^o_{eff} (kg/mm^2)	σ^o_{app} (kg/mm^2)	V_1/b^3	$(V_{b1}+V_{f2})/b^3$	Reference
5.00	-	45	-	45
2.50	-	25-42	-	42
2.50	-	30	-	40
2.50	-	45	-	43
2.50	-	50	-	44
2.32±.38	24.2±0.50	50± 17	403± 328	present*
2.00	-	50	-	28
2.00	-	55	-	43
1.26±.10	25.0±2.65	66± 25	551± 383	present*
1.25±.15	27.6±0.30	75± 33	85± 45	12
1.25	-	50	-	40
1.25	-	35-45	-	42
1.00	-	90	-	43
1.00	-	90	-	44
1.00	-	230	-	45
1.00±.03	25.8±2.04	104± 46	925±1047	present*
0.80	25.0	64	-	10
0.65±.06	27.5±2.60	97± 46	506± 289	present*
0.55±.10	15.1±0.10	300±100	600± 200	12
0.50	-	100	-	28
0.43	-	90	-	40
0.25±.15	5.2±.40	600±150	1400± 750	12
≳0	-	95-42	-	42

*The valuse of V_1 are from the strain dependence of the strain rate. For values obtained from the time dependence of strain, see Table III.

4. CONCLUSIONS

1. The deformation kinetics of pure iron at room temperature in creep was found to comprise of two consecutive barriers and the two barriers could not be in parallel.

2. The rate controlling mechanisms are believed to be associated with the overcoming of the Peierls-Nabarro stress field, whereby a double kink is formed and spreads laterally over a series of point defects in agreement with the stress relaxation study.[13]

3. Results indicated that the levelling off of creep curves maybe a result of backward activation[3]. Indications were that backward activation is over the double barrier system. Increase in the internal stress with creep strain strengthens the possibility of backward activation. Due to inconclusiveness of present results, it is suggested that creep tests of longer duration be performed to clarify whether such a backward activation is the cause of the levelling off of the creep curves.

4. In agreement with Taylor's[46] original observations, the internal stress in pure iron was found to increase with the square root of the creep strain.

5. It was concluded from the deformation kinetics analysis that, the limiting creep strain and limiting effective stress at which the rate becomes zero is proportional to $\Delta G_3^{\ddagger}$ and inversely proprotional to V_3. It follows that at zero rate the

effective stress is not necessarily zero and, therefore, that the internal stress is only approximately equal to the applied stress.

6. It is suggested that the sharp levelling-off of creep curves at the first applied stress level is a consequence of relatively large dislocation multiplication effects. The dislocation densities of the untested specimens are believed to be low, therefore, the effects of dislocation multiplication are relatively large.

7. From the rate theory description, the effect of temperature on creep behavior can be calculated. The calculated curves indicate that the delay time increases with decreasing temperature, however, the limiting creep strain is not directly effected by temperature.

APPENDIX I

ACTIVATION VOLUME VS. MECHANISM[3]

V/b^3	Mechanism
1	Climb
$10 - 10^2$	Peierels-Nabarro
$10 - 10^2$	Cross slip
$10^2 - 10^4$	Intersection
$10^2 - 10^4$	Nonconservative motion of jogs.

Note:b is the Burger's vector.

The activation volume, when expressed as a multiple of b^3, indicates the mechanism that might be operating. Some ranges of V correspond to more than one mechanism and therefore the activation energy should be determined to be more certain of the mechanism.

APPENDIX II

THE ESTIMATION OF $\Delta G_2^{\ddagger}$ AND $\Delta G_3^{\ddagger}$

The deformation kinetics description of the rate of a process in which two consecutive barriers are rate controlling is

$$\text{Rate} = \dot{\epsilon} = \delta\rho_1 \frac{1 - k_3/\nu}{\frac{1}{k_1} + \frac{1}{k_2}} \qquad (1)$$

where

$$k_i = \frac{\bar{k}T}{h} \exp\left(-\frac{\Delta G_i^{\ddagger} \pm V_i \tau_{eff}^{o}}{\bar{k}T}\right) \exp\left(\mp \frac{V_i H}{\bar{k}T} \epsilon\right) \qquad (2)$$

In terms of experimentally determined constants, Eq.1 can be expressed as

$$\dot{\epsilon} = \frac{1 - (A_3)_e \exp\left(\frac{V_3 H}{\bar{k}T} \epsilon\right)}{\frac{1}{(\delta\rho_1 A_1)_e} \exp\left(\frac{V_1 H}{\bar{k}T} \epsilon\right) + \frac{1}{(\delta\rho_1 A_1)_e} \exp\left(\frac{V_2 H}{\bar{k}T} \epsilon\right)} \qquad (3)$$

where $(\delta\rho_1 A_1)_e$, $(\delta\rho_1 A_2)_e$ and $(A_3)_e$ are experimentally determined.

Comparing Eq.1, Eq.2 and Eq.3, we find that

$$\delta\rho_1 \frac{\bar{k}T}{h} \exp\left(-\frac{\Delta G_1^{\ddagger} - V_1\tau_{eff}^{o}}{\bar{k}T}\right) = (\delta\rho_1 A_1)_e \qquad (4)$$

$$\delta\rho_1 \frac{\bar{k}T}{h} \exp\left(-\frac{\Delta G_2^{\ddagger} - V_2\tau_{eff}^{o}}{\bar{k}T}\right) = (\delta\rho_1 A_2)_e \qquad (5)$$

$$\exp\left(-\frac{\Delta G_3^{\ddagger} - V_3\tau_{eff}^{o}}{\bar{k}T}\right) = (A_3)_e \qquad (6)$$

In order to determine the activation free energies, it is necessary to perform temperature change tests. It is, however, possible to estimate the values of $\Delta G_1^{\ddagger}$ and $\Delta G_2^{\ddagger}$ if $\delta\rho_1$ is known, and $\Delta G_3^{\ddagger}$ from Eq.6.

Results reported in literature[10,13,40] indicate an activation free energy $\Delta G_1^{\ddagger}$ of about .7 to .74 ev for zero effective stress. Using these values, $\delta\rho_1$ can be estimated from

$$\delta\rho_1 = \frac{(\delta\rho_1 A_1)_e}{\frac{\bar{k}T}{h} \exp\left(-\frac{\Delta G_1^{\ddagger} - V_1\tau_{eff}^{o}}{\bar{k}T}\right)} \qquad (7)$$

which is a rearranged form of Eq.4. A listing of the $\delta\rho_1$ values calculated for $\Delta G_1^{\ddagger}$ = .7 and .74 ev is given in Table A-I.

Equation 5 can be rearranged as

$$\Delta G_2^{\ddagger} = V_2 \tau_{eff}^{o} - \bar{k}T \ln \frac{(\delta \rho_1 A_1)_e}{\delta \rho_1 \frac{\bar{k}T}{h}} \qquad (8)$$

Thus, the values of $\Delta G_2^{\ddagger}$ can be estimated using the calculated values for $\delta \rho_1$ from Eq.7. A listing of these values is also given in Table A-I.

There is great variation in the calculated values of $\Delta G_2^{\ddagger}$ $\Delta G_3^{\ddagger}$. This variation is believed to be due to one or both of the following:

i) The pre-exponential constants $(\delta \rho_1 A_1)_e$, $(\delta \rho_1 A_2)_e$ and $(A_3)_e$ are determined from semi-logarithmic graphs, as described in section 3.2. The inaccuracies involved in evaluating $(\delta \rho_1 A_1)_e$ are carried into the calculation of $\delta \rho_1$. This, along with the inaccuracy involved in the determination of $(\delta \rho_1 A_2)_e$ introduces greater inaccuracies in the calculation of $\Delta G_2^{\ddagger}$. The inaccuracy involved in determining $(A_3)_e$ is even greater because it is determined from very low strain rates.

ii) The dislocation density ρ_1 is considered to be constant for this evaluation. It has already been discussed in section 3.2 that the dislocation density changes. Also, it was pointed out that a more complete description is given by the use of ρ_t instead of ρ_1 where

$$\rho_t = \rho_1 + \rho_2$$

where ρ_2 is the concentration of flow units (mobile dislocation density) in front of the second type barrier.

TABLE A-I

ESTIMATED VALUES OF $\delta\rho_1, \Delta G_2^{\neq}$ AND $\Delta G_3^{\neq}$

Test Number	σ^o_{eff} (kg/mm^2)	$\Delta G_1^{\neq}$ = .7 ev $\delta\rho_1$	$\Delta G_2^{\neq}$(ev)	$\Delta G_1^{\neq}$ = .74 ev $\delta\rho_1$	$\Delta G_2^{\neq}$(ev)	$\Delta G_3^{\neq}$ (ev)
1.1	2.85	7.843×10^{-7}	.808	3.593×10^{-6}	.846	.060
3.1	4.21	3.339×10^{-8}	.720	1.522×10^{-7}	.759	.013
5.1	5.52	4.855×10^{-6}	.657	2.281×10^{-5}	.696	.059
6.1	2.59	1.454×10^{-6}	.706	6.747×10^{-6}	.744	-
6.2	2.58	3.566×10^{-6}	.722	1.654×10^{-5}	.750	-
6.3	1.93	1.261×10^{-7}	.571	5.848×10^{-7}	.611	.274
7.1	1.41	8.606×10^{-7}	.662	4.012×10^{-6}	.701	-
7.2	1.32	4.121×10^{-7}	.748	1.007×10^{-6}	.772	-
7.3	2.64	9.039×10^{-6}	.664	4.214×10^{-5}	.702	-.171*
7.4	1.11	4.236×10^{-6}	.428	1.975×10^{-5}	.466	.130
8.1	2.55	8.800×10^{-7}	-‡	4.099×10^{-6}	-‡	-10.98*
8.2	1.96	1.012×10^{-6}	.704	4.713×10^{-6}	.742	-17.59*
8.3	2.02	3.249×10^{-6}	.631	1.513×10^{-5}	.669	.355
8.4	1.37	7.319×10^{-7}	.664	3.409×10^{-6}	.683	.984*
9.1	1.94	4.023×10^{-8}	.664	1.876×10^{-7}	-.265*	-.104*
9.2	1.96	1.111×10^{-6}	.453	5.181×10^{-6}	.492	.083
9.3	1.98	2.742×10^{-6}	.714	1.278×10^{-5}	.753	.039
9.4	1.37	1.690×10^{-6}	.658	7.882×10^{-6}	.697	.097
10.1	2.08	1.579×10^{-6}	-‡	7.361×10^{-6}	-.637*	1.932
10.2	2.25	5.362×10^{-6}	.692	2.500×10^{-5}	.731	.145
10.3	2.36	9.002×10^{-6}	.461	4.197×10^{-5}	.500	.815
11.1	1.97	7.309×10^{-7}	-	3.122×10^{-6}	-	-
11.2	2.03	1.584×10^{-6}	.712	6.843×10^{-6}	.748	.018
11.3	2.01	9.329×10^{-6}	.658	4.002×10^{-5}	.695	.477
11.4	1.40	5.115×10^{-6}	.501	2.887×10^{-5}	.545	.160
12.1	4.17	2.701×10^{-6}	.027*	1.250×10^{-5}	.067*	1.316
12.2	2.10	6.845×10^{-6}	.447	3.166×10^{-5}	.486	.739*
12.3	1.98	1.909×10^{-5}	-	8.828×10^{-5}	-	-
13.1	2.27	2.179×10^{-6}	-‡	1.003×10^{-5}	-‡	.604*
13.2	2.01	8.377×10^{-8}	.735	3.876×10^{-7}	.773	.035*
13.3	1.30	6.066×10^{-8}	.518	2.929×10^{-5}	.558	.385
13.4	1.14	1.261×10^{-5}	.421	5.819×10^{-5}	.460	1.296
	Average energy values‡		.628±.113		.663±.113ev	.425±.554 ev

‡ In the calculation of these averages, the values marked by (*) were not included. The variations are one standard deviation.

‡ The values of $\Delta G_2^{\neq}$ could not becalculated from the experimental pre-exponential constants.

* These values were obtained from an analysis of two or three data points and are therefore not included in the averages.

APPENDIX III

ANALYSIS OF THE STRESS RELAXATION OF NICKEL SINGLE CRYSTALS

Results reported by Rhode and Pitt[11] on the stress relaxation of nickel single crystals show a sharp levelling off, as was observed in some of the creep tests on pure iron in the present investigation. The authors reported tests performed at 350°, 273°, 198°, 153°and 77°K. Their analysis was restricted to a single barrier-forward activation type kinetics analysis. They concluded that the rate controlling mechanism was associated with direct dislocation-dislocation interaction. They believed the observed decrease in the rate of relaxation to be a result of a decrease in the mobile dislocation density and an increase in the "long range back stress", i.e. the internal stress.

Their reported results at 350° and 273°K were analyzed to investigate what possibly causes a decrease in the relaxation rate. An increase in the total dislocation density can cause a proportional decrease in the mobile dislocation density. These effects, however, would be noticeable in the earlier parts of the experiments. Also, a change in the internal stress large enough to decrease the rate as observed is unlikely. The strains involved in stress relaxation are very low and therefore one would not expect a large change in the internal stress. The decrease in the rate of a deformation

process is usually due to backward activation over the single barrier system or another rate controlling mechanism becoming noticable.

The results at 350° and 273°K were analyzed in this light, it was found that with a sinlge exception of the nine test results, there was a second barrier that is rate controlling at lower stresses. The second barrier was found to be consecutive to the first,and a parallel combination is not possible.

Their results for the first barrier, forward activation, was reported to give and activation volume ranging from $4160b^3$ at 350°K to $1600b^3$ at 273°K. In the present analysis, the values ranged from $3550b^3$ at 350°K to $1670b^3$ at 273°K. The values are almost identical and indicate the possibility of the primary rate controlling mechanism to be the same, i.e. intersection or non-conservative motion of jogs.

At lower stresses, i.e. higher $\Delta\tau$, the activation volume of the second barrier was found to range at an average of $4x10^4b^3$ at 350°K to $1x10^4b^3$ at 273°K. At the lower temperature, the scatter in V_2 was considerable; the determined values ranging from $2x10^3b^3$ to $2.6x10^4b^3$. The large scatter is believed to be due to lack of more data. The values of V_2 are an order of magnitude larger than V_1 but are still indicative of the same mechanism(s).

The V_1 values determined from stress relaxation tests are considerably larger than those determined by etch-pitt

measurements ($V_1 \cong 600b^3$ at 273^oK). The difference has been reported to be due to the effect of the combined elastic modulus on the determination of activation volumes[3]. This effect was not investigated.

A deformation kinetics analysis was used in determining V_1 and V_2. Three typical experimental and calculated curves are shown in Figures A-1,2 and 3. The solid curves are calculated from the deformation kinetics description as

$$t = \frac{1}{\delta \rho_1 A_1 E} \frac{\bar{k}T}{V_1} \exp\left(\frac{V_1 \Delta\tau}{\bar{k}T}\right) + \frac{1}{\delta \rho_1 A_2 E} \frac{\bar{k}T}{V_2} \exp\left(\frac{V_2 \Delta\tau}{\bar{k}T}\right)$$

where E is the combined elastic modulus of the machine and specimen, and $\Delta\tau$ is the change in the stress. This equation is similar in form to Eq. 3.2.9, however, the "-1" term has been neglected on the RHS of the equation. The agreement between the experimental behavior was found to be good. The deviation observed at very early times is believed to be due to either non-negligible "-1" term or, more likely, the semi-logarithmic graphical presentation.

It should be noted that these experiments were of very short duration, an average of 15 to 20 seconds. Thus the results of the V_2 term were determined from few points. The description given in the present analysis gives a better fit

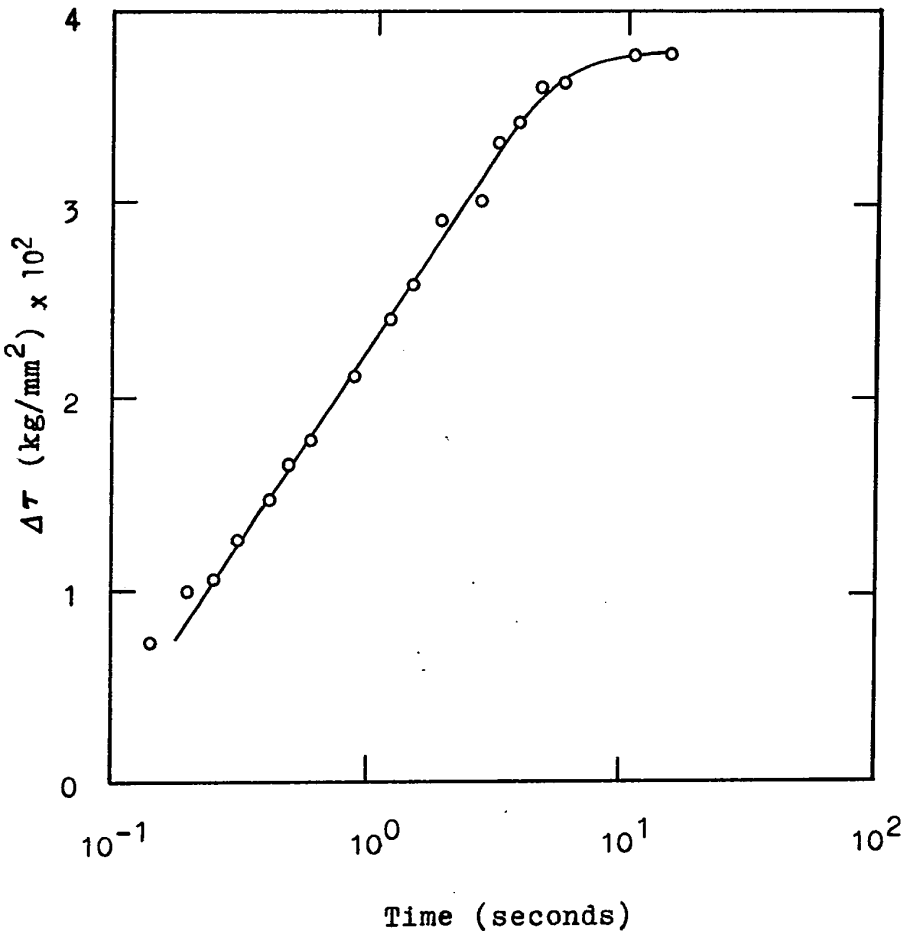

Fig. A -1. Stress relaxation of nickel single crystal, type P-4, at 350°K. The solid curve is calculated from Eq.1.

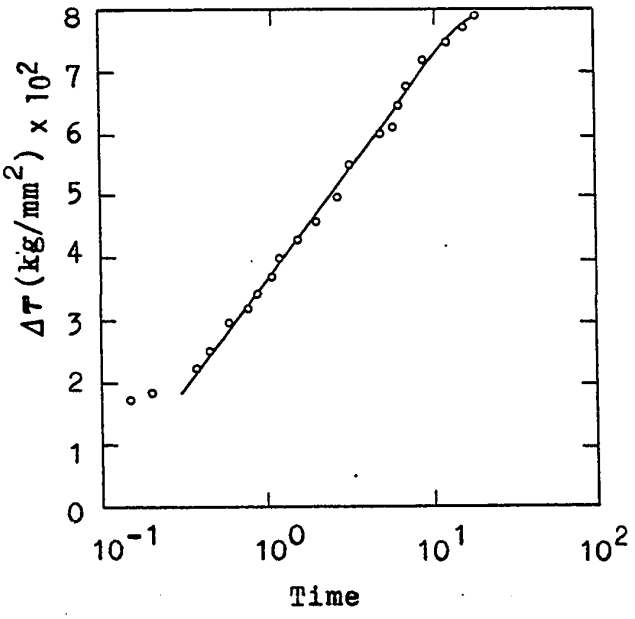

Fig. A-2. Stress relaxation of nickel single crystals, type P-4, at 273°K. The solid curve is calculated from Eq. 1.

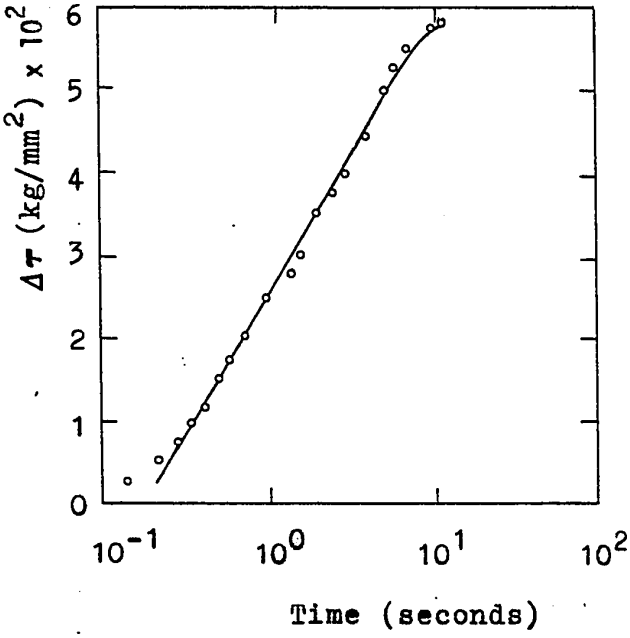

Fig. A-3. Stress relaxation of nickel sinle crystals, type Cu-12, at 273° K.

than the single forward term description. It may be possible that there is backward activation over the two barrier system causing the apparent levelling-off of the stress relaxation curves, however, this term cannot be determined from tests of such short duration.

APPENDIX IV

CREEP OF A "SUPERPLASTIC" ALLOY

Creep tests were performed on a Noranda Z-500 free machining alloy. The reported composition was 25% Al, 5% Cu, 0.5% Mg and Zn ballance. This material is believed to possibly have superplastic properties, i.e. a stress exponent close to unity.

The machined specimens were like the pure iron specimens, the difference being in gage lengths which varied from 42mm to 65mm. The tests were performed at room temperature. The material was found to creep extensively, up to 18% strain at an applied stress of 31.8 kg/mm^2.

The deformation kinetics analysis outlined in sections 1.4 and 3.2 was attempted. The step-by-step analysis could not be applied due to the non-linear creep behavior. A typical creep curve is given in Fig. A-4. It was therefore concluded that creep testing is not a suitable method for the study of the deformation kinetics of this material.

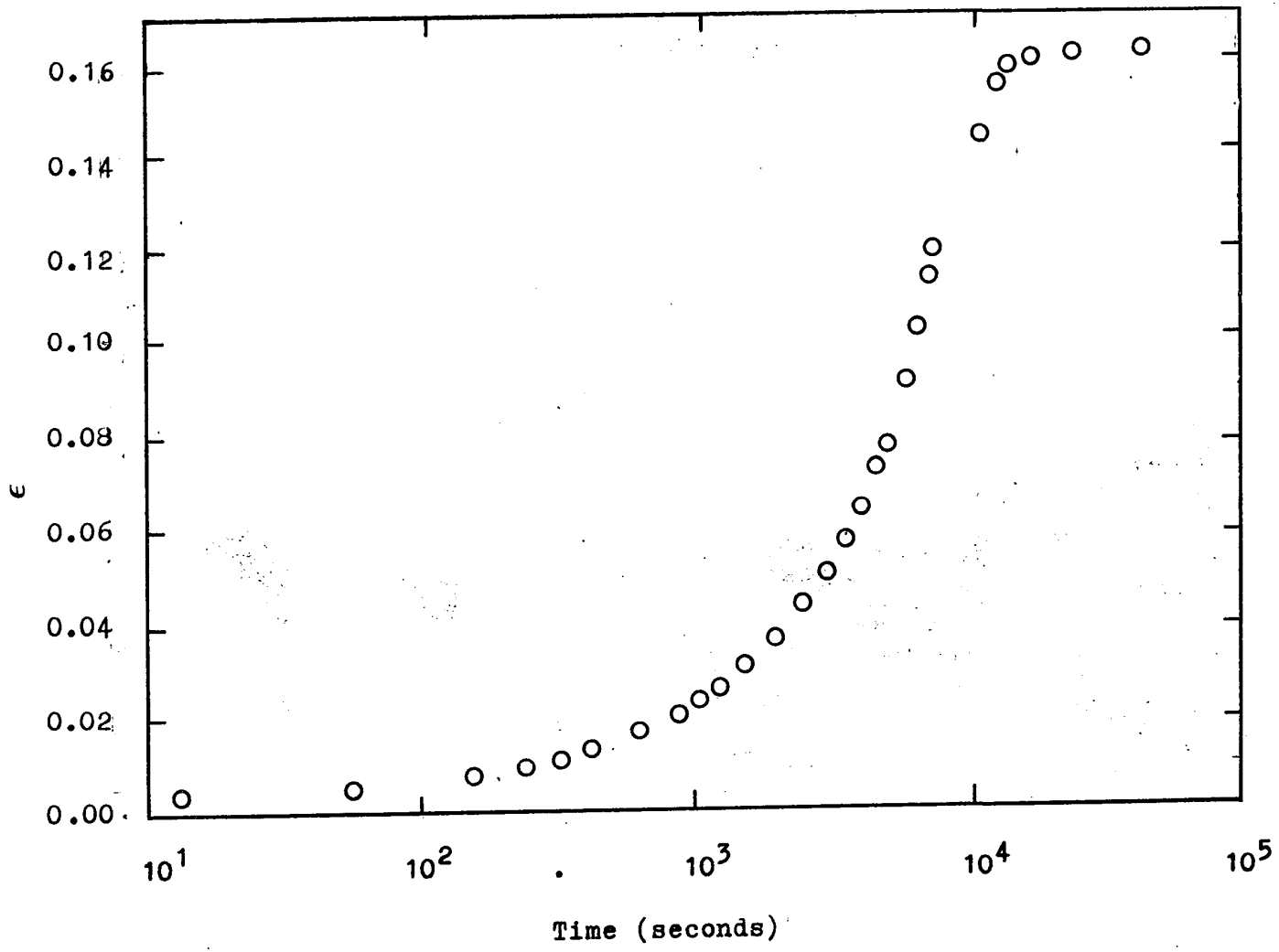

Fig. A-4. Experimental creep curve of Noranda Z-500, free machining alloy.

REFERENCES

1 Glen,J.,Phil.Mag.,1,400 (1956)

2 Andrade,E.N.daC.,Proc.Roy.Soc. (London) Ser.A, 1 (1910)

3 Krausz,A.S. and Eyring,H.,Deformation Kinetics,Wiley-Interscience(1975)

4 Phillips,F.,Phil.Mag.,9,513 (1905)

5 Wyatt,O.H.,Proc.Phy.Soc.(London)Ser.B,66,459 (1953)

6 Eyring,H.,J.Chem.Phys.,4,283 (1936)

7 Laidler,K.J.,Theories of Chemical Reaction Rates,McGraw Hill (1969)

7.1 Eyring,H. and Eyring,E.M.,Modern Chemical Kinetics, Reinhold Publising Corporation (1967)

8 Dorn,J.E.,Proc.Symp.Nat.Phys.Lab.(London),89(1956)

9 Altshuler,T.L. and Christian,J.W.,Phil.Trans.Roy.Soc. London,Ser.A,261,1121 (1967)

10 Basinski,Z.S. and Christian,J.W.,Australian J.Phys.,13, 299(1960)

11 Rhode,R.W. and Pitt,C.H.,J.Appl.Phys.,39,3186 (1968)

12 Hanley,T.O'D. and Krausz,A.S.,J.Appl.Phys.,45,2013 (1974)

13 Hanley,T.O'D.,Krausz,A.S. and Maheshwari,D.,Mat.Sci.& Eng.,16,155 (1974)

14 Gilman,J.J. and Johnston,W.G.,Solid State Physics,Academic Press,13,147 (1962)

15 Conrad,H.,Mat.Sci.&Eng.,6,265 (1970)

16 Ahlquist,N.,Scripta Met.,5,185 (1971)

17 Ahlquist,N. and Nix,W.D.,Scripta Met.,3,678 (1969)

18 Seeger,A.Z.,Naturforch,9.a (1954)

19 Gibbs,G.B.,Phil.Mag.,13,317 (1966)

20 Conrad,H. and Okazaki,K.,Scripta Met.,14,111 (1970)

21 Sargent,G. and Conrad,H.,Scripta Met.,3, 43 (1969)

22 Conrad,H.,J.Iron and Steel Inst.,364 (1961)

23 Maheshwari,D.,M.A.Sc. Thesis, Dept. of Mech. Eng., University of Ottawa, Ottawa (1972)

24 Mulla,G.A.,M.Eng. Thesis, Dept. of Mech. Eng., University of Ottawa, Ottawa,(1972)

25 Gilman,J.,Micromechanics of Flow in Solids,McGraw Hill (1969)

26 Bernstein,I.M.,Acta Met.,17,249 (1969)

27 Cadek,J.,Pahutova,M. and Rys,P.,Phys.Stat,Solidi,36, 351 (1969)

28 Conrad,H.,Mat.Sci.Lab. Aerospace Corpn.,El Segundo (1963)

29 Keh,A.S.,Phil.Mag.,12,9 (1965)

30 Krausz,A.S. and Aggarwal,M.L.,Appl.Sci.Res.,40,105 (1974)

31 Michalak,J.T.,Acta Met.,13,213 (1963)

32 Thomas,K.,Nature,213,172 (1967)

33 Smidt,F.A.Jr.,Acta Met.,17,381 (1966)

34 Krausz,A.S., submitted to Int.J.Frac. (1976)

35 Johnston,W.G.,J.Appl.Phys.,33,2716 (1962)

36 Gilman, J.,J.Appl.Phys.,36,2772 (1965)

37 Mukherjee,A.K.,Bird,J.E. and Dorn,J.E.,UCRL Report # 18526 (1968)

38 Arsenault,R.J.,Acta Met.,14,831 (1966)

39 Krausz,A.S.,Z.Naturforch,31.a (1976)

40 Harding,J.Acta Met.,17,949 (1969)

41 Wray,P.J. and Horne,G.T.,Phil.Mag,13,889 (1966)

42 Dorn,J.E. and Rajnak,S.,Trans.Met.Soc. of AIME,230, 1052 (1964)

43 Okazaki,K.,Kagawa,M. and Aono,Y.,Z.Metallkde.,67,47 (1976)

44 Spitzig,W. and Keh,A.S.,Acta Met.,18,1021 (1970)

45 Spitzig,W.,Mat.Sci. & Eng.,16,169 (1974)

46 Taylor,G.I.,Proc.Roy.Soc.(London)Ser.A,362(1934)